Fredrik Hekland

On the Design and Analysis of Shannon-Kotel'nikov Mappings for Joint Source-Channel Coding

Thesis for the degree doctor philosophiae

Trondheim, May 2007

Faculty of Information Technology,
Mathematics and Electrical Engineering
Department of Electronics and Telecommunications

NTNU
Innovation and Creativity

NTNU
Norwegian University of Science and Technology

Thesis for the degree doctor philosophiae

Faculty of Information Technology, Mathematics and Electrical Engineering
Department of Electronics and Telecommunications

ISBN 978-82-471-2260-0 (printed version)
ISBN 978-82-471-2274-7 (electronic version)
ISSN 1503-8181

Doctoral theses at NTNU, 2007:103

Printed by NTNU-trykk

Abstract

In this dissertation, we explore the possibility of transmitting discrete-time, continuous amplitude sources over discrete-time, continuous-amplitude channels by using non-linear direct source-channel mappings. This is a *joint source-channel coding* technique where there is no real distinction between the source coding part and the channel coding part. In contrast to traditional digital communication systems, these techniques are only suited for transmitting sources which tolerate a certain amount of distortion, e.g. images and sound. The reason for this restriction is that the channel noise is part of the total distortion, thus making error-free transmission impossible. However, the analog nature of the scheme provides both high spectral efficiency and robustness when the mappings are properly designed.

As there are no known non-linear maps which actually achieves optimality, we investigate the mechanisms which degrade the performance of source-channel coding systems, hoping to obtain some pointers on how to design systems with as little performance loss as possible. We identify several loss factors causing performance degradations; among them we mention mismatched channel symbol distribution and mismatched error-sequence distribution. Given an additive white Gaussian noise channel with an average power constraint, and a mean-squared error distortion measure, it is shown that both the loss from having non-Gaussian distributed channel symbols, and the loss from having non-Gaussian reconstruction error/noise, equals the relative entropy of the actual distribution and the capacity-achieving Gaussian.

A class of joint source-channel coding schemes which we have called *Shannon-Kotel'nikov mappings* is shown to provide both robustness to unknown channel conditions, and high spectral efficiency in the sense that the mappings operate close to the theoretical performance bounds. A mapping consist of a non-linear curve, or function, which maps a source point directly into the channel space. By having different dimensions of the source and channel spaces, both bandwidth reduction (compression) and bandwidth expansion (error control) can be achieved. The optimization of a

2:1 bandwidth-reducing system is shown, for both Gaussian and Laplacian sources over additive white Gaussian noise channels. These are shown to perform quite well relative to digital systems. Furthermore, a 4:1 bandwidth-reducing system consisting of a cascade of two 2:1 mappings is tried out as a way to avoid the complexity increase associated with higher dimensions, but this shows worse performance than known channel-optimized vector quantizers.

A problem with the analog nature of the Shannon-Kotel'nikov mappings is that they do not automatically interface with existing digital communication systems. Whether one wants to store the received mappings, or transmit them further through a digital transport network, a digitization step is necessary in order to obtain a bit-representation. We propose some very simple transcoding schemes which digitize the received channel symbols directly, instead of first decoding to native representation and re-encoding with a digital source coder. This proves to be simple, yet effective for interfacing the Shannon-Kotel'nikov mappings with a digital system. Moreover, the transcoding technique which produces multi-level channel symbols proves to be able to suppress most of the channel noise, enabling serial multi-hop communication without accumulation of channel noise.

Preface

This dissertation is submitted in partial fulfillment of the requirements for the degree of Philosophiae Doctor (PhD) at the Department of Electronics and Telecommunications, Norwegian University of Science and Technology (NTNU). My advisors have been Professor Tor A. Ramstand and Professor Geir E. Øien, both of whom are with the Department of Electronics and Telecommunications, NTNU.

The work, comprising research, compulsory courses as well as teaching assistant duties, was carried out from July 2002 to March 2007 with the Signal Processing group at NTNU.

The work included in this thesis was funded by The Research Counsil of Norway (NFR) through the IKT-2010 project called "Bandwidth-Efficient and Adaptive Transmission Schemes for Wireless Multimedia Communications" (BEATS). The assistantship was funded by the Department of of Electronics and Telecommunications, NTNU.

Acknowledgements

"The path to our destination is not always a straight one. We go down the wrong road, we get lost, we turn back. Maybe it doesn't matter which road we embark on. Maybe what matters is that we embark."

- Barbara Hall, Northern Exposure, Rosebud, 1993

During the spring of 2002, when I was about to finish my Master's thesis, I was more than ready to leave the university and get a "real" job in the industry. Pursuing a PhD was something I didn't really consider until Prof. Geir Øien informed me of the availability of several PhD grants. I applied, even thought I did't really think I would even be offered any. So, when I was notified that if I made up my mind over the weekend, the position would be mine, I seriously wondered what I should do. No matter who I talked to, they said I should take it; "This is perfect for you". So I accepted. Now that I'm sitting here several years later finalizing the report on my research, I can surely say that I'm happy that I grabbed this opportunity and embarked on the long road to obtain the doctoral degree. All the things I've learned, both on the personal and professional level. All the nice and intelligent people I've met. From them I had the chance to learn all kinds of things. The freedom to pursue the ideas and interest I had, without having a boss breathing down my neck. All of this made the long journey worthwhile. The hours of despair, with no sight of the end of the tunnel, is now forgotten.

I am deeply grateful to my main advisor; Professor Tor Ramstad. He has been a source of inspiration, and his insight and vision has made it possible for me to come this far. His cheerful character and generosity is unique. Although his source of ideas is running faster than my sink of research could ever consume, I managed to catch some of his ideas and make them come to life. The other significant person is my co-supervisor Professor Geir Øien, another smart and generous person I'm happy to have had as my advisor. I'm grateful for the fact that he offered me this opportunity, and that he all

along had a firm belief that I would make it. His encouragement and backing is priceless, and he was always available to help me whenever I needed it.

Another significant contributer to this dissertation is PhD student Pål Anders Floor. His arrival gave me an important discussion partner for details in my research, and we had many high-flying discussions (in a higher dimension?) which were really of great help. He also helped me with mathematical details, and provided valuable insight into the mystics of Shannon mappings through his own research.

Throughout all theses years, my office mate Greg Håkonsen was a great companion, and his green fingers made our office a rather nice place to be. Together we did reality checks on our ideas, and provided help whenever the other was stuck. I'm still irritated that I didn't manage to turn him into a coffee drinker, though. Luckily, other people in the group shared my interest in black fluids, the most prominent being Ole Morten Strand with whom I had several visits to the café for interesting discussions.

The signal processing group at NTNU is a unique collection of remarkable people, and I have cherished every moment with the people in this group. There are many people I should thank for making these years so memorable, and by naming a few of them I will certainly run the risk of insulting those I forgot. Therefore, I simply want to express my gratitude to all the people who crossed my path during these years at the signal processing group. The social events like food meetings, wine meetings and Christmas parties will be deeply missed.

I must not forget to extend a thought to the people close to me, outside the professional sphere. In particular, my family, which has always had a strong belief that I would make it through, backing me up both morally and economically whenever needed. Furthermore, a big thanks to my friends with whom I can just be myself and have fun without worrying about professional matters. All work and no play...

Last, but not least, the decision to take on this PhD made my path cross the path of the wonderful Anna Kim, who is now my partner. Apart from being a great supporter, constantly encouraging me, she also happens to be a Dr.Ing within the same area. Hence, she's also been an excellent discussion partner, providing insight and advise along the way. Moreover, having been through this process herself, she has been very understanding and tolerant in the last months toward the delivery. Her love has been a great source of energy for me during the most difficult times. `:-*`

Oslo, April 2007
Fredrik Hekland

Contents

List of Acronyms

1-D	one-dimensional
2-D	two-dimensional
3G	third generation wireless communication system
4B3T	4 binary, 3 ternary line code
ACM	adaptive, coded modulation
AWGN	additive white Gaussian noise
BCH	Bose-Chaudhuri-Hocquenghem
BER	bit-error rate
BPAM	block pulse amplitude modulation
BPSK	binary phase-shift keying
CD-ROM	compact disc read-only memory
cdf	cumulative density function
CLD	cross-layer design
COVQ	channel-optimized vector quantizer
CSI	channel-state information
CSNR	channel signal-to-noise ratio
dB	decibel
DSL	digital subscriber line
EFR	enhanced full-rate

ECVQ entropy-constrained vector quantizer

FEC forward error correction

FM frequency modulation

FPM frequency-position modulation

FTTH fiber to the home

GPS global positioning system

GSM global system for mobile communication

HDA hybrid digital-analog

HDTV high definition television

HSQLC hybrid scalar quantizer, linear coder

IA index assignment

i.i.d. independent, identically distributed

ISDN integrated services digital network

ISM industrial, scientific, medical

JPEG joint photographic experts group

JSC joint source-channel

JSCC joint source-channel coding

LDPC low-density parity check

MAP maximum a-posteriori probability

MBM mixed-base modulation

MD multiple description

MIMO multiple-input, multiple-output

ML maximum likelihood

MMSE minimum mean-squared error

MOR-VQ modulation-organized vector quantizer

MPEG moving picture experts group

MR multi-resolution

mse mean-squared error

OFDM orthogonal frequency-division multiplex

OPTA optimal performance, theoretically attainable

OSI Open Systems Interconnection

PAM pulse-amplitude modulation

PCCOVQ power-constrained channel-optimized vector quantizer

PCM pulse code modulation

pdf probability density function

PER packet error rate

PM phase modulation

pmf probability mass function

PPM pulse-position modulation

PSK phase-shift keying

QAM quadrature-amplitude modulation

R-D rate-distortion

RCPC rate-compatible punctured convolutional

SINR signal to interference-plus-noise ratio

S-K Shannon-Kotel'nikov

SNR signal-to-noise ratio

SOCC source-optimized channel coding

SPIHT set-partitioning in hierarchical trees

SQ scalar quantization

STBC space-time block-coding

TCM	trellis-coded modulation
UEP	unequal error protection
UMTS	universal mobile telecommunication system
VoD	video-on-demand
VQ	vector quantization

Nomenclature

$a(k)$	Quantized signal (channel 1 in the HSQLC)
α	Scaling factor for transmitted channel symbol
$b(k)$	Quantization error (channel 2 in the HSQLC)
B	Source bandwidth
β	Scaling factor for received channel symbol
C	Channel capacity
C'	Operational capacity
C^*	Channel capacity
c_i	PAM Representation level of transmitter-side transcoded mapping
$\circ$	Composition of two functions
D	Distortion
D_Q	Distortion due to transcoding
D_s	Distortion of unquantized spiral mapping
D_c	Distortion due to channel noise
δ	Quantizer step in transcoder
Δ_i	Spiral arm distance of the inner mapping in a cascade of two 2:1 mappings.
Δ_o	Spiral arm distance of the outer mapping in a cascade of two 2:1 mappings.

Δ	Spiral arm distance in 2:1 mapping
Δ_{opt}	Optimal Δ given γ
Δ_{opt}^{pre}	Optimized spiral arm distance for transmitter-side transcoding
$D(R)$	Distortion-Rate function
d_{th}	Distortion from incorrect decision
D_{tot}^{post}	Total distortion, receiver-side transcoding.
D_{tot}^{pre}	Total distortion, transmitter-side transcoding
E	Expectancy operator
ε_{th}^2	Average distortion from threshold effect
η	Constant used in the approximation of the curve length operator
$f_X(x)$	Probability density function
γ	Channel signal-to-noise ratio (CSNR)
$H(X)$	Entropy
$h(X)$	Differential entropy
$I(S;\hat{S})$	Mutual information
K	Number of links in a (serial) multihop network
k	Uniformity of Archimedean spiral
χ	Channel symbol (unscaled)
χ_q	Quantized channel symbol
λ	Scale parameter in Laplace distribution
M	Source dimension
m	Deformity parameter for Archimedean spirals
max	Maximum value
min	Minimum value

μ	Mean of random variable
N	Channel dimension
N	Noise power
$\mathcal{N}$	Normal distribution
Ω	Auxiliary variable used in transcoder optimization
ω	Auxiliary variable used in transcoding optimization
OPTA_{dB}	OPTA expressed in dB
P	Channel power
$\Pr[i]$	Probabiliy of event i
ψ	Dimension changing operation
$q()$	Approximation (projection) operator
R	Rate
$R'(D)$	Operational rate-distortion function
$R(D)$	Rate-Distortion function
$R^*(D)$	Rate-distortion function
$\mathbb{R}$	The set of real numbers
$\rho(f)$	Capacity loss due to mismatched channel symbol distribution f
σ_s^2	Source variance
$\sigma_{n,K}^2$	Channel noise variance of hop K
σ_n^2	Channel noise variance
σ_G	Standard deviation of a Gaussian random variable
σ_L	Standard deviation of a Laplacian random variable
σ_U	Standard deviation of a uniform random variable
$\text{SNR}_{gap,dB}$	The SNR gap to OPTA (in dB)

SNR_{dB}	SNR expressed in dB
$(\cdots)^t$	Matrix transposition
$T()$	Mapping/dimension changing operator
$\tau(g)$	Rate increase due to mismatched error sequence distribution g
$w()$	Distribution-warping function
W	Channel bandwidth
X, x	Transmitted channel symbol
Y, y	Received channel symbol
Z, z	Channel noise sample

Chapter 1

Introduction

"Give me six hours to chop down a tree and I will spend the first four sharpening the axe."

- Abraham Lincoln

Telecommunication is becoming increasingly important in modern societies, as it enables transportation of large amount of information in a very short time without being hampered by large distances. It is hard to imagine a world without telecommunications, since it would imply no television, radio, telephones, mobile phones, global positioning system (GPS), or Internet, to name a few important services. Although it is not within the scope of this dissertation to discuss the different benefits of telecommunications, being aware of them and knowing which areas that gain the most from increased research activity is indeed an advantage. Perhaps the most important development for long range communication was the introduction of the optical fiber. The evolution of fiber optics has revolutionized the telecommunication industry and helped boost the information age by providing "unlimited" capacities[1] on the backbone networks. Even fiber to the home (FTTH) is becoming more widespread as installation cost per provider is below $1000 [Wieland, 2006], enabling bandwidth hungry applications like video-on-demand (VoD) and high definition television (HDTV). The significantly increased bandwidth for Internet access has the potential

[1] Of course, the capacity is not infinite, but relative to wireless communication which is considered in this dissertation, the 2 Tbit/s over 9240 km achieved by [Yamada et al., 2002] can be considered to be infinite.

to change the broadcasting industry from the model we know today with fixed schedules and centralized control, to a model where the users can compose their own schedule, both in terms of content and time. Even user-produced content is gaining popularity, with services like YouTube.com and MySpace.com.

Wireless communication with its benefits such as mobility, flexibility, ease of deployment and reduced cabling, is becoming more and more popular. For users who do not have strict requirements on security and availability, wireless provides a tremendous convenience. There are, however, some important factors that impose restrictions on how much information can be sent per channel use (what we call channel capacity) for such systems. The most significant ones are the related issues of *limited available spectrum* and the fact that *a wireless channel is a shared medium*. Moreover, compared to wire-channels, wireless channels suffer from the fact that they are to different extents temporally, spatially and frequency-wise stochastically varying in quality. These factors limit the channel capacity of each user, as they are no longer free to use whatever amount of bandwidth or transmit power they wish. After all, most of the wireless spectrum is controlled through licenses in order to control the interference issues arising from users sharing the same frequencies. Only a few frequency bands are unlicensed (like the 2.4 GHz ISM band), but then the transmit power is limited. To further worsen the situation, available bandwidth and propagation characteristics are dependent on the carrier frequency. The lower the frequency, the longer the signals travel, thus increasing the interference for others using the same frequency. The usable spectrum for wireless communication spans from 300 kHz up to about 100 GHz [Proakis, 2001], with the lower end of the spectrum being the most crowded, and the less crowded higher end having a shorter transmission range (due to increased attenuation and line-of-sight requirements). When given the available transmit spectrum and power limitation, what limits the channel capacity is thermal noise in the receiver, interference from transmitters operating at the same frequency, and the properties of the channel.

In order to achieve high multi-cell spectral efficiency in cellular systems, aggressive frequency-reuse is necessary [Catreux et al., 2001; Gjendemsjø et al., 2006a; Kiani et al., 2006]. This necessarily reduces the signal to interference-plus-noise ratio (SINR) which again translates to lower throughput per user. In case the available bandwidth per user is fixed and the SINR is low, the most realistic way to increase the user throughput is to employ multiple antenna techniques like multiple-input, multiple-output (MIMO) techniques

[Paulraj et al., 2004] where the spectral efficiency can increase linearly with the number of antennas[2] without increasing the transmit power. MIMO has a limitation in the sense that it is dependent of rich multi-path diversity, potentially leaving little to no gain for certain applications, e.g. broadcasting in open landscape or short-range line-of-sight communication. Exploiting MIMO in line-of-sight scenarios is still possible, though [Bøhagen et al., 2005].

To enable high-bandwidth applications like HDTV over wireless and at the same time supporting a high number of users, spectrally efficient and robust solutions are essential. Moreover, low system complexity is desirable in order to obtain lower production costs and reduce battery consumption for mobile devices.

The purpose of this dissertation is to explore transmission techniques for analog sources which have the potential to be both spectrally efficient and robust, while maintaining a reasonably low complexity. The primary difference from traditional digital techniques is that instead of making the channel transparent, channel noise is a part of the total distortion of the reconstructed source at the receiver side. This is achieved by mapping a source point directly into the channel space using a mathematical function or curve. This makes both the encoder and decoder relatively simple, and also the channel symbols can be made memoryless.

1.1 Performance Bounds for Sources and Channels

In physical systems, noise will always limit the capacity of a given channel, thus dictating how much information that can be transmitted on the channel per use. When trying to build a communication system, it is desirable to have a performance criterion which serves as an upper achievable bound, in order to know how good the system actually can be. The goal is to make it perform optimally according to the chosen criterion. Ideally, the criterion should reflect the receiver's notion of quality, but usually more mathematically tractable criteria are used. The concept of optimal performance is thus often relative to the chosen criterion, but not necessarily to the receiver's opinion.

[2]This is only true for the single-cell scenario which is not interference-limited. For interference-limited operation the MIMO gains are, however, still significant over single-antenna system [Catreux et al., 2001].

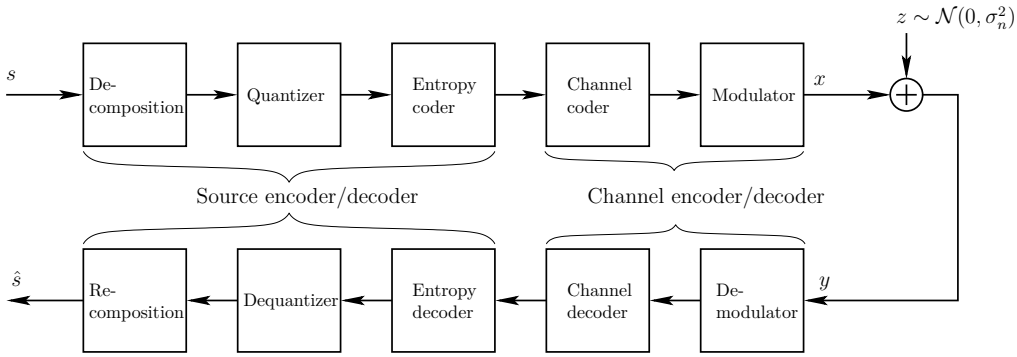

Figure 1.1: A source-channel coding system.

Figure 1.1 shows a commonly seen communication chain. We have a source coder which is responsible for compressing the source signal as much as necessary, and a channel encoder which is responsible for adapting the source data to the channel. These are the two basic operations in a source-channel coding system, and the theory providing the theoretical performance bounds of operation is described next.

1.1.1 Coding of Analog Sources

Analog sources, like images and sound, can be said to contain infinite amount of information; if we wish to describe them exactly without any loss we need infinite precision, which however is impossible in practical systems.

Since the amount of data from analog sources might grow very large, it is often of interest to make the approximate description of the source as coarse as possible in order to reduce the data rate, while introducing minimum distortion. This is what is called lossy source coding with a fidelity criterion [Shannon, 1959]. In essence, a source coder first tries to remove all redundancy by a decorrelating operation. Then further rate reductions can be achieved by removing imperceptible data, called *irrelevance*. This is normally done using a quantizer [Jayant and Noll, 1984]. Finally, if even lower rates are required quantizers can produce even coarser representations at the expense of introducing perceptible distortion. If the probabilities of the quantization indices are non-uniform, entropy coding can be employed to reduce the rate even further [Cover and Thomas, 1991]. Entropy coding, contrary to quantization, is a lossless operation and will not introduce any distortion.

The theory supporting lossy source coding is called rate-distortion (R-D) theory and was pioneered by [Shannon, 1959]. Rate-distortion theory has been less influential on source coding compared to information theory's impact on the channel coding community. This is partially due to the fact that simple systems using scalar quantization (SQ) with entropy coding or transform coders with scalar quantizers perform so well. At high rates, the scalar quantizer with entropy coding is only 0.255 bits, or 1.53 dB, away from the rate-distortion bound [Jayant and Noll, 1984] for any (memoryless) source, leaving very little gain for more complex systems [Lookabaugh and Gray, 1989]. On the other hand, vector quantization (VQ) can reach the rate-distortion bound if allowing infinite complexity and delay in the source coder, but still, the potential gain is only 1.53 decibel (dB) compared to the SQ.

For memoryless continuous sources, only the R-D function of the Gaussian source with a mean-squared error (mse) distortion measure exist in analytic form [Berger, 1971]:

$$R(D) = \begin{cases} \frac{1}{2}\log_2\left(\frac{\sigma_s^2}{D}\right), & D < \sigma_s^2, \\ 0, & \text{otherwise}, \end{cases} \tag{1.1}$$

where σ_s^2 is the source variance, D is the distortion and with base-2 logarithm the rate is bits. For source coders, the inverse of (1.1) can be more useful; this is called the distortion-rate function:

$$D(R) = \sigma_s^2 2^{-2R}, \quad R \geq 0. \tag{1.2}$$

The rate-distortion function for some other continuous-amplitude, symmetrically distributed sources can also be approximated for scalar quantization, by using (1.1), with a proportionality factor depending on the distribution [Berger and Gibson, 1998].

Turning to Figure 1.1 again, we look at the details of a source-channel coding system. Here, source coding is performed in the first three blocks, whereas channel coding is done in the last two blocks. First, the source is decomposed to produce statistically independent components, then quantizers are applied to remove all irrelevance and to introduce controlled distortion if lower rates are needed. Then, because of non-uniform probabilities of the quantizer outputs, entropy coding is applied to approach the entropy of the quantizer output (works by assigning short codewords to quantizer cells with high probability, and long codewords to less probable cells). When designing a source code without any knowledge of the channel, seriously reduced

performance might be experienced, especially in the case of entropy coding. Entropy codes which have variable length codewords are highly sensitive to bit-errors and will render further decoding impossible unless powerful channel codes are used, and resynchronization markers are inserted regularly into the data stream to enable recovery from bit-errors the channel decoder was unable to correct. To avoid this situation, one can abandon the entropy coding step and rather use fixed-length code words at the expense of higher rates R. The advantage of fixed-length codes for noisy channels is that they are decoded symbol-by-symbol. Hence, bit errors only affect one codeword and subsequent symbols can be decoded as normal. However, unless the quantizer is designed also taking the channel noise into account, suboptimal performance will be the result. Some work has been done on channel optimized quantization using fixed-length codes, see for instance [Kurtenbach and Wintz, 1969; Jayant and Noll, 1984; Farvardin and Vaishampayan, 1987], and even [Max, 1960] for the original Lloyd-Max quantizer design algorithm. Even though source codes can be made robust with respect to channel noise, the effectiveness of lossless entropy coding and the existence of powerful channel codes have made the noiseless source coder with a powerful channel code the most common approach in source-channel coding.

1.1.2 Communication over Noisy Channels

In a communication system we are always given a channel with a certain bandwidth, effectively limiting the channel symbol rate, and a cost constraint providing a certain number of information bits per channel symbol. The resulting capacity, which we define as the number of information bits per second, can be exactly calculated for certain channels. For linear, point-to-point channels with the cost given as an average power constraint and AWGN, the channel capacity is given as [Shannon, 1948],

$$C = W \log_2 \left(1 + \frac{P}{N}\right) \text{bits/s}, \tag{1.3}$$

where W is the bandwidth of the channel, P is the average transmitted power and N is the average noise power over the bandwidth W. This is the maximum rate of information which can be transmitted over a channel of bandwidth W and channel signal-to-noise ratio (CSNR) given as P/N. In order to achieve this, the bitstream must be formatted appropriately for the channel. This is usually done with a channel coder and modulator (Figure 1.1).

The channel coder is responsible for encoding the output of the source coder in such a way that the channel noise has the least impact on the source. In traditional bit-based systems this would be an error-correcting code which corrects erroneously detected channel symbols. Such codes work by adding structured redundancy to the source coder output, creating codewords with as large minimum distance as possible. The larger the distance between each valid codeword, the more erroneous bits can be corrected. Sometimes it is beneficial to include modulation in the channel coder, for instance when using Gray coding for higher-order modulation like quadrature-amplitude modulation (QAM) [Forney and Ungerboeck, 1998]. Other times the coding and modulation are jointly designed as in the case of trellis-coded modulation (TCM) where only constellation points that are close in the modulation space are protected by channel codes, thereby reducing the amount of redundancy [Ungerboeck, 1982].

Shannon proved the channel capacity theorem leading to (1.3) by applying a random coding argument, using long "random-like" codewords. This is exactly what turbo codes [Berrou et al., 1993] and Gallager codes[3] [Chung et al., 2001] mimic, and along with iterative decoding using soft-information they perform extremely well for low CSNR, using binary phase-shift keying (BPSK). The main "drawback" is that in order to achieve high information rates these codes require large channel bandwidths. Furthermore, the long codewords and the iterative decoding increases the coding delay which can be a problem for real-time communication. For higher CSNR values, there is no traditional coding scheme which performs arbitrarily close to the channel capacity. The most common approach is to use TCM, which comes as close as 4.5 dB from the capacity [Ungerboeck, 1982]. [Eleftheriou and Olcer, 2002] presents results for digital subscriber line (DSL) system, with AWGN which are about 3.5 dB in CSNR away from the capacity (with a target bit-error rate (BER) of 10^{-5}). Some attempts have been made using adaptive, coded modulation (ACM) for Rayleigh-fading channels, but still there is a gap to the theoretical bound (for Rayleigh fading channels) given in [Goldsmith and Varaiya, 1997]. For instance [Vishwanath and Goldsmith, 2003] come within 3 dB in CSNR from the Rayleigh fading bound, and [Myhre et al., 2002] are within 5 dB from the bound in (1.3).

[3] Also known as low-density parity check (LDPC) codes

1.1.3 The Separation Theorem

One of the most influential results of Shannon's original paper [Shannon, 1948] is the *separation theorem*. Given a source of rate R and a channel with capacity C, the theorem states that as long as $R \leq C$, the source can be transmitted over the channel with an arbitrarily small probability of error. This elegant result enables separate treatment of source and channel coding, and greatly simplifies system design since each module can be changed without affecting the other[4]. We refer to this concept as a *tandem coder* system. In essence, the source coder reduces the amount of information in the source to less than or equal to the channel capacity, and passes the bits (what we called information bits) to the channel coder. The channel coder tries to create a transparent channel for the information bits by using smart coding techniques. If no transmission errors occurs, the information bits are exactly recovered at the receiver, and the only distortion in the system is due to the information reduction (lossy compression) in the source coder.

In most communication systems today, the source coding and the channel coding are indeed separated. For applications where the assumptions of the separation theorem are valid, this works fine. These transmission scenarios include point-to-point communication where both coders are optimal and of infinite complexity and delay. (Of course, no practical system can have infinite complexity and are therefore strictly suboptimal). However, there are numerous examples where the assumptions leading to the separation theorem does not hold and thus a jointly designed source-channel coding system might be better. For instance, the separation theorem does not hold for channels which are not point-to-point, like network channels, broadcast and multiple access channels [Cover and Thomas, 1991; Gastpar et al., 2003]. In all these cases, jointly designed source and channel coding might outperform the separately optimized coders. Also, since one of the assumptions of the separation theorem is infinite delay and complexity in the coders, and given that infinite complexity is impossible, the resulting source and channel coders are suboptimal. In that case, each coder could be improved by letting the other coder have knowledge about the imperfections. As the restrictions on delay and complexity increase, the benefits of a system with jointly designed source and channel coders might also increase.

[4]However, there is a flip-side which is the fact that it has effectively created two separate camps of researchers; one which only works with source coding and one which only looks at channel coding.

Another question is whether or not it is best to introduce all the distortion in the source coder and suppress all channel noise, like the separation approach does. For sources which accept distortion, like sound and images, there is no particular reason for creating a transparent channel. Only when the system uses entropy coders which are highly sensitive to bit errors, will transparent channels be necessary. The possibility of letting the channel noise be a part of the total distortion will be one of the main topics in this dissertation.

1.2 Joint Source-Channel Coding

Whenever the separation theorem is not valid, there might exist systems with jointly optimized source and channel coders which perform better than separately optimized systems. This is what we call *joint source-channel coding* (JSCC), or combined source-channel coding. This can be done in many different ways, with the degree of co-optimization varying from a simple rate-allocator added to a tandem coder, to a fully combined coder when there is no distinction between the reduction of redundancy in the source coder and the adding of error protection in the channel coder. When transmitting analog sources, one could in the latter case envision a system where the source is put directly onto the channel, omitting explicit channel coding. This is what is considered in this dissertation. The increased robustness of these systems means that they provide good performance for a larger range of channel conditions than tandem coders. Hence, wireless channels with their inherent property of time-varying CSNR will benefit from such robust joint source-channel coding (JSCC) systems. Moreover, these systems can be made memoryless, enabling communication with very low delay. Obviously, these benefits does not come for free. The disadvantages with a JSCC system are the loss of modularity, where the whole system usually has to be re-optimized if either the source or the channel statistics changes, and possibly difficult optimization of the system.

A brief review of some JSCC techniques is found in [Zahir Azami et al., 1996]. This paper covers schemes like unequal error protection (UEP), index assignment (IA) for quantizers, channel-optimized vector quantizer (COVQ), modulation-organized vector quantizer (MOR-VQ), multi-resolution modulation, and rate-distortion source-channel coding. Other overview articles for JSCC over wireless channels are [van Dyck and Miller, 1999; Hagenauer and Stockhammer, 1999]. Some of the mentioned techniques plus some newer developments will now be discussed briefly.

Some of the earliest examples of practical joint source-channel coding are channel optimized quantizers, or quantization for noisy channels. [Kurtenbach and Wintz, 1969] optimized both uniform and non-uniform scalar quantizers for phase-shift keying (PSK) transmission over AWGN channels using an extension of Max's algorithm [Max, 1960]. However, some problems with realizability, optimal codeword assignment, and optimal number of quantizer levels were noted in [Farvardin and Vaishampayan, 1987]. They instead proposed an iterative method for designing the quantizer, where the encoder is determined for a fixed decoder, then the best decoder is found given that encoder, then one iterates until a local minimum for the distortion is found. The design of vector quantizers for noisy channels is more difficult than in the scalar case, and some of the first examples can be found in [Vaishampayan, 1989; Farvardin, 1990] and it is noted in [Farvardin and Vaishampayan, 1991] that encoding complexity of COVQs for bad channels is lower than a VQ with the same codebook size, due to a reduced number of encoding regions. [Fuldseth and Ramstad, 1997; Fuldseth, 1997] extends the work of Vaishampayan by adding a power-constraint, improving the initial conditions of the signal set and optimizing the minimum distance between signal points. MOR-VQ presented in [Skinnemoen, 1994] co-optimizes the vector quantizer and modulation using Kohonen's self-organizing maps. This approach ensures that transitions to neighboring modulation points, caused by channel noise, will only result in transitions to neighboring quantizer cells. This implies that small channel noise values will never induce large decoding errors.

Instead of designing the source coder with respect to the channel conditions as in the previous paragraph, it is also possible to turn the game around and do source-optimized channel coding (SOCC). [Heinen and Vary, 2005] proposes such an system, where instead of trying to minimize the BER, the total signal-to-noise ratio (SNR) is maximized. The benefits of using SOCC is that the source coder remains unchanged by the channel statistics.This means that one can benefit from the vast amount of good source coders designed for the error-free case, and just design the channel code given information about both the source statistics and the channel conditions. In a sense, this provides a form of implicit UEP which ensures that important bits are better protected than less important ones. UEP is perhaps the most widely employed JSCC method, with numerous practical examples like for instance the speech codecs in GSM [Paul et al., 2001] and 3G/UMTS, where it is recognized that different source bits have different significance and thus are protected to different degrees. In essence, UEP is a useful form of JSCC whenever source bits have different significance for the reconstructed source

at the receiver.

Perhaps the most obvious way of implementing joint source-channel coding in order to maximize the spectral efficiency is to implement a joint rate allocation for the source and channel coders. This technique has been called by several names, but here we will refer to it as *rate-distortion source-channel coding* [Bystrom and Modestino, 1998; Ruf and Modestino, 1999; Nosratinia et al., 2003]. The benefit is the possibility to use traditional, effective source coders, and protect the source bits according to the channel conditions. For this, rate-compatible punctured convolutional (RCPC) codes [Hagenauer, 1988] are commonly used to provide a variable degree of error protection given a certain channel state. They can provide UEP by protecting different bits from the source to different degrees. For such systems, transmitter-side knowledge about the channel is essential in order to prevent either over-protection of source bits (which would lead to increased quantization distortion), or under-protection (which would lead to source coder breakdown or at best unfavorable distortion). This inherently limits its usefulness in broadcast scenarios and hard-to-predict fast fading channels.

Whenever the source coder output has residual redundancy, the channel decoder can utilize such redundancy for error protection [Hagenauer, 1995], effectively providing joint source-channel *decoding*. The residual redundancy can be a result of imperfections in the source coder [Sayood and Borkenhagen, 1991], or intentionally introduced with for instance real BCH codes prior to quantization [Gabay et al., 2000] or by using oversampled filterbanks [Motwani and Guillemot, 2004; Labeau et al., 2005]. The benefits of the residual redundancy approach is that only the receiver has to be modified, whereas for the intentionally introduced redundancy, the entire communication chain might have to be redesigned. When there is residual redundancy, turbo-decoding principles are applicable in the decoding processing. Examples are turbo compression [Ruscitto and Biglieri, 1998], LDPC codes for combined compression/error protection [Poulliat et al., 2005] and Wyner-Ziv based techniques for JSCC [Girod et al., 2005; Xu et al., 2005]. The latter paper uses Fountain codes [Byers et al., 1998] which is an interesting technique for erasure protection.

Some research has been done on JSCC for MIMO systems, showing gains for fading channels. In [Song and Liu, 2002; Sun and Xiong, 2006], a set-partitioning in hierarchical trees (SPIHT) coder [Said and Pearlman, 1996] is used in combination with space-time block-coding (STBC) for transmit diversity [Alamouti, 1998] on orthogonal frequency-division multiplex (OFDM) systems [Zou and Wu, 1995], requiring no feedback to the trans-

mitter.

1.2.1 Coding or Direct Source-Channel Mapping

As we mentioned in Section 1.1.3, an important question is: *It is necessary to create a transparent channel when the source we are trying to transmit permits distortion in the reconstruction at the receiver?* After all, a traditional tandem source-channel coding system introduces distortion in the source coder in order to ensure that the rate is below the channel capacity, so it should be possible to let the channel noise contaminate the source instead of a quantizer. One might even question the use of bit representations when transporting information over waveform channels. A nice treatment of these questions can be found in [Gastpar et al., 2003]. Although the text is limited to discrete sources, it provides valuable insight into the source-channel coding problem.

One might argue that both source and channel coding are fields which are well developed, and abandoning the ideas and results from these areas would be a step in the wrong direction. Source coding for the error-free case shows impressive results, both for image coding, cf. instance JPEG 2000 [Taubman and Marcellin, 2002] and video coding, cf. MPEG-4/H.264. As for channel coding, coding for low-CSNR point-to-point channels is a very mature field where bandwidth and complexity are traded in for good performance. If anything, one could wish to make well-performing codes which are shorter (lower delay) and requiring less complex decoders (one might however argue that the latter is less of an issue these days thanks to ever-increasing processing power.) In the high-CSNR region, however, approaching the theoretical bounds is harder and requires careful consideration of both coding and modulation. Still, assuming that perfect channel-state information (CSI) is available, one can come fairly close to the bounds using for instance turbo trellis-coded modulation [Robertson and Wörz, 1998; Vishwanath and Goldsmith, 2003]. Again, it might be a problem that these systems have *high delays* and *complexities*. Hence, simpler systems with low delay might in some cases be desirable, especially for battery operated devices, since complex processing is also power-consuming.

Some attempts have been made to improve the performance in the low-CSNR (bandwidth-limited) regime and in the high-CSNR regime by creating *analog* error-correcting codes. For instance, in [Chen and Wornell, 1998], a chaotic dynamical system is used to provide error-protection of a continuous-

valued source. This system does not, however, provide good performance for higher CSNR, diverging from the theoretical optimum with 10 dB/decade for a bandwidth expansion factor two, and even more for higher bandwidth expansion factors. A similar approach using linear dynamical systems was investigated in [Vaishampayan and Costa, 2003], again with a relative large gap to the optimum (more than 20 dB in simulations). However, it should be noted that the authors prove the existence of codes which operate arbitrarily close to the theoretical bound.

Other problems with traditional channel codes are *robustness* and *adaptivity*. Designers of traditional channel codes strive to create codes with steep BER curves, meaning that above a certain CSNR the BER drops sharply toward zero. Obviously such codes are extremely robust provided that the actual CSNR on the channel is at least as high as the design CSNR for the code. However, below the design CSNR they quickly break down. Moreover, if the actual CSNR increases much above the design CSNR the source is over-protected, wasting bits on unnecessary error-protection. This means that traditional channel codes lacks both *graceful degradation* and *graceful improvement* properties. For time-varying channel conditions and imperfect CSI, this is an important issue. To improve the situation, systems are made *adaptive* with respect to the channel, usually requiring CSI at the transmitter [Goldsmith and Chua, 1998]. A feedback channel is then required, where the receiver can send the actual CSNR value back to the transmitter. Several proposals exist for slowly time-varying, frequency-flat fading channels [Goldsmith and Chua, 1998; Gjendemsjø et al., 2006b] where the channel state is assumed constant for a certain block length so that results from AWGN channels are applicable and a certain BER (or packet error rate (PER)) is guaranteed. In such a case, the practical range of CSNR values is divided into several regions, where each region is allocated a specific channel code and modulation constellation, effectively equipping the system with a set of codes, each providing good performance for their own CSNR region. As the channel state varies, the system switches between the different codes in the set to ensure as high a spectral efficiency as possible while providing the desired BER. If the channel state varies faster, meaning the channel quality changes quicker than the system can change the channel code, the BER cannot be guaranteed, potentially causing full breakdown in the source decoder if the source coder has not been made robust towards such error events. One intriguing concept for more adaptive source-channel coding systems is that of *multi-resolution* (MR) *modulation*, also known as *hierarchical modulation*. This concept is based on superposition coding proposed by [Cover, 1972]. MR modulation was introduced in [Ramchan-

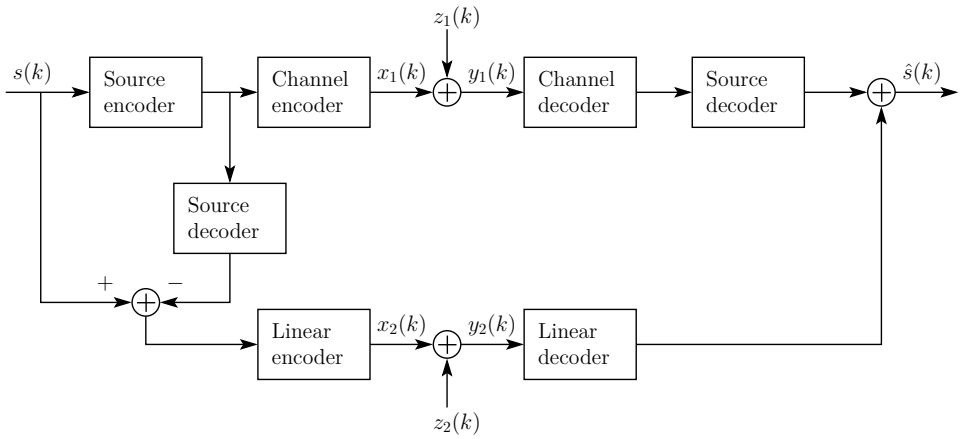

Figure 1.2: A general hybrid digital-analog (HDA) system.

dran et al., 1993; Kozintsev and Ramchandran, 1998; Zheng and Liu, 1999; Hossain et al., 2006] and reduces the need for exact CSI at the transmitter, making it suitable for broadcasting where the receivers have different CSNR (with high probability). The receiver simply decodes as many resolution layers as his CSNR allows, and when the source coder is multi-resolution based, the reconstruction quality improves as the number of decoded resolution layers increases.

To evade issues like the lack of graceful degradation/improvement in traditional channel codes, and the sensitivity of entropy coders explained in Section 1.1.1, it might be of interest to examine some alternatives to the approaches mentioned so far, and see if the mentioned issues could be avoided while not losing too much performance in the optimal point. One elegant approach to provide graceful improvement is that of *hybrid digital-analog* (HDA) systems, where a standard digital source-channel coder is connected in parallel with a linear analog coder which transmits the quantization error (Figure 1.2). Some examples exist in the literature, where a good starting point is [Mittal and Phamdo, 2002]. Here, different variations of the concept are presented, and achievable performance is analyzed. Perhaps the simplest variation of this concept is the scalar quantizer with a linear coder in [Coward and Ramstad, 2000]. This performs remarkably well compared to linear block pulse amplitude modulation (BPAM) [Lee and Petersen, 1976], where the latter is simply a repetition code. Other references include [Skoglund et al., 2002, 2006] where both bandwidth expansion or reduction is possible.

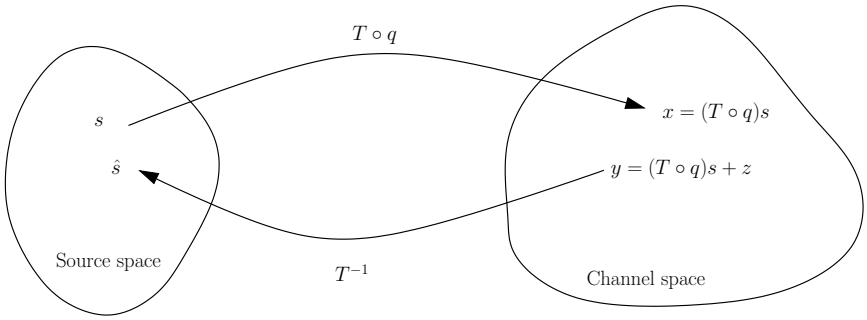

Figure 1.3: A general mapping between the source and channel spaces. The function q performs a projection from the source space of dimension M to a subspace of the source space. This makes it possible to have an invertible function T which performs the mapping from the sub dimension to the channel space of dimension N. The inverse of T brings the channel signal back into the source space and provides an estimate of the transmitted source signal.

1.2.2 Shannon-Kotel'nikov Mappings

Another interesting concept which has been little explored after the "digital revolution" is that of *direct source-channel mappings*. The core of this idea is a geometrical viewpoint to communication where both the source and the channel signals are regarded as points lying in vector spaces, possibly of different dimensions, and the source space is mapped directly onto the channel using a mathematical function. This is illustrated in Figure 1.3, where a source point s is projected directly onto the channel space using a given function or a curve. The channel symbol x is sent, and the received $y = x + z$ is decoded to give an estimate $\hat{s}$ of the original source signal.

This concept was proposed explicitly by [Shannon, 1949] and more implicitly in [Kotel'nikov, 1959][5]. [Berger and Tufts, 1967] demonstrated that for a certain special case, when the source and channel bandwidths are equal and the source is an independent, identically distributed (i.i.d.) Gaussian source and the channel is AWGN, the source-channel mapping is actually a linear multiplication factor. Actually, no other system performs better than this simple system. However, as soon as the source and channel bandwidths are not equal, linear systems are suboptimal. Instead of discarding the excess source bandwidth which does not fit on the channel (or repeating parts of the source bandwidths if it is smaller than the channel bandwidth) which

[5]This is an English translation of Kotel'nikov's dissertation in Russian from 1947.

is done for the linear system, using a non-linear function can significantly improve the performance if chosen carefully. In [Shannon, 1949], two examples were given; one was the so-called Shannon-Cantor coding for bandwidth reduction. This works by taking two numbers $0 \leq a, b \leq 1$ and representing these in decimal notation

$$a = 0.a_1a_2a_3\cdots$$
$$b = 0.b_1b_2b_3\cdots ,$$

and the resulting channel representation is found by interweaving the digits of a and b

$$c = 0.a_1b_1a_2b_2a_3b_3\ .\cdots$$

At the receiver site, the inverse operation is performed. The fidelity of the decoded a and b increases for increasing CSNR as more and more digits of c can be recovered correctly.

The other example can be seen in Figure 1.4, where the curve winding in the plane constitutes the non-linear mapping between the source and channel spaces. For bandwidth expansion, the one-dimensional source S lies along the curve and is mapped onto the two-dimensional channel using the associated tuple X_1 and X_2. This approach increases the noise immunity more compared to simply transmitting S twice and average. Bandwidth compression can be obtained by interchanging the source and channel in Figure 1.4. Then the source tuple (X_1, X_2) is projected down to the closest point on the channel space S. This produces lower distortion than simply discarding either X_1 or X_2 (provided that the mapping function is suited for the given source and channel statistics). This geometric approach to communication which we have termed *Shannon-Kotel'nikov (S-K) mappings*, can exploit the advantages of analog transmission, potentially providing both high spectral efficiency and robustness to channel impairments with very low delay. These properties make them interesting for different wireless communication scenarios. To give some examples we can mention real-time communication systems like voice and video telephony, sensor networks with requirements for low-complexity, feedback channels with low-delay in digital communication systems, and closed-loop control with strict delay constraints.

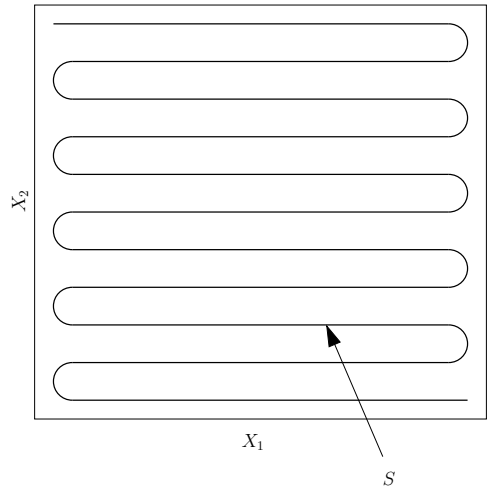

Figure 1.4: Shannon's example of a non-linear source-channel mapping.

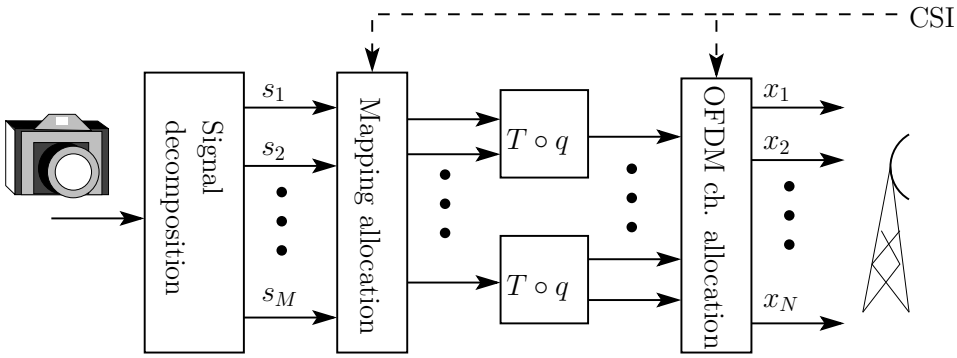

Figure 1.5: The transmitter side of a communication system using S-K mappings in conjunction with signal decomposition and OFDM. The sub-sources from the decomposed source are allocated different mappings and the mapping output is placed on an OFDM sub-carrier.

1.2.3 Optimal Performance Theoretically Attainable (OPTA)

The S-K mappings described in the previous subsection are a form of direct source-to-channel mappings, without any intermediate digital representation. Thus, some form of performance measure not depending on bit representations is needed. Since we are uniquely focused on analog sources which tolerate some distortion, to measure a system's performance we look at the decoded SNR for a given CSNR. This is equivalent to evaluating the operational distortion-rate performance with the source rate equal to the channel capacity. The operational performance would then be compared to what we call the optimal performance, theoretically attainable (OPTA), which is simply the distortion-rate function for the source, evaluated at the rate equal to the channel capacity. Equivalently, we can equate the rate-distortion function and the channel capacity, and express the SNR as a function of the CSNR [Berger and Tufts, 1967].

We limit our discussion of OPTA to the case of memoryless Gaussian sources and AWGN channels. This enables us to express OPTA in analytic form. This will also serve as a lower bound for other memoryless sources and channels. However, both the rate-distortion function and the channel capacity for non-Gaussian sources or channel noise can be estimated using the Arimoto-Blahut algorithm [Arimoto, 1972; Blahut, 1972].

We assume that we are given a source of bandwidth B and a channel of bandwidth W. If we perform sampling of the source at the Nyquist frequency ($2B$ samples per second), we will have a rate of $2BR$ nats per second. Furthermore, if we transmit with the Nyquist rate on the channel ($2W$ symbols per second), we have a capacity of $2WC$ nats per second. To find OPTA, we equate source rate given in (1.1) and channel capacity given in (1.3):

$$2B\frac{1}{2}\log_2\left(\frac{\sigma_s^2}{\sigma_q^2}\right) = 2W\frac{1}{2}\log_2\left(1+\frac{\sigma_x^2}{\sigma_n^2}\right), \tag{1.4}$$

where σ_s^2 is the source variance, σ_q^2 is the distortion, σ_x^2 is the transmit power, and σ_n^2 is the channel noise power. Solving this for the SNR, we obtain

$$\frac{\sigma_s^2}{\sigma_q^2} = \left(1+\frac{\sigma_x^2}{\sigma_n^2}\right)^{W/B}. \tag{1.5}$$

The bandwidth ratio W/B can only be obtained by combining (or distributing) M source samples into (or over) N channel samples, depending on whether $B > W$ or $B < W$. Assuming that N and M are sufficiently large,

this would give us $N/M \approx W/B$ and we thus have

$$\frac{\sigma_s^2}{\sigma_q^2} = \left(1 + \frac{\sigma_x^2}{\sigma_n^2}\right)^{N/M}. \tag{1.6}$$

We say that we have an M:N bandwidth reduction system if $M > N$, and an M:N bandwidth expansion system if $M < N$.

In Figure 1.6 the resulting curves for (1.6) with different bandwidth ratios are seen. Comparing this to the linear solution, BPAM [Lee and Petersen, 1976] in Figure 1.7 where the SNR only increases with 3 dB per channel doubling for expansion, and drops a little less per channel halving, the (non-linear) S-K mappings can improve decoded source fidelity considerably relative to linear solutions. This is true for both bandwidth expansion and reduction except for very low CSNR where the gain is less pronounced.

1.2.4 Scope of the dissertation

Both source coding and communications are vast fields with numerous variations, and a dissertation can only cover a small range of the possible topics. Here, we have chosen to study S-K mappings used for lossy source-channel communication. The motivation behind this is the factors already mentioned: high spectral efficiency and robustness against channel impairments, while providing low delay. We constrain ourselves to the simplest case of linear Gaussian point-to-point channels and continuous-valued memoryless sources. This provides some analytical tractability while at the same time representing some relevant scenarios, such as transmitting decorrelated subband coefficients from for instance an image, over a point-to-point wireless channel with little or no fading. The channel has an average power constraint and the distortion measure for the channel is the MSE. The reason for choosing such a simple channel model is primarily to ease the analysis in order to gain more insight into the potentials and limitations of the concept of mappings. Besides, the AWGN channel model can be used to approximate slowly flat-fading channels and multi-carrier sub-channels. Hence, this model has relevance even for some wireless scenarios. As for the choice of using a memoryless source instead of more general Gauss-Markov sources, we can assume that it is decorrelated by a decomposition operation or similar prior to applying the mapping.

The main purpose of this dissertation is thus to investigate the potential of some specific S-K mappings; in particular, how close to the theoretical

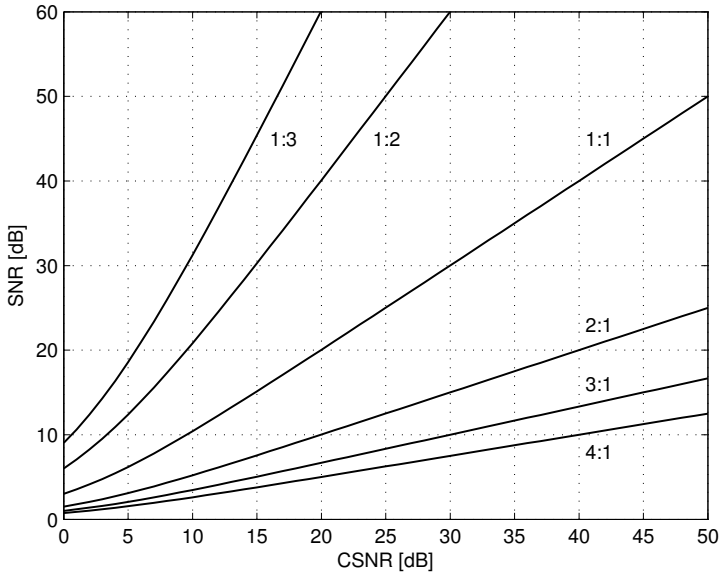

Figure 1.6: OPTA for i.i.d. Gaussian source and AWGN channel, with bandwidth reduction factor indicated on the curves.

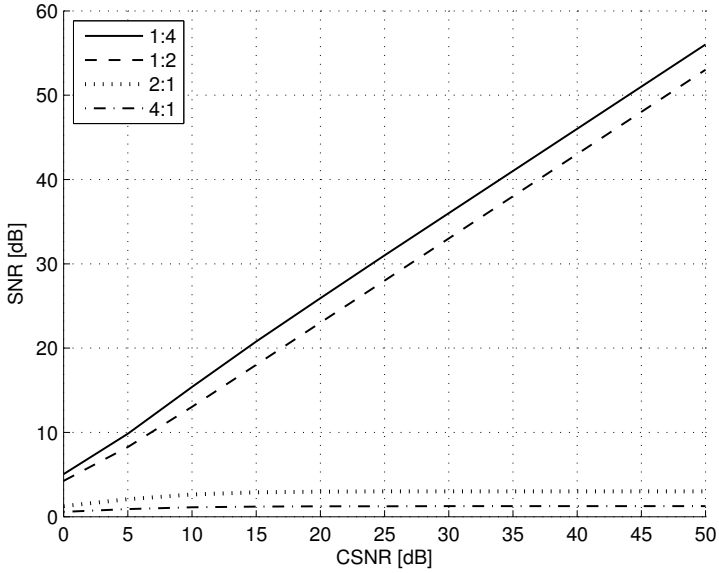

Figure 1.7: The linear solution to direct source-channel coding for memoryless vector channels, BPAM, seen for four different source-to-channel bandwidth ratios.

bounds they can get, and how robust toward incorrect (or unknown) CSI and incorrect source distribution they are. Moreover, since the received signal is continuous in amplitude, an important question is whether they can interface with digital transport networks without too much loss.

1.3 Outline of This Thesis

The main content of the dissertation is contained in three chapters. Even though they can be read independently, reading them in the presented order is recommended since terminology and notation defined in earlier chapters may be omitted in the later chapters.

Ch. 2 - Quantifying the Losses in Source-Channel Coding Systems
A discussion about the different loss factors in source-channel communication is given. This is not restricted to the mapping approach and some of the results therein are applicable to more standard source-channel coding system. This chapter is based on [Hekland et al., 2007] and partially on [Hekland et al., 2005].

Ch. 3 - Shannon-Kotel'nikov Mappings
The concept of S-K mappings for joint source-channel coding is introduced through some examples. The source distribution's influence on the mapping geometry is illustrated and some approaches to deal with different source distributions are proposed. This work is based on [Hekland et al., 2005, Submitted] with the addition of some as of yet unpublished material.

Ch. 4 - Quantization of the Shannon-Kotel'nikov Mappings
Since the S-K mappings are usually continuous-amplitude one has to transcode or digitize the received mappings before further transmission on fully digital transport networks or storage channels. Some simple, yet effective transcoding methods are proposed and the need for jointly optimized mapping and transcoding is discussed. This chapter is based on [Hekland and Ramstad, 2005, 2006a,b] and some unpublished material.

Chapter 2

Quantifying Losses in Source-Channel Coding Systems

"We know that communication must be hampered, and its form largely determined, by the unconscious but inevitable influence of a transmitting mechanism, whether that be of a merely mechanical or of a physiological character."

- Oliver J. Lodge

2.1 Introduction

As stated in the previous chapter, the aim of source-channel coding is to reconstruct a signal at the receiver with as little distortion as possible, given a cost constraint, or the other way around; minimize the cost given a distortion constraint. As there exist theoretical bounds on how well a source can be reconstructed when communicated over a noisy channel, there also exist an optimal point of operation when given the system constraints (e.g. source rate, transmit power). Obviously, we want our systems to operate at the theoretical optimum, but this is rarely the case in practice. The purpose of this chapter is the following: Using information theoretical concepts, we want to describe the factors which lead to sub-optimal performance, especially in the case of direct source-channel mappings. Ideally, this should lead to concrete suggestions on how to improve a specific system. Unfortunately, what is often the case with information theory is that *what should be done*

can be inferred from the calculations, but exactly how to do it in practice is left for the engineers.

Figure 1.7 shows that the linear solution for direct source-channel mapping presented in [Lee and Petersen, 1976] performs relatively far away from OPTA (Figure 1.6) whenever the source and channel bandwidths are different. In order to approach OPTA in these situations, non-linear systems are necessary.

In an effort to improve the performance for the case of unequal source and channel bandwidths, we have proposed some schemes for joint source-channel coding which we have termed *S-K mappings* [Ramstad, 2002; Hekland et al., 2005; Floor and Ramstad, 2006b]. This concept will be discussed more in detail in the next chapter. These use non-linear maps to project source samples directly into the channel space, and can achieve either bandwidth reduction (compression) or bandwidth expansion (error control) with very low delay. However, none of them achieve actual optimality (in the OPTA sense). What is apparent from past work, however, is that systems which do compression come much closer to the theoretical bounds than when performing expansion. Intrigued by this, we try to identify more in detail which loss factors come into play when designing a source-channel coding system, in order to obtain some hints on what to do to reduce the system's gap to the theoretical bound. The loss factors, which together constitutes the gap, will be described in terms of information theoretic expressions as far as possible. Thus, they are not specific to S-K mappings or other direct source-channel mappings. Indeed, traditional schemes with separable quantizers and channel coders can also be analyzed, although our main emphasis in the example will be on JSCC systems.

A good discussion about lossy source-channel coding system can be found in [Gastpar et al., 2003]. This paper covers the information theoretical aspects of optimal source-channel coding, and, through Theorem 6 therein, provides a criterion which can be used to check whether or not a system performs optimally. However, no clues are given on how to determine the actual loss whenever a system is not optimal. As most systems (especially those with delay or complexity constraints) do not achieve optimality, it is interesting to quantify these loss factors. This would enable us to know how much we can hope to improve a system, which parts of the system are responsible for the biggest losses, and thus where it pays off the most to make improvements.

This chapter is organized as follows. First we identify the different loss factors; mismatched channel symbol distribution, under-utilization of the chan-

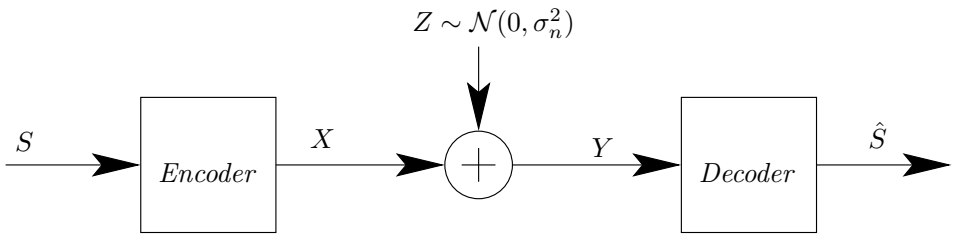

Figure 2.1: A generic communication system with an AWGN channel.

nel, inter-channel correlation, mismatched source distribution, source coding redundancy, suboptimal receiver structures, and decoding errors. Then we exemplify some of these with a 1:2 bandwidth-expanding JSCC system, demonstrating that simulation results match the analytical predictions of the total loss.

2.2 Loss Factors

Based to some extent on intuition, we will initially make some conjectures about what causes suboptimal performance in joint source-channel coding systems under a mse distortion measure. The reason for using the mse distortion measure is its widespread use, and mathematical tractability. Whether the mse is a suitable distortion measure for a given application is a different matter, and is outside the scope of this dissertation. However, one should keep in mind that the mse is not the best distortion measure to use for all applications, as it does not necessarily reflect the receivers' perception of quality.

The conceptual communication chain we assume is seen in Figure 2.1 where $S$is the source symbol, X, is the transmitted channel symbol, $Z$is the channel noise, $Y$is the received channel symbol, and $\hat{S}$ is the reconstructed source symbol. The encoder and decoder might be any joint source-channel coding system, or in fact even a traditional separate source and channel coding system. Moreover, the losses are stated in bits, but this does not limit us to looking at bit-based systems. In short, we want to determine the loss due to the inequalities in the proof of [Gastpar et al., 2003, Lemma 2], for

convenience repeated here:

$$R(D) = \min_{f_{\hat{s}|s}:\mathsf{E}\left[d(S,\hat{S})\leq D\right]} I(S;\hat{S}) \overset{a)}{\leq} I(S;\hat{S}) \overset{b)}{\leq} I(X;Y) \overset{c)}{\leq} \max_{f_x:\mathsf{E}[\sigma_x^2]\leq P} I(X;Y) = C(P), \tag{2.1}$$

where E denotes the expectation operator with respect to the source distribution, $d(\cdot,\cdot)$ is the distortion measure, $I(\cdot;\cdot)$ denotes mutual information. A system performs optimally whenever the distortion-rate function is attained with the rate equal to the channel capacity, i.e. when all the relations in (2.1) are equality signs[1]. Equality in a) is achieved for the rate-distortion bound achieving error distribution (given the distortion measure), equality in b) is achieved for an information lossless encoder-decoder pair (when going from the source space to the channel space, and back), and finally equality in c) is achieved for the capacity-achieving channel symbol distribution (given the capacity-cost function).

It is worth noting that for an optimal pair $R(D) = C(P)$, one cannot lower D (or P) without changing $R(D)$ (or $C(P)$) accordingly. This means that if the source rate is higher than the channel capacity, the information content must be reduced (i.e. D must be increased such that the equality is satisfied) before transmission (D will be increased by the channel noise in the case of analog transmission).

2.2.1 Loss from Mismatched Channel Symbol Distributions

We now show how much we lose by using non-Gaussian distributed channel symbols on an AWGN channel, causing an inequality in c) of (2.1). This result was shown for a single channel case in [Hekland et al., 2005], but is shown here for the parallel channel case.

We know from information theory that Gaussian distributed channel symbols maximize the mutual information between a transmitted and received sequence over any memoryless channel with an average power constraint [Cover and Thomas, 1991]. For the specific example of a N-dimensional AWGN channel with an average power constraint, the channel capacity is

[1] This is a simplification of the discussion in the original paper, and the interested reader is urged to read the original for a more rigorous presentation.

defined as [Cover and Thomas, 1991]

$$C = \max_{f(x_1,\ldots,x_N):\sum \sigma_{x_i}^2 \leq P} I(X_1,\ldots,X_N;Y_1,\ldots,Y_N). \tag{2.2}$$

Whenever we have a marginal channel symbol distribution $f(x_i) \nsim \mathcal{N}$ of the same power as in (2.2), the achievable transmission rate will be less than the capacity of this specific channel, i.e.

$$C' = I(X_1,\ldots,X_N;Y_1,\ldots,Y_N)\big|_{f(x_i)\nsim\mathcal{N}} = C - \sum_{i=1}^{N} \rho(f(x_i)),$$

where $\rho(f)$ denotes the associated capacity loss for the distribution f. Expanding the mutual information in (2.2), and assuming that the signal and noise are uncorrelated, one can show that [Cover and Thomas, 1991]

$$I(X_1,\ldots,X_N;Y_1,\ldots,Y_N) \leq \sum_{i=1}^{N} \{h(Y_i) - h(Z_i)\}, \tag{2.3}$$

where Z_i is the channel noise in channel i and $h(\cdot)$ denotes the differential entropy. Assuming that the covariance matrix of $(X_1,\ldots,X_N)$ is diagonal so that there is no correlation between the channels, the only loss we would experience is when the X_i's are not Gaussian distributed. To determine this loss, we expand the first term on the right hand side of (2.3). Since we always integrate over the same variable y, we write f_i instead of $f_{Y_i}(y)$ to increase the readability, although this in some sense is abuse of notation. Expanding the differential entropy, we obtain

$$\begin{aligned} h(Y_i) &= -\int f_i \log f_i = -\int f_i \log\left(f_i \frac{f_i^*}{f_i^*}\right) \\ &= -\int f_i \log f_i^* - \int f_i \log\left(\frac{f_i}{f_i^*}\right) \\ &\overset{(a)}{=} -\int f_i^* \log f_i^* - \int f_i \log\left(\frac{f_i}{f_i^*}\right) \qquad (2.4) \\ &= h^*(Y) - I(f_i \| f_i^*), \qquad (2.5) \end{aligned}$$

where $I(\cdot\|\cdot)$ is the relative entropy (also known as I-divergence, Kullback-Leibler distance or cross-entropy) between two distributions[2], and (a) is valid

[2]We are using the less common form $I(\cdot\|\cdot)$ instead of $D(\cdot\|\cdot)$ in order to avoid confusion with the distortion D used later.

when f_i^* is the Gaussian distribution and f_i is any continuous distribution with zero mean and same variance as f_i^*. To see why this is true, consider

$$\begin{aligned} -\int f \ln f^* &= -\int f \ln\left(\frac{1}{\sqrt{2\pi}\sigma_G} \mathrm{e}^{\frac{-y^2}{2\sigma_G^2}}\right) \\ &= \frac{1}{2\sigma_G^2}\int y^2 f + \ln\left(\sqrt{2\pi}\sigma_G\right)\int f \\ &= \frac{1}{2\sigma_G^2}\int y^2 f^* + \ln\left(\sqrt{2\pi}\sigma_G\right)\int f^* \\ &= -\int f^* \ln f^*, \end{aligned} \tag{2.6}$$

which is valid for any well-behaved distribution f with zero mean. Inserting (2.5) and (2.3) into the definition of the channel capacity in (2.2) we obtain the maximum achievable transmission rate for output distributions f_i as

$$\begin{aligned} C' &= \sum_{i=1}^{N} h^*(Y_i) - h(Z_i) - I(f_i \| f_i^*) \\ &= \sum_{i=1}^{N} \{C_i - I(f_i \| f_i^*)\}, \end{aligned} \tag{2.7}$$

which is the sum of the channel capacity of each channel minus the relative entropy between the mismatched distribution of each channel and the Gaussian. I.e., $\rho(f_i) = I(f_i \| f_i^*)$.

2.2.2 Loss From Incorrectly Decoded Channel Symbols

Whenever the channel impairments induce incorrect decisions in the decoder, we have an information loss responsible for an increasing inequality in relation *b*) of (2.1). What this loss translates to, depends strongly on the actual system. For a communication system using entropy coding, bit errors can cause catastrophic breakdown ruining the entire transmission. For strong channel codes with steep BER curves, the error rate increases rapidly below a certain CSNR threshold. In both cases, this effect is often referred to as the *threshold effect*, since the performance above a certain CSNR threshold is good, but rapidly deteriorates below the threshold. Direct modulation of a scalar quantizer, however, only causes increased distortion when incorrectly decoding to neighboring intervals. This might provide increased robustness

ala fixed-length source codes. The idea of direct modulation will be explored more in detail in the next chapter.

Bandwidth-expanding systems cannot be designed to avoid the threshold effect, since it is impossible to perform a mapping from a higher to a lower dimensional space in a continuous manner [Shannon, 1949]. This means that small channel noise values might induce large source distortion. For bandwidth-reduction, on the other hand, the threshold effect is avoided as the decoder *can* perform a continuous mapping from the channel space to the higher dimensional source space.

2.2.3 Loss From Information Rate Less Than the Operational Channel Capacity

Obviously, we cannot attain the theoretical optimum if the actual information rate of the symbols transmitted over the channel is strictly below the channel capacity, i.e. if relation b) in (2.1) is a strict inequality. This is for instance the case for channel codes with insufficient puncturing using more parity bits than necessary to achieve a certain BER [Hagenauer, 1988]. Another case leading to a loss is when there is a strict inequality in relation c) in (2.1), caused by using a too small modulation constellation for the current channel condition[3]. Both these loss factors corresponds to [Gastpar et al., 2003, Eq.(8)], where $I(X;Y)-I(S;\hat{S})$ is the loss induced by too many parity bits, leaving too few bits for the source encoder (relation b) in (2.1)). $C - I(X;Y)$ would be the resulting loss for using a too small modulation constellation (relation c) in (2.1)).

When communicating a continuous source over an AWGN channel, the Gaussian channel noise contaminating the source ensures that the first inequality sign in (2.1) is satisfied with equality. Furthermore, by plugging the source directly onto the channel and using the optimal (linear) Wiener filter as the receiver, the second inequality sign is satisfied with equality too. This means that we have $R = C'$, where C' is defined in (2.7). The only loss will be caused by the non-Gaussian channel symbol distribution as described in Section 2.2.1.

For a bandwidth expanding system (which is prone to the threshold effect), operating at a rate equal to the channel capacity might not be possible

[3] In the previous section, relation c) was caused by an incorrect distribution f_x. Here, the loss is caused by not producing an input sequence X with enough information, by using a too small modulation constellation.

without inducing too much distortion. Hence, some channels must be underutilized in order to reduce the probability of the threshold effect.

2.2.4 Loss from Correlated Channels

In a system with parallel communication channels, the information transmitted over the different channels should be mutually uncorrelated in order to maximize the total achievable capacity. This is especially an issue in bandwidth-expanding systems, where a source must be "stretched out" to fill the entire channel bandwidth without simply repeating parts of it.

For independent noise Z, a reasonable assumption in many communication systems, we have the following inequality for the mutual information:

$$\begin{aligned} &I(X_1, X_2, \ldots, X_N; Y_1, Y_2, \ldots, Y_N) \\ &\quad = h(Y_1, Y_2, \ldots, Y_N) - \sum_i h(Z_i) \\ &\quad \leq \sum_i \{h(Y_i) - h(Z_i)\}, \end{aligned} \tag{2.8}$$

where equality is only achieved by independent Y's. Expanding the differential entropy of the Y's we have [Cover and Thomas, 1991]

$$h(Y_1, Y_2, \ldots, Y_N) = \sum_{i=1}^{N} h(Y_i)|Y_1, Y_2, \ldots, Y_{i-1}), \tag{2.9}$$

and consequently we have

$$h(Y_1, Y_2, \ldots, Y_N) \leq \sum h(Y_i), \tag{2.10}$$

since conditioning reduces entropy. The resulting rate loss would be the difference

$$\sum h(Y_i) - \sum h(Y_j)|Y_1, Y_2, \ldots, Y_{j-1}).$$

For examples of systems suffering from correlated channels, one could think of spatial correlation in MIMO systems, or OFDM systems with sub-channel gains correlated in frequency. However, we will not discuss MIMO or OFDM here, and we refer the reader to [Goldsmith et al., 2003; Zou and Wu, 1995].

We will also classify the case of encoder-induced correlation into this section. By this we mean inter-channel correlation introduced by the encoder,

as opposed to e.g. the spatial correlation leading to reduced rank MIMO channels. The worst-case example would be BPAM [Lee and Petersen, 1976] for bandwidth expansion, where replicas of the source is transmitted in parallel ("repetition code"). Provided that the total power is doubled when the number of channels is doubled, the SNR is only increased by 3 dB per doubling of channels. The slopes of the SNR vs. CSNR curve in Figure 1.7 remain constant for all expansion factors, instead of increasing for higher expansion factors which is the case for OPTA. This is due to the fact that the channels carry fully correlated information, thus the available bandwidth is poorly utilized and the only gain comes from the increased channel power.

Figure 2.2 shows a specific 1:2 bandwidth expanding system (to be described more in detail in Section 2.4.2). The line segments in the plane constitute the source space, and the plane constitutes the channel space. BPAM with the same expansion factor would be a represented by a diagonal line in the plane. This means that the encoder introduces full correlation between the two channels and the channel space (the plane) is poorly utilized. The system shown in the figure has much less correlation and fills the channel space better.

2.2.5 Loss from Source Coder Imperfections

In order for a communication system to perform optimally, it also has to operate at the R-D bound (relation a) in (2.1)), and the source coder rate must thus be equal to the channel capacity [Gastpar et al., 2003]. The loss experienced from a non-optimal source coder is given as the excess rate required to achieve the same distortion as the R-D function evaluated at the channel capacity.

When performing source coding, the rate must be reduced to the desired level in a controlled manner. To do so, any redundancy should first be removed from the source by applying for instance a frequency decomposition. Then any non-perceptible information (irrelevance) can be removed using for instance quantizers (or more generally, lossy source coding). For further rate reductions, perceptible distortion will be introduced. After quantization, the resulting indices often have a non-uniform probability distribution and entropy coding can be used to provide shorter average codeword length. Omitting the entropy coding will give a rate increase, with the amount of increase depending on the probability density function (pdf) [Jayant and Noll, 1984] of the indices, and on the remaining source redundancy not

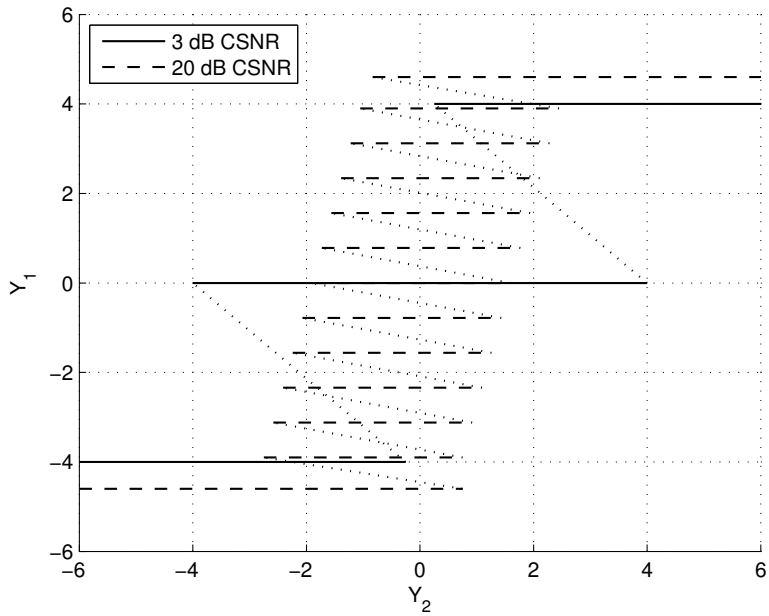

Figure 2.2: HSQLC Quantizer for two different channel states. The source space is aligned along the lines in the plane, and the resulting channel symbols are given along the axes. $a(k)$ is the output of a scalar quantizer, and $b(k)$ is the corresponding quantization error.

removed in the decomposition.

Entropy coding alone, however, cannot achieve the R-D bound. For instance, a scalar quantizer can at best be 0.255 bits away from the R-D bound [Jayant and Noll, 1984], regardless of the source pdf. This is due to the fact that the quantization noise cannot be shaped properly (to be a Gaussian) when we have only one dimension in the quantizer. vector quantization (VQ) can, on the other hand, reach the R-D bound if given infinite dimensions. This is referred to as the *space-filling advantage* in [Lookabaugh and Gray, 1989]. We will thus refer to the gap relative to an ideal VQ as the *space-filling loss*, and it applies to any source coder failing to produce Gaussian reconstruction-error noise.

Usually, the space filling loss is described in terms of high-resolution theory [Lookabaugh and Gray, 1989]. However, we present an alternative way of looking at the space filling loss by examining the reconstruction (or quantization) noise which appears in the derivation of the R-D function for a Gaussian source. Given the squared error distortion measure, Gaussian-distributed quantization noise is needed in order to reach the rate-distortion

bound [Cover and Thomas, 1991], regardless of the input source distribution. This is because for an allowed distortion D, a Gaussian-distributed reconstruction error will minimize the mutual information between the original and reconstructed sequences. We now determine the loss of a non-Gaussian reconstruction noise. The R-D function is defined as [Cover and Thomas, 1991]

$$R(D) = \min_{g(\hat{s}^M|s^M):\mathsf{E}\left[d\left(S^M,\hat{S}^M\right)\right]\leq D} I(S^M;\hat{S}^M), \tag{2.11}$$

where $d(\cdot,\cdot)$ is the chosen distortion metric, i.e. the mse in our case.

Assuming that the coder produces reconstruction noise which is not Gaussian distributed, we have an operational R-D function, $R'(D)$, which is higher than the R-D bound $R(D)$ given in (2.11):

$$R'(D) = I(S^M;\hat{S}^M)\big|_{g(\hat{s}^M|s^M)\nsim\mathcal{N}} = R(D) + \tau(g), \tag{2.12}$$

where $\tau(g)$ is the penalty term due to the non-Gaussian reconstruction noise distributions. Looking at the mutual information, we can expand it as follows:

$$\begin{aligned} I(S^M;\hat{S}^M) &= \sum_{i=1}^{M} h(S_i) - \sum_{i=1}^{M} h(S_i|S^{i-1},\hat{S}^M) \\ &\geq \sum_{i=1}^{M} h(S_i) - \sum_{i=1}^{M} h(S_i|\hat{S}_i) \qquad (2.13) \\ &= \sum_{i=1}^{M} h(S_i) - \sum_{i=1}^{M} h(S_i-\hat{S}_i|\hat{S}_i) \\ &\geq \sum_{i=1}^{M} h(S_i) - \sum_{i=1}^{M} h(S_i-\hat{S}_i), \qquad (2.14) \end{aligned}$$

where (2.13) and (2.14) are due to the fact that conditioning reduces entropy. Using the definition of the differential entropy we can furthermore expand the last addend of (2.14) as follows (again slightly abusing notation):

$$\begin{aligned} h(S_i-\hat{S}_i) &= -\int g_i \log g_i = -\int g_i \log\left(g_i\frac{g_i^*}{g_i^*}\right) \\ &= -\int g_i \log g_i^* - \int g_i \log\left(\frac{g_i}{g_i^*}\right) \\ &= -\int g_i^* \log g_i^* - \int g_i \log\left(\frac{g_i}{g_i^*}\right) \qquad (2.15) \\ &= h^*(S_i-\hat{S}_i) - I(g_i\|g_i^*), \qquad (2.16) \end{aligned}$$

where (2.15) is valid when g_i^* is the Gaussian distribution and g_i is any continuous distribution with zero mean[4] and the same variance as g_i^*, due to the same arguments as in (2.6). Inserting (2.16) into (2.14) we obtain

$$I(S^M;\hat{S}^M) \geq \sum_{i=1}^{M} \left\{ h(S_i) - h^*(S_i - \hat{S}_i) + I(g_i \| g_i^*) \right\}, \tag{2.17}$$

where the two first addends on the right hand side correspond to $R(D)$ in (2.12) and the last term corresponds to the penalty $\tau(g)$ in (2.12). This gives us the operational R-D function

$$R'(D) = \sum_{i=1}^{M} \left\{ R(D_i) + I(g_i \| g_i^*) \right\}, \tag{2.18}$$

i.e. the loss factor in (2.12) is $\tau(g) = \sum_{i=1}^{M} I(g_i \| g_i^*)$. This result is similar to the discrepancy shown in Section 2.2.1, in the sense that the penalty for having a non-optimal distribution is the "distance" between the actual and the optimal distribution[5]. To the authors' knowledge, this result has not been previously reported in the literature.

2.2.6 Loss From Mismatched Source Distribution

When designing a source coder, knowing the source's input pdf is important to ensure optimal performance. However, exact knowledge about the source is usually not available and it is usually estimated from data, resulting in mismatch in the source coder. We will call the resulting loss *source mismatch loss*.

Some work has been done on this for high-rate entropy-constrained vector quantizers [Gray and Linder, 2003], where they show that the loss incurred by designing the quantizer for a pdf f and applying a pdf g is equal to the relative entropy between the two, i.e. $I(f\|g)$. The restrictions on this result is that f/g must be bounded, which in many cases is not true.

Results valid for arbitrary quantizers are not known, however, and the source mismatch loss must be determined for each specific system.

[4] This is not a restricting assumption, since the mean can always be subtracted before encoding the source.

[5] The relative entropy, also known as the Kullback-Leibler distance, is not a true distance metric, but still it provides a measure of the rate difference of two distributions.

2.2.7 Loss Due to Suboptimal Receiver Structures

The design of the receiver is crucial for the system performance, since it is responsible for extracting the transmitted signal from the contaminating channel noise, and deal with other impairments such as fading and interference. Moreover, depending on whether the source symbols are uniformly distributed or not, the optimal receiver would be either be a maximum likelihood (ML) or a maximum a-posteriori probability (MAP) receiver [Barry et al., 2004]. The former is basically a minimum-distance detector for the AWGN channel, but in some cases, even an ML detector might become prohibitively complex, and more simpler receiver structures are employed. Any sub-optimality in the receiver of course results in degraded performance. Often there is a certain correlation between channels, either because of non-optimal source coding or deliberately introduced to aid decoding. However, if the decoder is not decoding the channels jointly, but rather independently, performance degradations will occur [Laneman et al., 2005].

It is, however, rather difficult to quantify this degradation in general terms, since it is very system dependent. Usually, this is a trade-off between the complexity of the receiver and performance. This will usually be a design (or cost) question where the designer must choose where on the cost-performance curve to put his/her system.

2.3 What insight have been gained?

Although we have not provided any practical method to construct good source-channel coding systems, some design pointers have been given in the preceding sections. Apart from more "obvious" factors, like using optimal receivers and minimizing the probability of the threshold effect, we see that having the correct distributions in both the channel symbols and the error sequence matters. Let us see what the effects of these are for a system with source bandwidth B and channel dimension W.

According to Section 2.2.1, the operational rate-distortion function is

$$R'(D) = R^*(D) + I(g\|g^*), \tag{2.19}$$

where $I(g\|g^*)$ is a rate increase due to non-Gaussian error sequence distribution g, whereas the optimal distribution is Gaussian g^*.

According to Section 2.2.5, the operational channel capacity is

$$C' = C^* - I(f\|f^*), \tag{2.20}$$

where $I(f\|f^*)$ is a capacity decrease due to non-Gaussian channel symbol distribution f, whereas the optimal distribution is Gaussian f^*.

If we assume sampling the source which has a bandwidth B at the Nyquist rate, the source produces $2B$ samples per second, and thus $2BR$ bits per second. Similar for the channel when assuming Nyquist signaling, the channel capacity is $2WC$ bits per second.

Now, using the operational terms (2.19) and (2.20) in place of R and C, and setting the source rate equal to the operational capacity, we have

$$\begin{aligned} 2BR' &= 2WC' \\ 2B(R^* + I(g\|g^*)) &= 2W(C^* - I(f\|f^*)) \\ R^* &= \frac{W}{B}\Big(C^* - I(f\|f^*)\Big) - I(g\|g^*), \end{aligned} \tag{2.21}$$

where R^* and C^* are the R-D function for a Gaussian source (1.1) and AWGN capacity (1.3), respectively [Cover and Thomas, 1991]. Inserting those into (2.21), we have

$$\begin{aligned} \frac{1}{2}\log_2(\mathrm{SNR}) =& \frac{W}{B}\left(\frac{1}{2}\log_2(1+\gamma) - I(f\|f^*)\right) - I(g\|g^*) \\ \mathrm{SNR} =& 2^{\frac{W}{B}(\log_2(1+\gamma) - 2I(f\|f^*)) - 2I(g\|g^*)} \\ \mathrm{SNR}_{dB} =& 10\Bigg(\frac{W}{B}\left\{\log_2(1+\gamma) - 2I(f\|f^*)\right\} \\ & - 2I(g\|g^*)\Bigg)\log_{10}(2), \end{aligned} \tag{2.22}$$

where we introduced $\gamma = P/N$ for the CSNR. The expression for OPTA is

$$\mathrm{OPTA}_{dB} = 10\log_{10}(1+\gamma)^{W/B} = \frac{10W}{B}\log_{10}(1+\gamma). \tag{2.23}$$

Hence, the gap to OPTA is

$$\mathrm{SNR}_{gap,dB} = \left[\frac{20W}{B}I(f\|f^*) + 20I(g\|g^*)\right]\log_{10}(2). \tag{2.24}$$

This indicates that for a bandwidth reducing system ($B > W$), the incorrect channel symbol distribution has reduced impact for decreasing W/B,

whereas for the bandwidth expanding system, the loss is proportional to the bandwidth ratio. As for the incorrect error sequence distribution, it appears to be independent of the bandwidth ratio.

One thing which has not been explored is the dependency between the different loss factors. Obviously, some of them are dependent and must be analyzed jointly. For instance, the threshold effect and information rate on the channel are closely linked. This, however, is now covered in this dissertation and is subject to future research.

2.4 Examples

We now present some examples of joint source-channel coding systems, where the relevant loss factors described in Section 2.2 are shown to be able to completely explain the discrepancy between the systems' performance and the theoretical optimum. Even though these systems do not operate with bit representations, the losses are stated in bits and converted to decibels with the common 6.02 dB per bit rule [Jayant and Noll, 1984]. This is valid for the case of scalar, memoryless sources with a squared-error distortion measure.

2.4.1 1:1 Uncoded Laplacian Source over an AWGN Channel

When transmitting a Laplacian source over an AWGN channel of the same bandwidth by using direct pulse-amplitude modulation (PAM), the channel signal distribution would be Laplacian, whereas a Gaussian distribution is required for optimality. According to Section 2.2.1, this loss should be equal to the relative entropy between the actual Laplacian distribution and the

optimal Gaussian one. We find the loss to be [Hekland et al., 2005]

$$\begin{aligned} D\left(f\|f^*\right) &= \int f \ln \frac{f}{f^*} = -h(f) - \int f \ln f^* \\ &= -h(f) + \int f \ln\left(\sqrt{2\pi}\sigma_G\right) + \int f \frac{y^2}{2\sigma_G^2} \\ &= -h(f) + \ln\left(\sqrt{2\pi}\sigma_G\right) + \frac{1}{2\sigma_G^2}\int y^2 f \\ &\overset{(b)}{=} -\ln 2\lambda - 1 + \ln\left(\sqrt{2\pi}\sigma_G\right) + 1/2 \\ &= \ln\left(\frac{\sqrt{2\pi}\sigma_G}{2\lambda\sqrt{\mathrm{e}}}\right). \end{aligned} \tag{2.25}$$

In (b), $h(f)$ is given from [Cover and Thomas, 1991], and to have equal power (or variance, since the mean, $\mu = 0$) in the two distributions, we set $\int y^2 f = \sigma_L^2 = 2\lambda^2 = \sigma_G^2 \Rightarrow \sigma_G = \sqrt{2}\lambda$. Inserting this into (2.25) we finally obtain

$$D\left(f\|f^*\right) = \ln\left(\sqrt{\frac{\pi}{\mathrm{e}}}\right) = \frac{1}{2}\ln\left(\frac{\pi}{e}\right) \approx 0.072 \text{ nats} = 0.104 \text{ bits}. \tag{2.26}$$

When applying the 6.02 dB per bit rule this loss is 0.63 dB. This is exactly the loss found if using the Arimoto-Blahut algorithm to compute the R-D bound for a Laplacian source (Figure 2.3). In this case none of the other mentioned sources of loss come into play.

2.4.2 1:2 HSQLC, Gaussian Source and AWGN Channel

The hybrid scalar quantizer, linear coder [Coward and Ramstad, 2000; Coward, 2001] is a bandwidth-expanding joint source-channel coding scheme with two channels, where the total channel bandwidth is twice that of the source bandwidth. The bandwidth expansion is a way of performing error control, which allows higher SNR of the reconstructed source than for equal source and channel bandwidths. The schematic diagram of the HSQLC system is shown in Figure 2.4, and an example of the corresponding quantizer levels is seen in Figure 2.2. The input signal $x(k)$ is first quantized by a uniform scalar quantizer, and the quantized signal $a(k)$ is allocated a certain amount of power and transmitted over the channel as a multilevel PAM-symbol. The quantization error $b(k)$ is allocated the rest of the power and transmitted with direct PAM over the other channel. For high CSNR

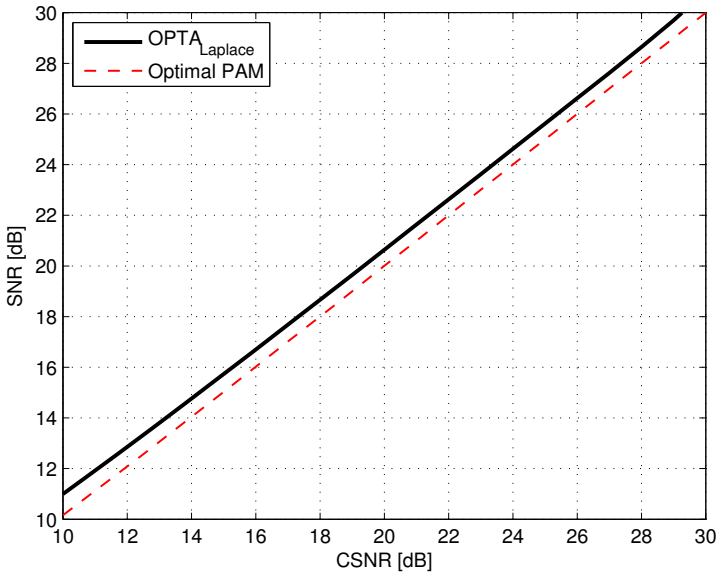

FIGURE 2.3: Laplacian source and AWGN channel of equal bandwidths. OPTA is estimated using the Arimoto-Blahut algorithm.

($>$ 30 dB) and a Gaussian source the optimization described in [Coward, 2001] divides the available transmit power equally between the two channels. We assume that the two channels have equal characteristics. The receivers are not optimal, as the two channels are decoded independently. However, simulations confirm that the difference in performance between the optimal and simplified receivers is negligible at high CSNR [Coward and Ramstad, 2000; Coward, 2001]. Theoretically, as previously mentioned, the best we can achieve is OPTA which is found by equating the rate-distortion function with the channel capacity (Section 1.2.3). For a bandwidth expansion factor of two, for a Gaussian source and an AWGN channel, we have

$$2B_s \cdot \frac{1}{2}\log_2(\text{SNR}) = 2B_c \cdot \frac{1}{2}\log_2(1+\text{CSNR})$$
$$\text{SNR} = (1+\text{CSNR})^{\frac{B_c}{B_s}} = (1+\text{CSNR})^2. \qquad (2.27)$$

In dB, this becomes

$$\text{SNR}_{dB} = 20\log_{10}(1+\text{CSNR}) \approx 2 \cdot 10\log_{10}\text{CSNR} = 2\text{CSNR}_{dB}. \qquad (2.28)$$

The HSQLC system's performance is, however, far away from this bound. At around 30 dB CSNR when the two channels are allocated the same amount of power by the optimization algorithm, the system performance is a little

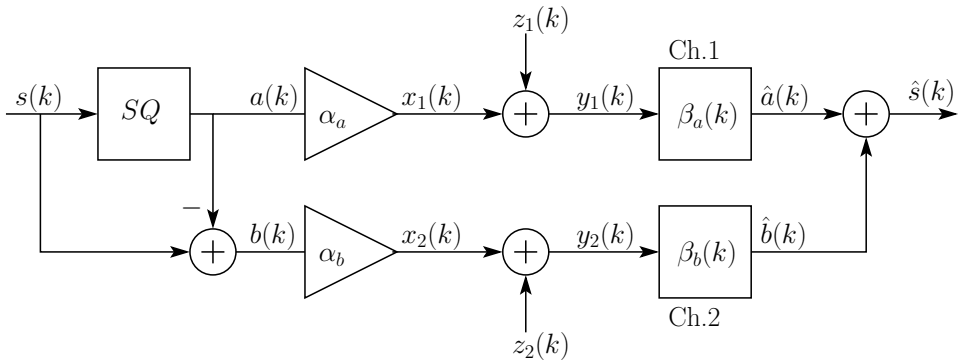

Figure 2.4: The HSQLC system

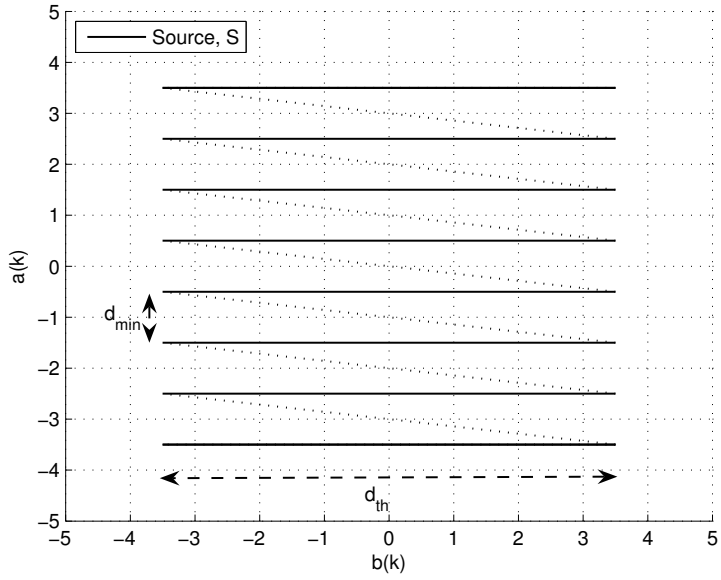

Figure 2.5: Quantizer levels of the simplified HSQLC system.

less than 8 dB away from OPTA. To make the calculation of the performance loss factors tractable, we will consider a simplified system where the distance to OPTA is 8.5 dB at 30 dB CSNR. The quantizer levels of this system is seen in Figure 2.5. We will now scrutinize this simplified system in order to try to identify the main causes of this big loss. We restrict ourselves to the high CSNR region, since as mentioned in this region the optimization algorithm distributes the power equally on the two channels (hence we have the same CSNR on the two channels, i.e. we assume equal noise power on the two channels). Moreover, in this region, the quantizer has sufficiently

high rate allowing us to assume that the quantizer output and quantization error are uncorrelated (given that the usual required conditions for this approximation to be valid are fulfilled). Also, in the high CSNR case, the effect of the non-ideal receivers is more or less negligible.

As previously mentioned, to facilitate the analysis we abandon the optimized quantizer characteristics (Figure 2.2), and instead stack the quantizer levels directly above each other (Figure 2.5). This degrades the performance slightly since incorrectly decoded symbols $\hat{a}$ will induce higher distortion, and furthermore the error-signal distribution will be uniform instead of something closer to a Gaussian. For CSNR above 30 dB, the original system has little shift, but still the difference between the original and the simplified system is approximately 0.5 dB. Below 30 dB the original system increases the shift of the quantizer levels as can be seen in Figure 2.2. Analysis is harder in this case, as we would have to calculate both the relative entropy between discrete and continuous variables. Also we would have to calculate the conditional entropy of a discrete variable, given a continuous variable. Moreover, stacking the quantization levels directly above each other further reduces correlation between the channel representations, reducing the need for joint decoding.

Loss from mismatched channel symbol distributions: Since the signal on channel 2, $x_2(k)$, is transmitted as direct PAM, it will have the same distribution as the quantization error $b(k)$. The scalar quantizer is of high rate (at high CSNR) and thus the quantization error is approximately following a uniform distribution (Figure 2.7). According to Section 2.2.1 we should thus experience a loss equal to the relative entropy between the actual uniform distribution and the optimal Gaussian channel symbol distribution of the same variance. Denoting the uniform distribution as f and the Gaussian as f^* we have

$$\begin{aligned} I(f\|f^*) &= \int f \ln \frac{f}{f^*} = -h(f) - \int f \ln f^* \\ &= -h(f) + \ln\left(\sqrt{2\pi}\sigma_G\right) + \int f \frac{y^2}{2\sigma_G^2} \\ &= -\ln(\max(x_2) - \min(x_2)) + \ln\left(\sqrt{2\pi}\sigma_G\right) + 1/2 \\ &\overset{(c)}{=} -\ln\sqrt{12\sigma_U^2} + \ln\left(\sqrt{2\pi\sigma_G^2}\right) + \ln\sqrt{e} \\ &= \frac{1}{2}\ln\left(\frac{2\pi e\sigma_G^2}{12\sigma_U^2}\right) = \frac{1}{2}\ln\left(\frac{\pi e}{6}\right), \end{aligned} \tag{2.29}$$

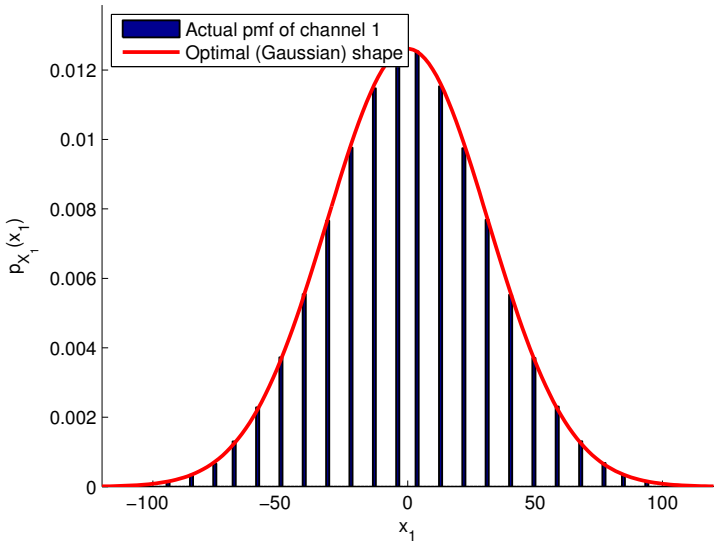

Figure 2.6: At 30 dB CSNR, the pmf of the channel symbols on channel 1 is clearly following a Gaussian distribution, and there is no loss due to mismatched channel symbol distribution.

where we use the fact that $\sigma_U^2 \equiv \sigma_G^2$ (comparing distortion at the same power level), and in (c) we use the fact that the variance of the uniform distribution on channel 2 is given as $\sigma_U^2 = 1/12(\max(x_2) - \min(x_2))^2$ [Zwillinger, 2003]. In bits, this loss is $0.5\log_2(\pi e/6) = 0.255$. This value is confirmed by estimating the relative entropy of the simulated quantization error and a Gaussian distribution of the same variance, using the method described in [Wang et al., 2005]. In decibel, this loss is 1.53 dB which is equal to the potential shaping gain of 1.53 dB in modulation [Forney and Ungerboeck, 1998]. The quantized signal $a(k)$, transmitted over channel 1 with direct PAM will have a discrete distribution approximating the continuous Gaussian distribution (Figure 2.6, and there will be almost no loss due to incorrect channel symbol distribution as long as the number of levels is sufficiently high.

For lower CSNR values, the situation changes since the quantizer levels of the HSQLC should not be stacked directly on top of each other, but rather with a horizontal displacement as seen in Figure 2.2. If we try this, we notice that the displacement means that the distortion occurring from incorrectly decoded y_1 is reduced and the pdf on channel 2 becomes more Gaussian. However, the power on channel 2 will increase without increasing

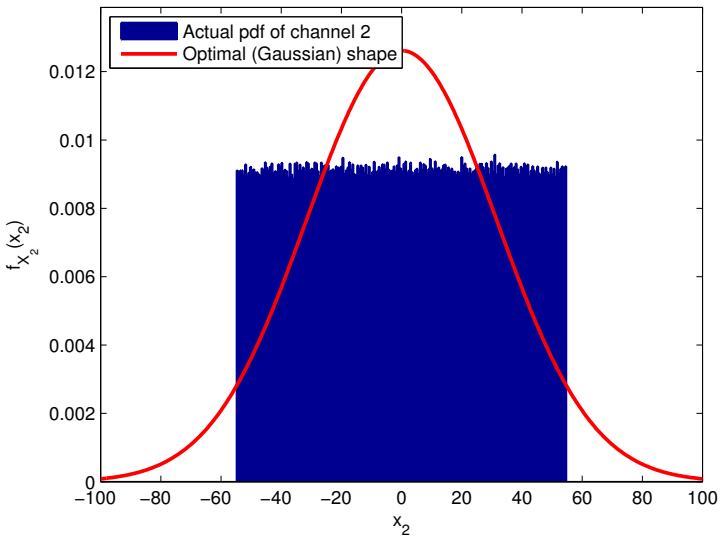

FIGURE 2.7: At 30 dB CSNR, the channel symbol distribution on channel 2 is uniformly distributed, and causes a capacity loss of 0.255 bits.

the decoded SNR[6], and channel 1 will be correlated with channel 2 thus reducing the information content on channel 1. These two benefits and two drawbacks will balance each other for a certain quantizer level shift given a CSNR, thus providing an optimal shift given the CSNR. We also not that the reduced rate on the quantizer has made the distribution on channel 1 non-Gaussian (Figure 2.8).

Loss from threshold effect: Channel 1 has multi-level symbols with no explicit error protection. Channel noise will therefore cause transitions to neighboring symbol levels, and we will have a loss as discussed in Section 2.2.2. This implies that in order to obtain an acceptable symbol error rate, each channel symbol must carry strictly less information than the channel capacity allows. However, since we in the HSQLC use direct modulation of the quantized values without entropy coding or bit-representation, and the channel symbols are memoryless, a symbol error will not cause complete breakdown in the coder. Only one source sample is affected, allowing for a higher symbol error rate compared to digital systems.

Calculation of the mse caused by the threshold effect in channel 1 is done

[6]This is becaue the increased power has not been used to "stretch" the channel signal curve to minimize the effect of channel noise. See [Floor and Ramstad, 2006a].

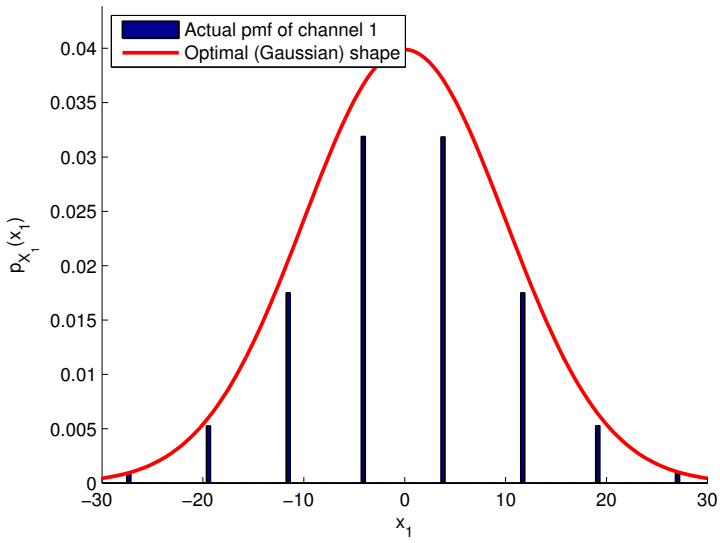

Figure 2.8: The pmf on channel 1 corresponding to the HSQLC characteristics for 20 dB CSNR shown in Figure 2.2. The distribution is no longer following a Gaussian, and will experience a certain capacity loss. This is, however, difficult estimate since the distribution is discrete whereas the optimal Gaussian is continuous.

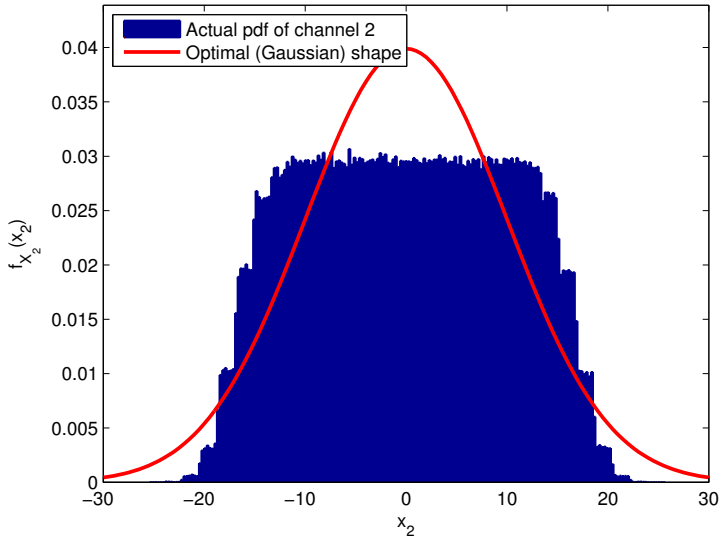

Figure 2.9: Channel 2 has a more Gaussian distribution compared to Figure 2.7, but the increased power usage due to the quantizer level shifts reduces the channel noise suppression. Moreover, channel 1 will now be more correlated with channel 2 reducing the amount of new information transmitted.

as follows. The length of each source segment in Figure 2.5 is

$$d_{th} = \frac{s_{max} - s_{min}}{L}, \tag{2.30}$$

where L is the number of levels. Since the simplified system has the source segments stacked on top of each other, the distortion caused by a jump to neighboring levels is simply $\|j \cdot d_{th}\|^2$, where j is the number of jumps caused by the channel noise. The total mse from the threshold effect is the distortion from all jumps to neighboring levels, multiplied by the probability of transitions, integrated over the entire source S:

$$\varepsilon_{th}^2 = \sum_{i=1}^{L} \sum_{j=1}^{L} \int_{s_i}^{s_i + d_{th}} ((i-j)d_{th})^2 Q\left(\frac{|i-j|d_{min}}{2\sigma_n}\right) f_S(s) ds, \tag{2.31}$$

where $Q(\cdot)$ is the Q-function which returns the tail area under the standardized normal distribution, d_{min} is the distance between quantizer levels on the channel ($x_1(k)$), $s_1 = s_{min}$, $s_L = s_{max}$ and $s_i = s_{i-1} + d_{th}$ (assuming that the overload distortion is negligible).

Translating the mse in (2.31) into its associated SNR loss in an exact manner is not trivial. We can try to approximate the value, but it is admittedly quite clumsy and should be found by some other mean. Starting with the expression for the total SNR

$$\text{SNR} = 10 \log_{10}\left(\frac{\sigma_s^2}{\varepsilon_{ch.2}^2 + \varepsilon_{th}^2}\right), \tag{2.32}$$

we can approximate the SNR loss by taking the difference of the SNR from only channel 2 and the total SNR

$$\Delta\text{SNR}_{th} = 10 \log_{10}\left(\frac{\sigma_s^2}{\varepsilon_{ch.2}^2}\right) - \text{SNR}. \tag{2.33}$$

This is not exact, however, since $\log(a+b) \neq \log a + \log b$, but when the mse from the threshold effect is small it gives a reasonably accurate result.

Loss from rate lower than C: Since the channel symbols are memoryless and no entropy coding is involved, the HSQLC system can allow a certain amount of symbol errors. Still, the threshold effect calculated as above restricts the rate to a number strictly lower than the channel capacity. At 30 dB CSNR the number of PAM-levels is 28 (for the simplified system). Using [Jayant and Noll, 1984, Eq. 4.108] for a Gaussian distribution with the optimal step size, we find the resulting entropy to be 3.89 information bits. This is 1.09

bits below the channel capacity. The symbols on channel 2, carrying the quantization error, are continuous-amplitude and has a rate equal to the channel capacity. The only loss in this channel is from the incorrect channel symbol distribution as explained above.

Loss from channel symbol correlation: Since the quantizer has relatively high rate and the input distribution is Gaussian, we can treat the quantization error and the input as uncorrelated random variables. Since the quantizer output is a deterministic function of the input, we can also treat the quantization error and the output as uncorrelated random variables. This means that the correlation between the two channels is close to zero, and thus there is no loss as explained in Section 2.2.4. This, however, is a simplification which does not hold for low CSNR, where the rate on channel 1 drops. Furthermore, looking at Figure 2.2, we see the quantizer levels of the original HSQLC system [Coward and Ramstad, 2000] are shifted to the right relative their neighbors below. The dashed and solid lines in the plane represents the source at two different channel states, and a source point along these lines determines the resulting channel symbols x_1 (Ch.1) and x_2 (Ch.2) which are used for transmission. Neighboring points along the line segments are neighbors in the one-dimensional source space, and the dotted lines indicates the neighbors of the different line segments. Now, we can see that the optimization algorithm is shifting each line segment toward the right in order to reduce the impact of incorrectly decoded $\hat{a}$. We also see that the shift is bigger for lower CSNR. The shift introduces correlation between channel 1 and 2. This means that the information content $H(x_1|x_2) < H(x_1)$ on channel one is reduced, leading to a loss. The dependence between the two channels should ideally be exploited in the receiver, as discussed in Section 2.2.7, in order to reduce the probability for the threshold effect. The optimal receiver, however, is significantly more complex to derive, and provides at best no more than 0.5 dB improvement [Coward, 2001].

Table 2.1 sums up all the redundancy factors of the simplified HSQLC-system and shows the estimated loss in decibels, calculated from the 6.02 dB per bit rule. The total estimated loss of 8.56 dB is very close to the loss we see from simulations, with simulation results varying a bit due to the threshold effect contribution. When the probability of the threshold effect is estimated correctly in (2.31), the calculated and simulated loss agree within 0.02 dB if we reduce the rate on channel 1 to eliminate the threshold effect, theory and simulation agree fully. At lower CSNR values, it is harder to calculate the loss explicitly since the power is no longer divided equally between the two

Loss (30 dB CSNR)	Sec.	**bits**	**dB**
Mismatched pmf (Ch.1)	2.2.1	$\sim$0	$\sim$0
$R_{Ch.1} < C$	2.2.3	1.09	6.56
Mismatched pdf (Ch.2)	2.2.1	0.255	1.53
$R_{Ch.2} < C$	2.2.3	$\sim$0	$\sim$0
Inter-channel correlation	2.2.4	$\sim$0	$\sim$0
Source Coder Redundancy	2.2.5	$\sim$0	$\sim$0
Suboptimal receiver	2.2.7	$\sim$0	$\sim$0
Threshold effect (Ch.1)	2.2.2	-	0.47
Sum		**1.345**	**8.56**
Simulation			8.58

Table 2.1: Loss account for the simplified HSQLC, Gaussian source and AWGN channel.

channels, and since the quantizer rate is reduced, inter-channel correlation is introduced.

As the reduced rate on the channel 1 is responsible for 81% of the loss for the HSQLC, it would make sense to try to include a more efficient coding on that channel, like for instance a bandwidth-efficient LDPC-coded modulation [Eleftheriou and Olcer, 2002][7]. Using this on channel 1, we could get as close as 3.88 dB to the Shannon limit with a BER of 10^{-7}. This translates to a capacity loss of 0.643 bits per symbol. Assuming no incorrectly decoded symbols, the calculated distance to OPTA would be $0.643 \cdot 6.02 + 1.53 = 5.39$ dB. For a capacity-achieving code, the distance to OPTA would be only 1.53 dB.

To further improve the performance, a higher dimensional vector quantizer in place of the scalar quantizer must be employed, since that is the only way to produce a more Gaussian distributed quantization noise.

2.5 Concluding Remarks

In this chapter, we have tried to identify factors in (lossy) joint source-channel coding systems leading to sub-optimal performance. We only considered systems with a squared-error distortion measure and an average power constraint on the channel.

[7] This would, however, further reduce the system's robustness compared to direct modulation.

The loss factors identified are the following; Non-Gaussian channel symbol distribution (Sec.2.2.1), decoding errors (Section 2.2.2), operational rate lower than the channel capacity (Section 2.2.3), correlation between channels (Section 2.2.4), source coder redundancy (Section 2.2.5), mismatched source distributions (Section 2.2.6), and suboptimal receiver structures (Section 2.2.7). The list of loss factors is not exhaustive, but should cover the most important loss factors of source-channel coding systems. By means of two examples some of the identified factors were shown to be able to explain the loss experienced and to provide important hints on where to start when trying to improve a given system's performance.

Chapter 3

Shannon-Kotel'nikov Mappings

"The reasonable man adapts himself to the world; the unreasonable one persists in trying to adapt the world to himself. Therefore all progress depends on the unreasonable man."

- George Bernard Shaw (1856 - 1950), Man and Superman (1903) "Maxims for Revolutionists"

This chapter introduces the concept of S-K mappings, which is a class of lossy joint source-channel coding schemes based on the geometrical interpretations of communication due to [Shannon, 1949; Kotel'nikov, 1959][1]. The idea of this approach is to exploit the analog nature of waveform channels in order to provide both high spectral efficiency and robustness against channel fluctuations, while at the same time ensuring low delay and complexity.

The concept of S-K mappings assumes that both the source and the channel are represented by amplitude-continuous[2] and time-discrete symbols. That is, the source is sampled, but not quantized, and the channel has distinctive symbols with continuous or multi-level amplitudes. The discrete-time nature implies that both the source and the channel will require a particular bandwidth, given by the sampling rate. The source is then projected, or mapped, directly onto the channel using a mathematical function, or a composition of several functions. This takes a point from the source space and

[1] Note that the book from 1959 is an English translation of Kotel'nikov's doctoral thesis from 1947.

[2] The channel representation can also be multi-level symbols like the example in Section 2.4.2. The point is that there are no bit-representations involved.

places it in the channel space, hopefully in a close to optimal manner. The decoder should bring the point from the channel space (the channel symbol) back into the source space, introducing as little distortion as possible into the reconstruction at the receiver side. Figure 1.3 illustrates the conceptual process of the S-K mappings, where the composition $T \circ q$ constitutes the encoder, and T^{-1} the decoder. If the source bandwidth is larger than the channel bandwidth, the function q is responsible for reducing the information content of the source so that it can be "fitted" onto the channel. In this case, q will not be injective, and the encoding function is not invertible (not lossless). On the other hand, of the channel bandwidth is larger than the source bandwidth, the function q is not needed and will simply be the identity operator. The bijective function T performs the mapping from the source to the channel space, and is obviously invertible. Since both the source and the channel symbols have continuous amplitude, channel noise will introduce distortion in the reconstructed source symbol at the receiver. A good choice of encoder-decoder pair is required to minimize the effect of the channel noise.

In order to put the S-K mapping schemes in perspective, a quick comparison with the "standard" approach to communication of analog sources (sound, images, video etc.) is in order. In digital communications, the (analog) source is first approximated to a discrete and countable set, usually by sampling and quantization. This reduces the information content of the source to some value R, called the rate. The source set is mapped, using a bijective mapping, onto a discrete and countable set of channel symbols. As long as R is below the channel capacity C, the channel can be made to be virtually error free (transparent) by utilizing forward error correction (FEC). After the invention of Turbo codes [Berrou et al., 1993] and re-invention of LDPC codes [Chung et al., 2001], this approach comes very close to the optimum for low channel CSNRs using BPSK.

The principal difference between the fully digital approach and the S-K mappings is how the issue of channel noise is addressed. In the former, the channel is made transparent and the distortion at the decoder side comes solely from the necessary information reduction performed in the source coder. However, as both the source and the channel are analog and the source tolerates a certain level of distortion, there is no particular requirement for the channel to actually be transparent. So instead of reducing the information content to a rate below the channel capacity, and achieving error-free transmission, S-K mappings explicitly allow channel noise to contaminate the source, with the possible benefit of higher spectral efficiency,

higher robustness and lower end-to-end delay. This concept has its roots in non-linear analog communication, and thus display many similarities to that and to robust source coding like channel-optimized vector quantization. Thus, a quick review of these related schemes is also in order.

An article which explores the theoretical limitations of analog communication [Goblick, 1965] shows that for low-CSNR channels, the potential gain from bandwidth expansion is vanishing, and in that respect the benefits of analog communication over digital systems using turbo codes and BPSK would be lower delay and complexity. With respect to non-linear analog modulation techniques, several methods exist; pulse-position modulation (PPM), frequency-position modulation (FPM), frequency modulation (FM) and phase modulation (PM). These systems all have performances relatively far away from the theoretical optimum for small bandwidth expansion factors [Wozencraft and Jacobs, 1965; Timor, 1970]. However, as the channel bandwidth goes to infinity, these systems do approach optimum modulation schemes, in the sense that no other systems have a faster decaying mean-squared error. Systems which build on Kotel'nikov's geometric interpretation using nonlinear continuous curves (*signal curves*) for communication [Kotel'nikov, 1959] have shown improved performance for the bandwidth expansion case, with bandwidth expansion factors less than or equal to 5 [McRae, 1971; Thomas et al., 1975]. These schemes, which are called *mixed-base modulation* (MBM), achieve expansion by performing a mapping through the signal curve, from the source space (dimension 1) to the channel space (dimension N). The bandwidth expansion factor is equal to the dimension increase, and the performance improves compared to the PPM-like systems for small bandwidth expansion factors. A common expression for MBM, PPM, FPM and FM is *twisted modulation* [Wozencraft and Jacobs, 1965].

More recent examples, usually termed *hybrid digital-analog* (HDA) *joint source-channel codes*, can be found in [Skoglund et al., 2002; Mittal and Phamdo, 2002; Skoglund et al., 2006]. These systems strongly resemble the earlier mentioned systems, but as they incorporate channel codes in the digital parts, the breakdown below the design CSNR is more abrupt, whereas the analog part ensures graceful improvement if the CSNR is higher. Recently, we have presented some "purely analog" bandwidth-expansion schemes resembling the MBM systems which uses parametric curves or surfaces to perform the dimension change. These perform on par with or even better than the HDA schemes [Floor and Ramstad, 2006a,b,c; Cai and Modestino, 2006]. The 1:2 bandwidth expansion mapping introduced in Chapter 2

[Coward and Ramstad, 2000] is commonly referred to as a HDA system, as it has the same structure as the previously mentioned HDA systems. However, as the system has no bit representation, but rather employs a direct modulation of the quantized source, this system can be classified as a S-K mapping.

For bandwidth reduction, there are several more examples, and they generally come closer to the theoretical bounds than the existing schemes for the expansion case. Most common are COVQ, where the codebook indices are mapped directly onto the channel [Vaishampayan, 1989; Skinnemoen, 1994; Fuldseth and Ramstad, 1997]. Instead of using discrete vector quantizers, parametric curves or surfaces can be used as "continuous codebooks". The functions should be matched carefully to the source and channel [Chung, 2000; Hekland et al., 2005], but general design methods for constructing these functions are at present still not known to exist. Performance is comparable to the COVQ systems with the added benefit of simpler encoding and decoding.

3.1 Preliminaries for Shannon-Kotel'nikov Mappings

Before presenting specific examples of S-K mappings, necessary assumptions, notation and performance measures are introduced. Unless noted otherwise, these hold for the following chapters too.

For simplicity, only memoryless i.i.d. sources are considered. Correlation is assumed removed through preceding operations such as filterbanks or transforms.

For measuring the distortion between the source and the reconstruction at the receiver, only the mean-squared error distortion measure is used. This is chosen for mathematical simplicity and because it provides a closed-form expression for the rate-distortion function for the Gaussian source. Furthermore, its wide utilization as an objective distortion measure makes it easier to compare to other systems.

A practical system is always constrained in terms of available resources. The design space, i.e. bandwidth, power, complexity etc. has in practice always some kinds of imposed constraints. The main limitations in this discussion is:

- Bandwidth of both the source and the channel is assumed to be lim-

ited, and in general the source and channel bandwidths are different. However, we only consider relative differences between the source and channel bandwidths.

- The channel has an average power constraint as this is simpler mathematically, although practical systems usually have peak power limitations, and even an amplitude limitation.

Obviously, in a practical system the bandwidth cannot be exactly restricted to a specific value since filters have a smooth roll-off instead of an ideal brick-wall characteristics. However, this fact is disregarded and ideal filters are assumed to simplify analysis, but obviously has to be taken into account when designing a practical system. With regards to the channel power constraint, it should also be noted that it is possible to use different kinds or several simultaneous constraints like average power and peak amplitude limitations when optimizing the mappings.

3.1.1 Dimension Change as a Mean to Achieve Bandwidth Change

Since we assume time-discrete operation, any time-continuous source must be sampled before transmission. Throughout the entire thesis, the sources are assumed to be strictly bandwidth-limited[3]. According to the Shannon-Whittaker-Kotel'nikov sampling theorem [Zayed, 1993], a source with a bandwidth W can be sampled and accurately reconstructed using a sampling frequency of $2W$. Hence, the source outputs $2W$ samples per second. For a channel with bandwidth W and using Nyquist signaling rate, one can transmit $2W$ symbols per second. This implies that one can transmit a source of bandwidth W over a Nyquist channel of bandwidth W while achieving the same performance as direct analog transmission. As was discussed in Section 1.2.3, we achieve either bandwidth reduction by combining M source samples into N channel samples, or bandwidth expansion by distributing M samples over N channel samples. This is can be expressed as

$$\psi : \mathbb{R}^M \rightarrow \mathbb{R}^N, \tag{3.1}$$

where the dimension change will provide the needed bandwidth change, given that the numbers M and N are sufficiently large for the approximation $M/N \approx W/B$ to hold with good accuracy.

[3]The bandwidth limitation can be natural or imposed through a preceding low-pass filtering operation, but in either case only the bandwidth-limited source is considered.

Using a non-linear operator ψ has benefits both for compression and expansion. For a linear mapping, and where the source bandwidth is larger than the channel bandwidth, there are two options for achieving compression and thereby fitting the source on channel. Either the source can be low-pass filtered and resampled to such a rate that it fits on the channel, or it can simply discard the excess samples, transmitting only the most important samples. Both approaches increase the distortion, however in different ways. A non-linear mapping on the other hand, would retain the full bandwidth of the source and not discard any samples, but rather represent each sample with less precision. To achieve a 2:1 compression, the linear mapping would discard every second sample (or resample to half the bandwidth), whereas the non-linear mapping would combine two and two samples and represent them as one single channel sample. This can potentially increase the resulting SNR at the receiver side, especially for high CSNR. As for bandwidth expansion, a linear system can only achieve expansion through sending several copies of the same source signal and average at the receiver. This translate to only 3 dB increase in SNR per doubling of channels, provided that the power doubles too. The reason for this small gain is the poor utilization of the channel space. When using this kind of repetition code, fully correlated information is transmitted on the channels, thereby "wasting" bandwidth which could be used to send new information. By using a non-linear mapping, the different channel representations can be made to carry unique information, thereby improving the channel utilization. According to what we found in Section 2.2.4, the difference between the linear (BPAM) and the optimal nonlinear mapping can be assessed through evaluating the expressions of the channel capacity

$$C = \max_{f(x_1,x_2,\ldots,x_N):\sum \mathsf{E}[X_i^2]\leq P} I(X_1, X_2, \ldots, X_n; Y_1, Y_2, \ldots, Y_N), \tag{3.2}$$

where X_i are the transmitted symbols, Y_i are the received symbols.

With the noise Z_i independent of the signal X_i, the mutual information in (3.2) can be written as

$$\begin{aligned} &I(X_1,X_2,\ldots,X_k;Y_1,Y_2,\ldots,Y_N) \\ &\qquad = h(Y_1,Y_2,\ldots,Y_N) - \sum_i h(Z_i). \end{aligned} \tag{3.3}$$

For the linear system with fully correlated channel symbols, i.e. the joint

differential entropy is $h(Y_1, Y_2, \ldots, Y_N) = h(Y_1)$, (3.3) becomes

$$I(X_1,X_2,\ldots,X_N;Y_1,Y_2,\ldots,Y_N) = h(Y_1) - \sum_i h(Z_i) \overset{a)}{=} \frac{1}{2}\log\left(1 + \frac{\sum_i P_i}{Z_i}\right), \tag{3.4}$$

where it in a) is assumed capacity achieving distributions and that all the available power, P, is put into one channel (equivalent to transmitting the same information on all the channels and averaging out the noise). For the nonlinear systems with independent channel symbols, (3.3) becomes

$$I(X_1,X_2,\ldots,X_N;Y_1,Y_2,\ldots,Y_N) = \sum_i h(Y_i) - h(Z_i) \overset{a)}{=} \sum_i \frac{1}{2}\log\left(1 + \frac{P_i}{Z_i}\right), \tag{3.5}$$

where $P_i = \mathsf{E}\left[X_i^2\right]$ and $\sum P_i = P$. Comparing these expressions, assuming $P_i/\sigma_{n,i}^2 \gg 1$ and equal $P_i/\sigma_{n,i}^2$ on all the channels, the capacity in the linear solution grows logarithmically with the number of channels N, whereas in the nonlinear solution it grows linearly with N.

3.2 Mappings providing 2:1 Dimension Reduction

With a 2:1 dimension reducing mapping, we can transmit a source of bandwidth $2W$ over a channel with bandwidth W, with the theoretical lower bound SNR $= (1 + \text{CSNR})^{1/2}$ (Section 1.2.3). The lower bound describes the case of transmitting a Gaussian source over an AWGN channel. Other sources like Laplacian sources are "easier" to describe (lower rate) and this increases the SNR for a given CSNR. Likewise, Gaussian noise minimizes the capacity of (3.2), and all other noise distributions increase the capacity, thus increasing the SNR as well. The mapping process works by applying the function $q()$ to the source. This function performs a projection from the source space, which is two-dimensional, to a subspace. This effectively creates an approximated version of the source where the information content is sufficiently reduced so that it fits on the channel. The subspace in which the approximated source resides can be mapped with an invertible function $T()$ onto the one-dimensional channel.

The key to good performance is to find the q and T which minimize the distortion at the receiver side. The geometry of q, i.e. the geometry of the

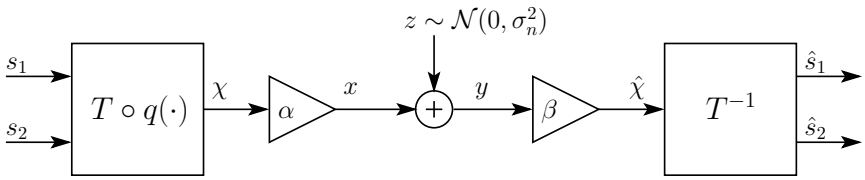

FIGURE 3.1: A generic $2:1$ dimension (bandwidth) reducing Shannon mapping. The $q(\cdot)$ operator projects the 2-D source tuple onto a point on a 1-D curve in $\mathbb{R}^2$. This operation is not invertible when the curve has finite length. The $T(\cdot)$ operator is an invertible one-to-one mapping between the curve and the channel space. The scaling factor ensures that the power-constraint is fulfilled.

subspace, determines the approximation noise (equivalent to quantization noise) introduced when reducing the information content. The function T is responsible for taking the approximated source into the channel space and back in an optimal manner. Ideally, the channel symbol distribution should be Gaussian, as discussed in Section 2.2.1, but at the same time, the impact of the channel noise should be minimized. Moreover, the total noise contribution, from both the approximation step and the channel noise, should ideally be Gaussian distributed with a power no greater than what is needed to equate the rate-distortion function with the channel capacity.

Determining what q and T should be, given the source and channel statistics, is not trivial. The two functions together both determine the channel symbol distribution and the resulting noise distribution, thus decoupling the design of them will most likely lead to suboptimal results. For now, the only ways to determine q and T are to either make intelligent guesswork, or to look at the results of a power-constrained channel-optimized vector quantizer (PCCOVQ) [Fuldseth, 1997] which is closely related to S-K mappings. The major difference from the S-K mappings is that instead of using a function or curve to describe the subspace in the approximation step q, an ordered vector quantizer is used. By increasing the number of codebook entries in the PCCOVQ, a continuous function can be approximated. Figure 3.2 shows the resulting codebook from the PCCOVQ for a Gaussian source and an AWGN channel for different channel qualities. Using a codebook size of 1024, the codebook vectors become so closely spaced that they approximate a continuous function. For sources and channels resulting in such regular codebooks as this, we can hope to find similar looking functions which can be used to describe the subspace q in our mappings.

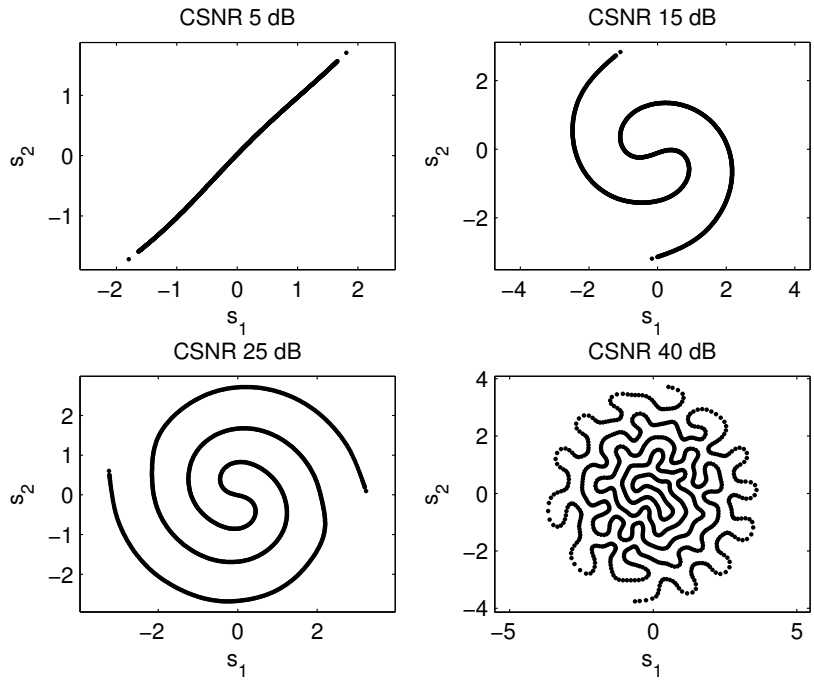

Figure 3.2: 2:1 PCCOVQ codebook for a Gaussian source and an AWGN channel, created using the algorithm described in [Fuldseth, 1997]. Interestingly, for low CSNRs the PCCOVQ produces a linear system, whereas for higher CSNR the result is a non-linear system. For intermediate CSNRs the codebook shows a very regular structure resembling a double intertwined Archimedes' spiral, wheres for very high CSNRs the codebook shows a more irregular behavior (which is shown to be suboptimal).

3.2.1 Gaussian Source, AWGN Channel

We now assume that we are given an i.i.d. Gaussian source S with zero mean, and form tuples of two consecutive samples. This can be represented as a source vector $\mathbf{s} = (s_1, s_2)$. We want to perform a bandwidth reduction by transmitting a combination of the two source samples as one channel sample. To achieve this we perform a mapping operation from the two-dimensional source space onto a subspace which must consist of line segments. This is represented by the $q(\cdot)$ in Figure 3.1, where any point in $\mathbb{R}^2$ is mapped to the closest point in the subspace defined by q. In our case, the subspace is given as the double Archimedes' spiral, defined by the radii

$$r_+(\theta) = \frac{\Delta}{\pi}\theta \quad \text{and} \quad r_-(\theta) = \frac{\Delta}{\pi}(\theta + \pi), \tag{3.6}$$

for the solid and dashed spiral arms in Figure 3.4 respectively. Here, Δ is the distance to neighboring spiral arms in Figure 3.4 and $\theta \in \mathbb{R}$ is the angle from the origin to a point on the spiral. The curve length of the spiral arm is given as

$$\ell(\theta) = \frac{1}{2}\Delta\left(\theta\sqrt{1+\theta^2} + \sinh^{-1}\theta\right). \tag{3.7}$$

The Archimedes' spiral belongs to a family of Archimedean spirals given as $r_+(\theta) = \frac{\Delta}{\pi}\theta^{1/k}$, where the difference from (3.6) is the term k which determines whether the distance between the spiral arms increases for higher θ ($k < 1$), is uniform ($k = 1$), or the spiral arm distance decreases for higher θ ($k > 1$). The family of Archimedean spirals can also be given in parametric form as

$$\mathbf{u}_\pm(\theta) = \pm\frac{\Delta}{\pi}\theta^{1/k}\left(\cos\theta\vec{i} + \sin\theta\vec{j}\right), \tag{3.8}$$

where $\mathbf{u}_+$ and $\mathbf{u}_-$ determine the solid and dashed spiral arms in Figure 3.4 respectively.

The choice of the double Archimedes' spiral as the subspace in q is based on the observations of the codebook of the PCCOVQ in Figure 3.2. Figure 3.3 shows the PCCOVQ and the double intertwined Archimedes' spiral superimposed, indicating that it is a sensible choice as a subspace for q. It was discovered that results on such a system were already presented in [Chung, 2000], but since most of the derivations of the results were omitted there, and no publications on the results exist, a more complete description of the optimization process is presented in the following.

First, a source vector is approximated, or projected, onto the closest point on the spiral. In Figure 3.4 this can be seen as the star point being approximated by the circle point on the spiral. The approximated source vector is still two-dimensional, but is restricted to the Archimedes' spirals. Then we perform a mapping using the invertible operator $T(\cdot)$ in Figure 3.4 from the two-dimensional subspace to a one-dimensional channel representation. In this case, we use the square of the angle,

$$T_+(\theta) = +\eta\theta^2 \quad \text{and} \quad T_-(\theta) = -\eta\theta^2 \tag{3.9}$$

for the solid and dashed spiral arms respectively in Figure 3.4. The parameter $\eta = a\Delta$ with $a = 0.16$ makes this T-operator an approximation of the length along the spiral given in (3.7). This is then scaled to satisfy the power constraint and sent as an analog symbol over the channel.

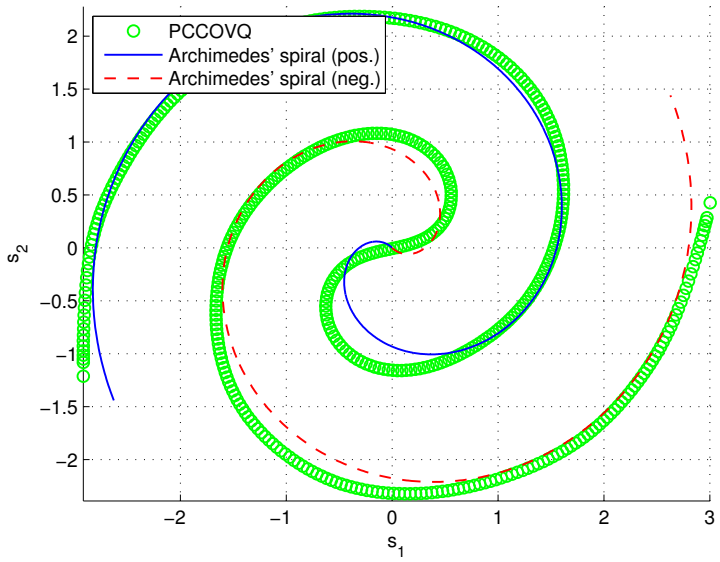

Figure 3.3: Comparing the structure of codebooks at 20dB CSNR.

The optimal Δ depends on the channel noise and the transmit power constraint, and is the parameter to be determined. In the receiver, the square-root of the received symbol is taken. This leads to signal dependency of the channel noise. However, simulations suggest that in the high-CSNR region this effect is minimal, so we disregard this factor in the following.

When optimizing the spiral mapping, the goal is to find the Δ that minimizes the total distortion, given an average power-constraint P. That is,

$$\Delta_{opt} = \underset{\Delta:\mathsf{E}[x^2]\leq P}{\operatorname{argmin}} \left[D(\Delta)\right], \tag{3.10}$$

where $D(\Delta)$ is the resulting distortion after reception when using Δ as the spiral arm distance, and $\mathsf{E}\left[x^2\right]$ is the average channel symbol power. The power-constraint will limit the range of θ, so we have $\theta \in \mathcal{S} \subset \mathbb{R}$.

We define the resulting distortion per source symbol after decoding at the receiver side as

$$D_s \overset{def}{=} \frac{\mathsf{E}\left[\|\mathbf{s}-\hat{\mathbf{s}}\|^2\right]}{2},$$

where $\mathbf{s}$ and $\hat{\mathbf{s}}$ are the original and decoded source vectors respectively. The denominator accounts for the fact that the distortion is distributed on two source symbols. As in the thesis by Chung [Chung, 2000] we decompose the

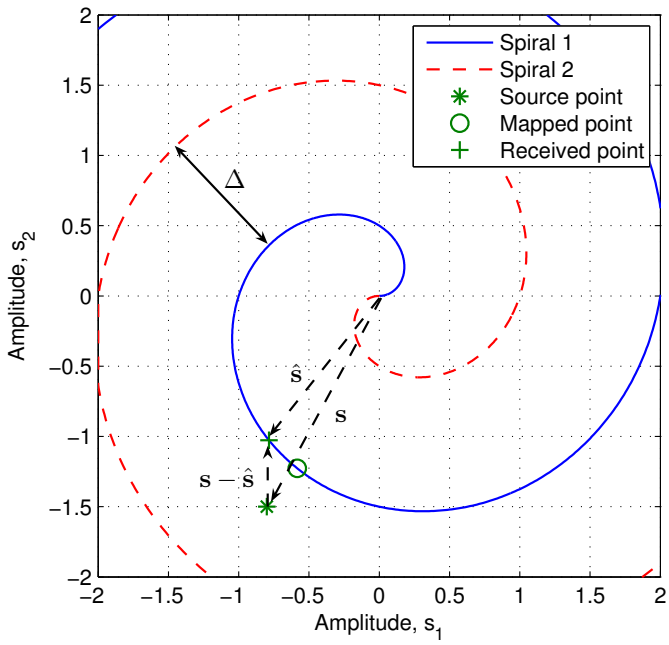

Figure 3.4: Indicates the error components from the mapping process. The total error $\|\mathbf{s}-\hat{\mathbf{s}}\|$ can be decomposed into two orthogonal components: A radial component from the approximation $q(\cdot)$ in Figure 3.1, and an angular component, $\|\hat{\mathbf{s}}\|\,(\angle\mathbf{s}-\angle\hat{\mathbf{s}})$, from the channel noise which moves the mapped point along the spiral.

error into a radial component resulting from the approximation operation $q(\cdot)$ in Figure 3.1 and an angular component from channel noise Z:

$$D_s = D_r + D_\theta = \frac{1}{2}\mathsf{E}\Big[\left(\|\mathbf{s}\| - \|\hat{\mathbf{s}}\|\right)^2\Big] + \frac{1}{2}\mathsf{E}\Big[\|\hat{\mathbf{s}}\|^2\left(\angle\mathbf{s} - \angle\hat{\mathbf{s}}\right)^2\Big]. \tag{3.12}$$

This decomposition is possible under the assumption of high CSNR when the spiral is sufficiently dense at the origin, so that the average error is approximately equal in the two source samples after projecting the combined source point onto the spiral. The radial distortion will increase with increasing Δ, which is obvious since the distance to the closest spiral arm increases. The angular distortion will, however, increase with decreasing Δ. This is because the source will have to be down-scaled as a result of the power constraint. The corresponding up-scaling at the receiver end will then amplify both signal and noise. Hence, there is an optimal value of Δ which produces the minimum total distortion.

Balancing the Distortion Contributions

Since we allow noise from both the approximation step and the channel to affect the source signals, we want to determine the optimal balance between these two noise contributions. That is, we want to determine the optimal Δ which minimizes the total distortion. Then we will show that this implies $D_r = D_\theta$.

We need an expression for the total distortion, containing both distortion components, and then we must minimize this under the given power constraint. This expression is

$$D_s(\Delta, \sigma_n) = D_r(\Delta) + D_\theta(\Delta, \sigma_n). \tag{3.13}$$

The power constraint in (3.10) implies that we have to scale the channel input signal with a factor α in order to satisfy the average power constraint $\mathsf{E}\big[(\alpha\chi)^2\big] = \alpha^2\mathsf{E}\big[\chi^2\big] = \alpha^2\sigma_\chi^2$, where $\alpha = \sqrt{P/\sigma_\chi^2}$. The received channel signal must be up-scaled accordingly to obtain the original source power. Even though the inverse of the scaling parameter on the transmitter side is sub-optimal compared to a Wiener-type scaling factor (i.e. an minimum mean-squared error (MMSE) receiver), we use $\beta = \alpha^{-1}$ for simplicity. The scaling on the receiver side implies that the channel noise will also be scaled as:

$$\mathrm{Var}\left[\beta Y\right] = \beta^2 \mathrm{Var}\left[Y\right] = \beta^2\sigma_n^2 = \frac{\sigma_\chi^2}{P}\sigma_n^2. \tag{3.14}$$

For the two distortion terms in (3.13), we introduce some approximations valid in the high CSNR (i.e. dense spiral) case. First, looking at Figure 3.4, we realize that the approximation step which projects the source point (star) to the approximated point (circle) moves the point (approximately) in the radial direction. Since the spiral arms are uniformly spaced, and densely packed for high CSNRs, the approximation operation can be interpreted as a standard uniform scalar quantizer (except near the origin). Therefore we can introduce the well-known expression for the quantization error in a scalar quantizer, $\sigma_q^2 = \Delta^2/12$. With regard to the problems around the origin, it seems reasonable to assume that with a sufficiently dense spiral the approximation should still be valid except for a disc with a small radius. The anomaly around the origin will be insignificant for dense spirals, but will result in modeling errors as the CSNR is reduced since the spirals become less dense. For the distortion in the angular direction, the scaled noise

variance in (3.14) is used. Inserting into (3.13) we obtain

$$D_s(\Delta, \sigma_n) = \frac{1}{2}\left(\frac{\Delta^2}{12}\right) + \frac{1}{2}\left(\beta^2\sigma_n^2\right) = \frac{1}{2}\left(\frac{\Delta^2}{12}\right) + \frac{1}{2}\left(\frac{\sigma_\chi^2}{P}\sigma_n^2\right) \tag{3.15}$$

where σ_χ^2 is a function of Δ. To determine σ_χ^2, we assume that in the high-CSNR region the spiral is sufficiently dense to disregard the approximation step for this particular purpose. This means we can calculate the density on a circle around the origin. This is done by evaluating $Y = g(s_1, s_1) = \pm\eta\theta^2 = \pm\eta(s_1^2+s_2^2)$, from the expression of the radius (3.6). See Appendix A for details on how to determine $f_\chi(\chi)$ and the corresponding σ_χ^2. For a 2-D Gaussian circular symmetric source, using the T-operator in (3.9) gives a Laplace distribution with variance

$$\sigma_\chi^2 = 2\lambda^2 = 2\left(2\eta\frac{\pi^2}{\Delta^2}\sigma_s^2\right)^2, \tag{3.16}$$

where σ_s^2 is the variance of the source, and η equals $a\Delta$ as in (3.9). Setting $a = 0.16$ will provide an approximation of the curve length, and this will be used in the remainder of this thesis. Inserting into (3.15) we have

$$D_s(\Delta, \sigma_n) = \frac{\Delta^2}{24} + \frac{8(0.16\pi^2\sigma_s^2\sigma_n)^2}{\Delta^2 \cdot 2P}. \tag{3.17}$$

We thus see, as stated above, that the radial distortion will decrease with smaller Δ whereas the angular distortion will increase with smaller Δ. Therefore we will have a distinct Δ which provides the minimal distortion for the given noise variance and power constraint. To find this minimum we differentiate D_s with respect to Δ and equate the resulting expression to zero.

$$\frac{dD_s}{d\Delta} = \frac{\Delta}{12} - \frac{8(0.16\pi^2\sigma_s^2\sigma_n)^2}{\Delta^3 P} = 0. \tag{3.18}$$

Solving this expression for Δ we obtain

$$\Delta_{opt} = 2\pi\sigma_s\sqrt[4]{\frac{6\cdot 0.16^2\sigma_n^2}{P}} = 2\pi\sigma_s\sqrt[4]{\frac{6\cdot 0.16^2}{\gamma}}, \tag{3.19}$$

where we defined the CSNR as $\gamma = P/\sigma_n^2$.

Using the distortion expression in (3.17), and inserting (3.19) into (3.17), we find that with minimal total distortion, both distortion contributions are

$$D_r = D_\theta = \frac{\Delta_{opt}^2}{24} = \pi^2\sigma_s^2\sqrt{\frac{0.16^2}{6\cdot\gamma}}. \tag{3.20}$$

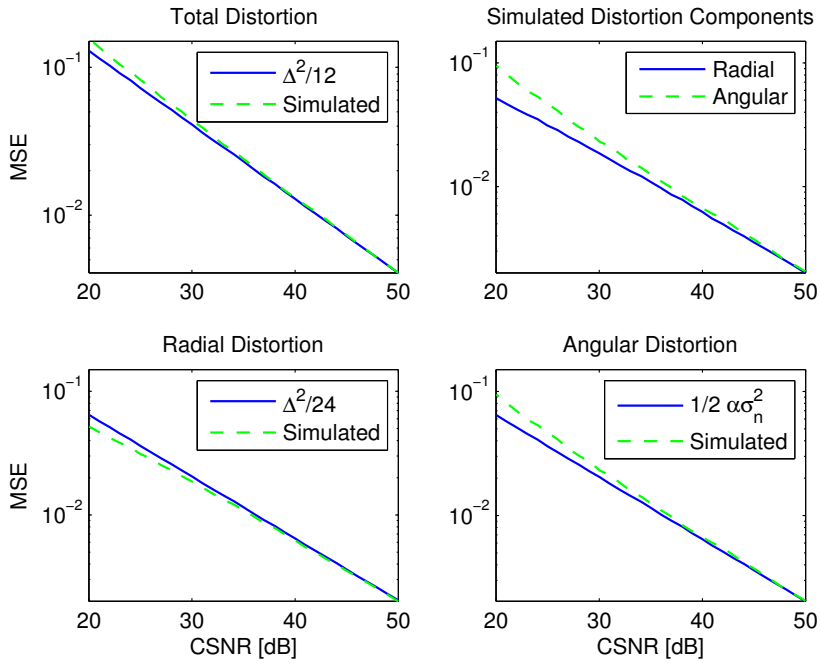

Figure 3.5: A comparison between the distortion model (3.15) and simulations. The radial distortion denotes the distortion due to the approximation operation, whereas the angular distortion denotes the distortion due to channel noise. The model shows good correspondence above 35 dB CSNR.

Thus, the total distortion is minimized when the approximation and channel noise are equal, and it is given as

$$D_s = \frac{\Delta_{opt}^2}{12} \tag{3.21}$$

The SNR is defined as

$$\begin{aligned} \text{SNR} &= \frac{\sigma_s^2}{D_s} = \frac{\sigma_s^2}{\Delta_{opt}^2/12} = \frac{\sqrt{6}}{2 \cdot 0.16 \cdot \pi \cdot \pi}\sqrt{\gamma} \\ &\approx \frac{\sqrt{6}}{\pi}\sqrt{\gamma}, \end{aligned} \tag{3.22}$$

and comparing this to OPTA for the $2:1$ case:

$$\text{SNR} = \sqrt{1+\gamma}, \tag{3.23}$$

we see that the asymptotic gap from OPTA is $\sqrt{6}/\pi \approx 1.1$ dB, which agrees with the findings of [Chung, 2000].

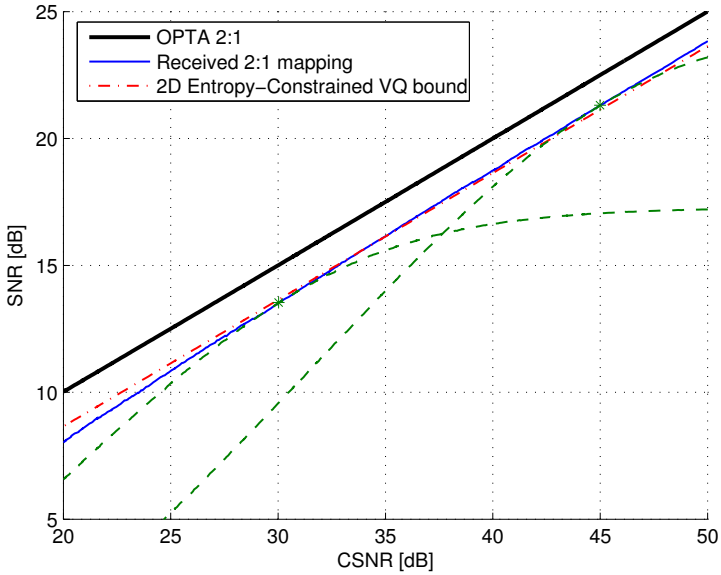

Figure 3.6: SNR vs. CSNR for 2-D i.i.d. Gaussian source and AWGN channel. Comparison of the optimized spiral mapping and the theoretical bound for 2-D ECVQ. The green dashed curve illustrates the robustness of the system for incorrect CSI at the transmitter.

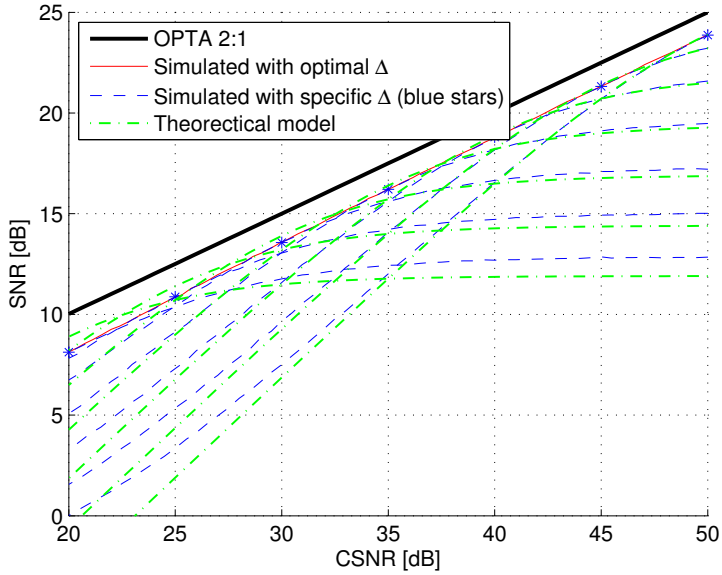

Figure 3.7: SNR vs. CSNR for 2-D i.i.d. Gaussian source and AWGN channel. Comparison of simulations and the analytic model in (3.17).

A comparison between this optimized spiral mapping, OPTA for 2:1 bandwidth reduction, and the ideal entropy-coded vector quantizer with perfect channel coder can be seen in Figure 3.6. It is observed that the proposed system outperforms the vector quantizer in the high-CSNR region where the assumptions hold, whereas below 20-25 dB CSNR, the assumptions in Section 3.2.1 are no longer valid, causing higher distortion. It is stressed that in contrast to the ideal entropy coded vector quantizer with a capacity achieving code for the channel, the proposed system is memoryless and does not attain the theoretical channel capacity. Furthermore, it is very robust in the sense that incorrect CSI in the receiver will not cause a break-down in the decoder. The systems shows both graceful degradation and improvement for all CSNR, as can be seen in the blue dashed curves in Figure 3.7.

Since the optimal Δ in (3.19) depends on the source variance σ_s^2, incorrect estimates of σ_s^2 will result in degradations. However, unless the source sample set is very small so that estimating the source variance is hard to do accurately, this will be a small issue since the curve in Figure 3.8 is relatively flat around the assumed σ_s^2. More than 50% estimation error of the variance will still provide a performance within 2 dB from OPTA. Since we chose the geometry on the basis of the PCCOVQ, it is reasonable to compare the performance of the two to see how they perform relative to each other. If we assume perfect CSI and known σ_s^2 at the transmitter side, the spiral used for simulations is found using (3.19), whereas the codebooks for the PCCOVQ are trained using the algorithm in [Fuldseth, 1997] with a training set consisting of $4 \cdot 10^6$ vectors. The codebooks are trained for each integer CSNR value to make the comparison fair in terms of optimality. Keep in mind that this would require massive storage requirements, so in practice a few codebooks for different CSNRs would be used relying on the robustness of the PCCOVQ for CSNR values in between. This would effectively reduce the performance of the PCCOVQ slightly in a practical system, whereas the spiral mapping, given the CSI, can obtain the exact parameter by simply evaluating (3.19); thus no storage is required in this case.

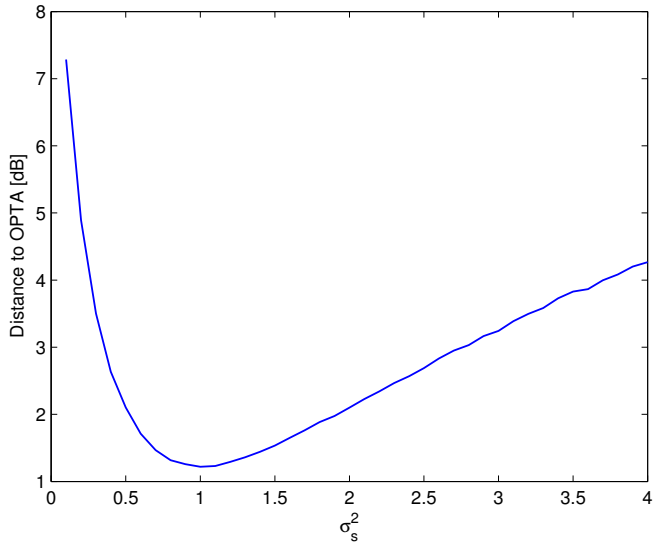

Figure 3.8: The sensitivity of the Archimedes' spiral with respect to mismatched source variance. The spiral arm distance Δ is calculated assuming $\sigma_s^2 = 1$ whereas the true variance is given along the x-axis, resulting in degraded performance.

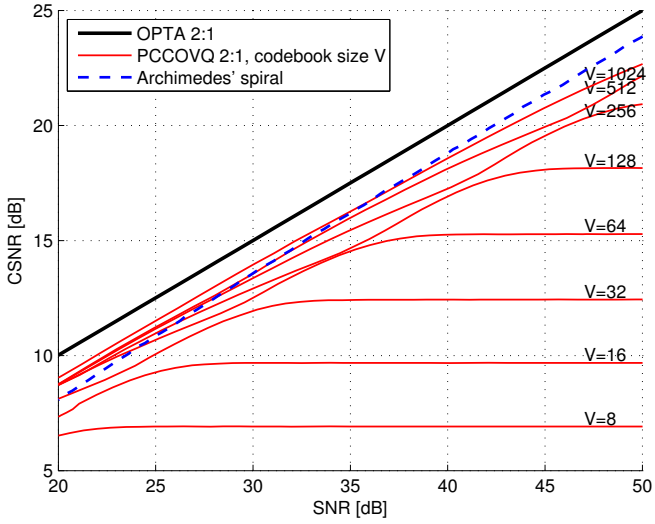

Figure 3.9: Comparing the performance of the Archimedes' spiral with the PCCOVQ with different codebook size, given a Gaussian source and an AWGN channel. The PCCOVQ is not optimal for higher CSNR where the codebooks start to become irregular (lower right plot in Figure 3.2), whereas the PCCOVQ outperforms the spiral mapping below 35 dB where the model no longer is accurate.

3.2.2 Laplacian Source, AWGN Channel

Another common distribution in source coding is the Laplace distribution [Weisstein]. Both the signal to be residually coded in speech and audio, and the high-frequency coefficients which are coded in transform coding of images are well modeled by this distribution [Robinson, 1994; Lam and Goodman, 2000; Taubman and Marcellin, 2002], thus it would be of interest to find a good mapping for this source distribution. Obviously, as the Laplacian is "peakier" around the center and the tails are longer compared to the Gaussian, a different geometry than the Archimedes' spiral in Section 3.2.1 is necessary. Again, not knowing how to determine the optimal shape given the source and channel statistics, looking at the codebook of the PCCOVQ optimized for a Laplacian distributed source and AWGN channel might provide some clues. Figure 3.11 shows the PCCOVQ optimized for 25 dB CSNR, and the resulting codebook is more diamond shaped, similar to the Laplace distribution seen in Figure 3.10. Another option is to warp the Laplace distributed source into a more Gaussian distributed source, then apply the results in Section 3.2.1 with the proper parameters, and unwarp after decoding. These two approaches will be explored and compared in the

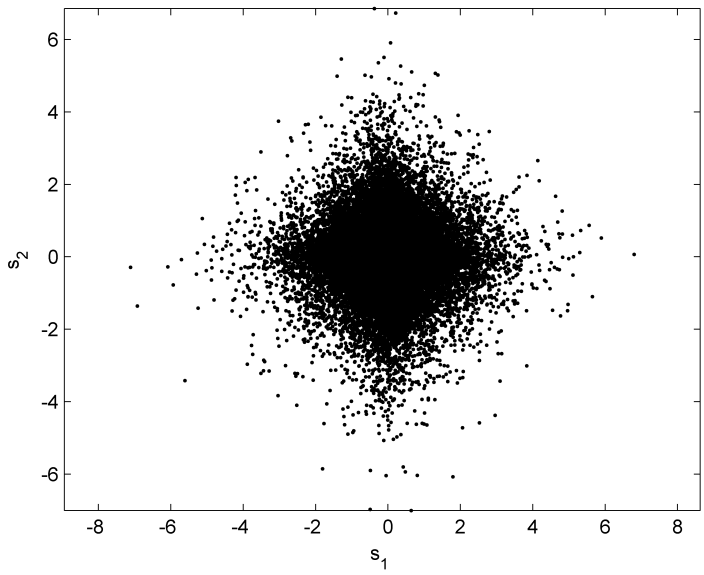

Figure 3.10: Two-dimensional i.i.d. Laplacian source.

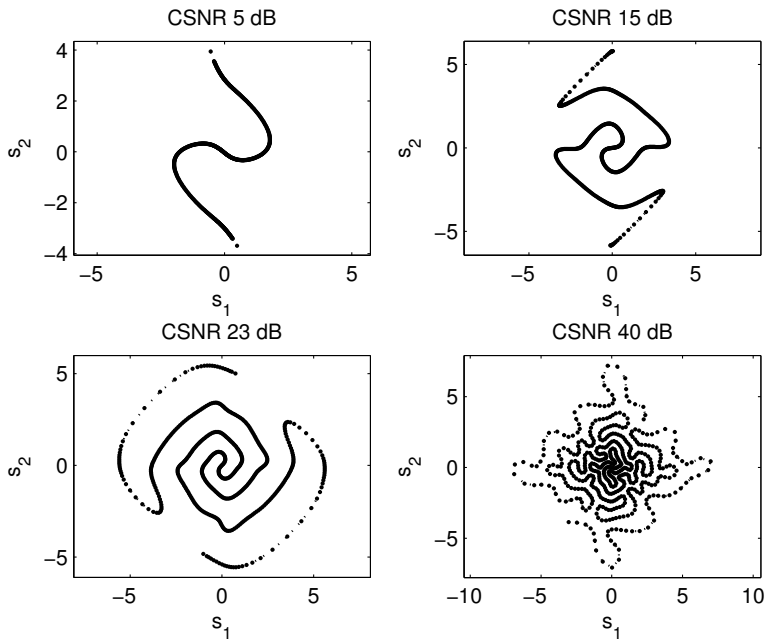

Figure 3.11: The PCCOVQ codebook trained for a Laplacian distributed source and AWGN channel using the algorithm proposed in [Fuldseth, 1997].

following sections.

Deforming the spiral mapping

Looking at the shape of the codebook in Figure 3.11 does not bring any immediate association with known space-filling curves. However, since the codebook's shape is similar to the Archimedes' spiral in the sense that it is doubly intertwined, unwinding from the center and out, one possibility is to try to deform the Archimedes' spiral to better match the PCCOVQ codebook. This was suggested in [Floor, 2003] for a 4:1 bandwidth reducing system consisting of two cascaded 2:1 mappings where the input to the inner mapping is Laplacian distributed.

Here, we use the same deformation approach to evaluate the performance of a 2:1 mapping for transmitting a Laplacian distributed source over an AWGN channel. The deformation can be done by representing the parametric representation of the spiral in its Fourier series expansion. Then, by changing the parameters, the shape of the spiral will change. With some

trial and error, it is possible to find a somewhat resembling shape, but as there are three parameters determining the shape, it is very difficult to try to optimize the parameters, given the source and channel distribution. In parametric form, the two spiral arms are given as [Floor, 2003]

$$\begin{aligned}\mathbf{u}_1 =& \frac{\Delta}{\pi}\theta^{1/k}\left[\cos\left(\theta - \frac{3\pi}{16}\right) + m\sin\left(3\theta\right)\right]\vec{i} \\ &+ \theta^{1/k}\left[\sin\left(\theta - \frac{3\pi}{16}\right) + m\cos\left(3\theta\right)\right]\vec{j}. \qquad (3.24)\\ \mathbf{u}_2 =& \frac{\Delta}{\pi}\theta^{1/k}\left[\cos\left(\theta - \frac{3\pi}{16} - \pi\right) + m\sin\left(3\theta - \pi\right)\right]\vec{i} \\ &+ \theta^{1/k}\left[\sin\left(\theta - \frac{3\pi}{16} - \pi\right) + m\cos\left(3\theta - \pi\right)\right]\vec{j}, \qquad (3.25)\end{aligned}$$

where $m \in [0, 0.3)$ determines the deformity (shape) of the spiral; $m = 0$ being no deformity, giving a circular mapping (Figure 3.12d) and $m = 0.3$ being most deformed, giving a diamond shaped mapping (Figure 3.12a). The parameter k determines how the spiral arms unwind; $k = 1$ provides a uniform distance between the spiral arms, $k > 1$ decreases the spiral arm distance as the spiral winds outwards (Figure 3.12d), and $k < 1$ increases the distance, making it less dense as it winds outwards (Figure 3.12a-c). Whereas Figure 3.12a most resembles the Laplace distribution in Figure 3.10 and Figure 3.12b most resembles the PCCOVQ codebook in Figure 3.11, what provides the best result is in fact the geometry in Figure 3.12c. In this case, using the PCCOVQ codebook was not successful, and a geometry which is more circular works the best. What seems more important is to have the spiral arm distance grow as radius (or angle) increases. This is intuitive, as the Laplacian is a more peaky distribution than the Gaussian.

In any case, hoping to optimize the geometry for the Laplacian case may seem futile as the three parameters Δ, k, and m are strongly coupled and the distortion statistics change considerably when adjusting the parameters. This makes it very difficult to find an analytic expression for the distortion, and for now we have to rely on the iterative approach where the range of one parameter is swept while keeping the others fixed, and do this for each parameter in turn.

Warping the input distribution to fit the Gaussian spiral

Instead of trying to create a mapping with a geometry matching the Laplacian source distribution, we might try to warp the source in such a way that

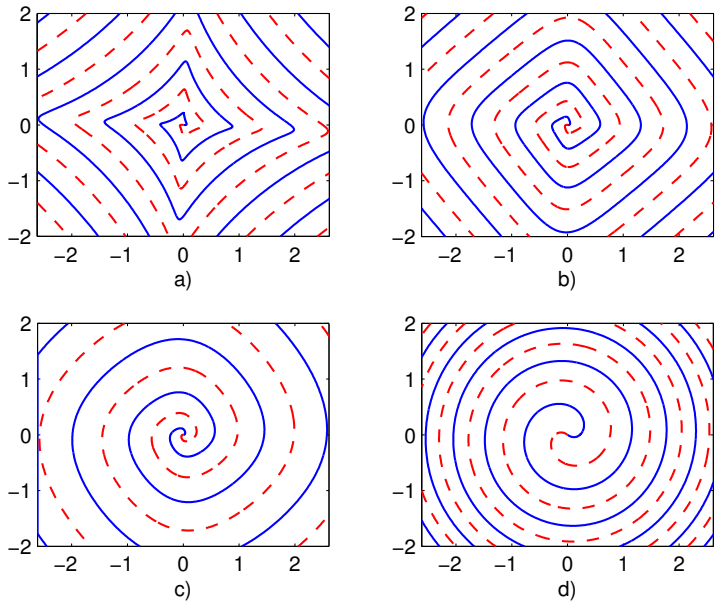

FIGURE 3.12: Shows the effect of the parameters in (3.24). a) $\Delta = 0.2$, $k = 0.8$, $m = 0.25$, b) $\Delta = 0.15$, $k = 0.8$, $m = 0.1$, c) $\Delta = 0.1$, $k = 0.68$, $m = 0.03$, d) $\Delta = 0.1$, $k = 1.5$, $m = 0$.

the distribution becomes more Gaussian-like. That would enable us to use the Archimedes' spiral and the optimization results from Section 3.2.1. If this warping-approach could be applied without too much negative impact in terms of amplified channel noise, several problems would be avoided:

1. The problem of actually finding the optimal geometry of the mapping for the Laplacian case. As explained in the previous section, there are three parameters, more or less inter-dependent, which have to be determined.

2. By using the Archimedes' spiral with its regular structure, the encoder would be simpler.

3. With fewer parameters needed to describe the geometry, there is less side information to transmit. (Although this is less important.)

The warping can be achieved as a simple transformation of a random variable $S \in \mathbb{R}$. If the input distribution is given as S, the desired warped distribution is $\tilde{S} \in \mathbb{R}$, then we need to determine the monotonic function w which gives

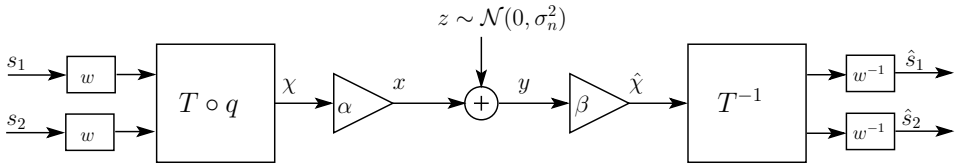

FIGURE 3.13: 2:1 Shannon mapping for Laplacian distributed source. The input is warped from Laplacian to Gaussian by applying the function $w(s)$.

us $\tilde{S} = w(S)$. This is slightly different from the standard problem of finding the resulting distribution from a transformation of a random variable, but the starting point is the same. Defining our sample spaces $\mathcal{S}$ and $\tilde{\mathcal{S}}$ as follows,

$$\mathcal{S} = \{s : f_S(s) > 0\} \tag{3.26}$$

$$\tilde{\mathcal{S}} = \{\tilde{s} : \tilde{s} = w(s) \text{ for some } s \in \mathcal{S}\}, \tag{3.27}$$

where $f_S(s)$ is continuous on $\mathcal{S}$ and $w^{-1}(\tilde{s})$ has a continuous derivative on $\tilde{\mathcal{S}}$ then we have [Casella and Berger, 2002, Theorem 2.1.5]

$$f_{\tilde{S}}(\tilde{s}) = f_S(w^{-1}(\tilde{s})) \left| \frac{dw^{-1}(\tilde{s})}{\tilde{s}} \right| \quad , \tilde{s} \in \tilde{\mathcal{S}}. \tag{3.28}$$

Substituting $\tilde{s} = w(s)$ and $w^{-1}(\tilde{s}) = s$ into (3.28) and rearranging, we obtain the following differential equation:

$$f_{\tilde{S}}\left(w(s)\right) \left| \frac{dw(s)}{ds} \right| - f_S(s) = 0. \tag{3.29}$$

Now, we want the $\tilde{S}$ to be Gaussian distributed with zero mean:

$$f_{\tilde{S}}(\tilde{s}) = \frac{1}{\sqrt{2\pi}\sigma} e^{-\frac{\tilde{s}^2}{2\sigma}}, \tag{3.30}$$

and S to be Laplacian distributed with zero mean:

$$f_S(s) = \frac{1}{2\lambda} e^{-\frac{|s|}{\lambda}}. \tag{3.31}$$

Substituting (3.30) and (3.31) into (3.29) we obtain

$$\frac{1}{\sqrt{2\pi}\sigma} e^{-\frac{w^2(s)}{2\sigma^2}} \left| \frac{dw(s)}{ds} \right| - \frac{1}{2\lambda} e^{-\frac{|s|}{\lambda}} = 0 \tag{3.32}$$

Solving this analytically with respect to $w(s)$ is impossible as the Gaussian does not have an closed-form cumulative density function (cdf), so we have to utilize some numerical method like the Runge-Kutta method [Edwards and Penney, 1996]. Since the Laplacian tails are significantly longer than the Gaussian, we have to make $\sigma^2_{\tilde{S}}$ smaller than σ^2_S to avoid clipping the large values. The variance of a Laplace distribution is $\sigma^2 = 2\lambda^2$, so we relate the variances of the the input σ^2_S with the output $\sigma^2_{\tilde{S}}$ as $\sigma^2_S = 8\sigma^2_{\tilde{S}}$. This was found through trials to produce good results. The numerical solution to (3.32) is shown in Figure 3.14 as the blue solid line. Since one can obtain a Laplace distribution by summing two squared Gaussians (Appendix A) and the the solution in the figure shows square-root behavior, it seems reasonable to try to perform a curve-fit of a square-root function onto the numerical solution. The simplest good fit which was found was

$$w(\pm s) = \pm\sqrt{(\pm s)^{1.022} + 0.379} \mp 0.616. \tag{3.33}$$

To check how well this warping function work, we try it on a Laplacian distributed variable. Figure 3.15 shows the resulting histograms along with a true Gaussian with the same variance as as the warped variable in b). The warping function does not produce a true Gaussian, and using the algorithm described in [Wang et al., 2005] estimates the relative entropy between Figure 3.15b and Figure 3.15d to be 0.0195 bits. One problem with the warping function, though, is the tendency to create either peaks or gaps around zero if the initial distribution is not a true Laplacian. Another more serious problem is illustrated in Figure 3.15c, where we see that the inverse $w^{-1}(\tilde{s} + z)$ amplifies noise, whether noise comes from the approximation process or the channel. If we try to reduce the loss described in Section 2.2.1, by forcing the Laplacian distributed *channel* symbols in Section 3.2.1 into a more Gaussian distribution using the warping function $w(s)$, we see no gain, but rather a drop in performance due to the amplified channel noise. However, using the warping function to reduce the input distribution mismatch described in Section 2.2.6 when the input is Laplacian distributed, the gain from having a correct input distribution outweighs the noise amplification, and we see a 1 dB SNR gain compared to just using the Archimedes' spiral without modifications.

Simulation

To determine which of the two methods presented in Section 3.2.2 are better for handling the Laplacian source, all we can do is to run simulations since

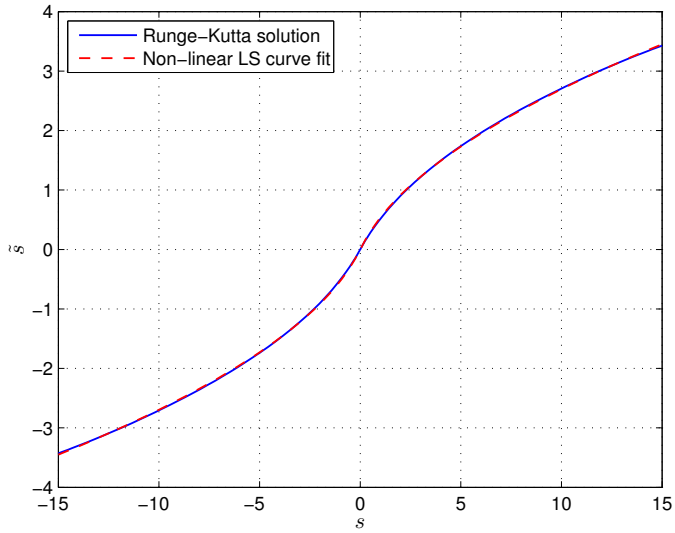

Figure 3.14: The output from the Runge-Kutta solver to the warping function (3.32), with the according curve-fit solution in (3.33).

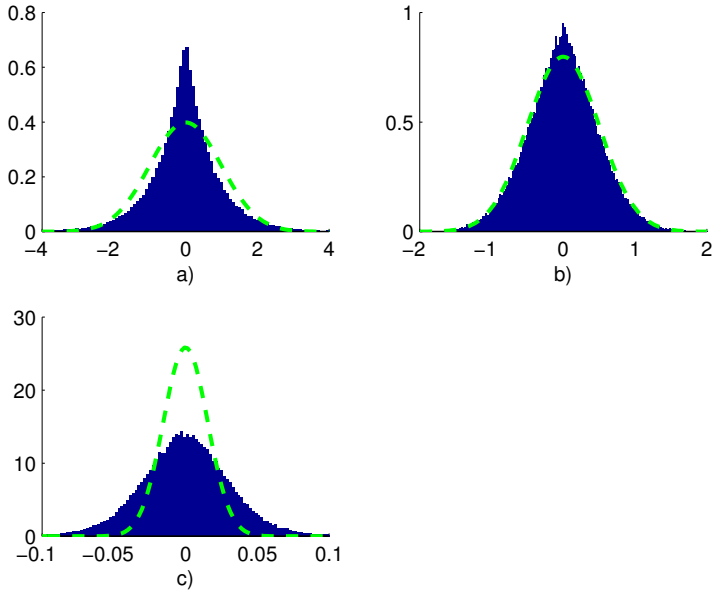

Figure 3.15: Histograms showing the results of the warping function (3.33). a) Original Laplacian distributed variable (blue) with the desired Gaussian (green dashed), b) warped variable (blue) with the optimal Gaussian of the same variance (green dashed), c) The de-warped noise distribution (blue) with the original added Gaussian noise (green dashed).

we have no theoretical model of neither one of them. Whereas the warping approach benefits from the optimizations in Section 3.2.1 while suffering from noise amplification in the unwarping. The deformation approach suffers from the fact that the parameters cannot be optimized at the time of writing, and they have been determined by fixing two parameters and varying one, then vary another while keeping two parameters fixed. Then, go back to the first and do the same iterations again until the result does not improve any longer. Still, we see from the simulation results in Figure 3.16 that the deformation approach has 0.2 dB advantage over the warping approach, since the warping function in (3.33) results in signal dependent channel noise. Still these two systems are only 1.4 and 1.6 dB away from OPTA for a Laplacian source and an AWGN channel, despite not being properly optimized.

Since we used the codebooks from the PCCOVQ to determine the geometry of the subspace in the approximation function q, we compare the performance of the Shannon mapping using the deformed Archimedes' spiral, with the results of the PCCOVQ. The codebooks of the PCCOVQ were trained using $4 \cdot 10^6$ training vectors drawn from an i.i.d. Laplacian source, and an AWGN channel. Codebook sizes ranging from 8 to 1024 were trained for each (integer) CSNR value. Again, like in the Gaussian case, this requires a significant amount of storage and in practice codebooks for only a few number of channel states would be used. This would slightly reduce the performance for the PCCOVQ. The Shannon mapping using the simple warping approach needs no storage, and its parameters are determined using the results from Section 3.2.1. The deformed mapping, however, must be determined for different CSNR values. However, no storage is needed here either, since the parameters can be determined using a polynomial curve fit on the parameter data.

Looking at Figure 3.17, the deformed Archimedes' spiral performs quite respectably, beating the PCCOVQ for CSNR values above 30 dB. Considering that fact that our system is not properly optimized, there might be room for improvements too. Similar to the Gaussian case, the training algorithm of the PCCOVQ produces codebooks with increasingly irregular structure as the CSNR increases, indicating that there is room for improvement in the PCCOVQ's training algorithm as well.

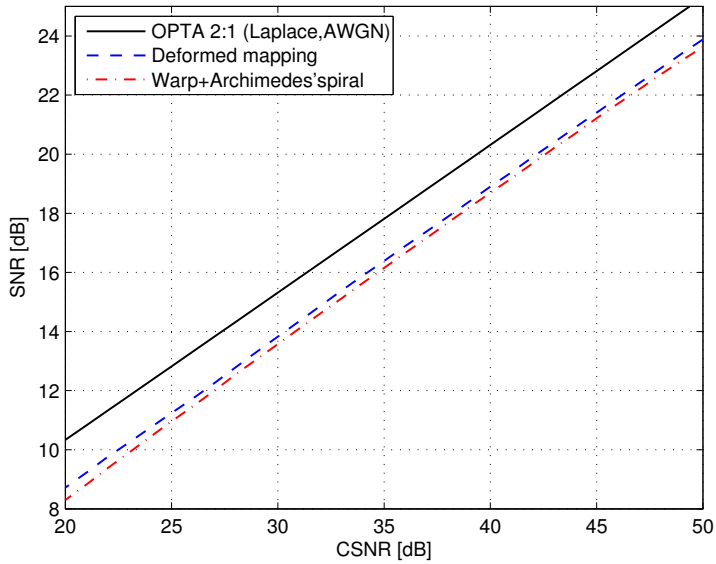

Figure 3.16: SNR vs. CSNR for the 2:1 bandwidth reduction mappings for an i.i.d. Laplacian source and an AWGN channel. The two techniques described in Section 3.2.2 are compared, showing a slight advantage to the deformed mapping.

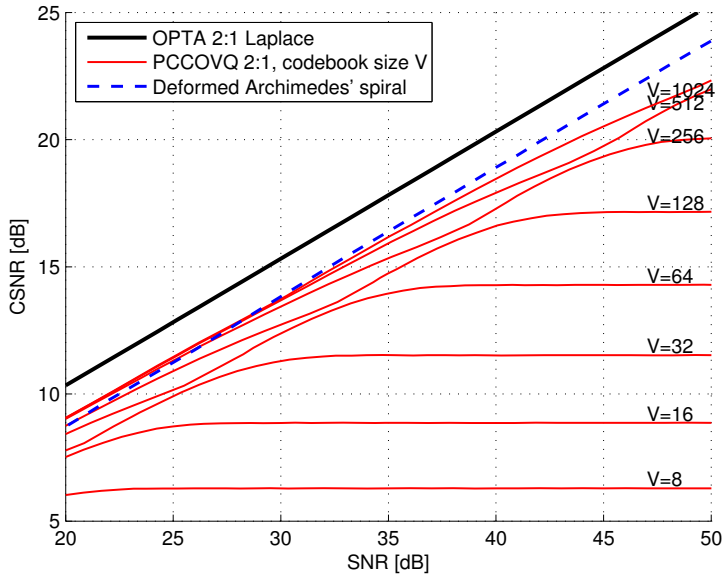

Figure 3.17: SNR vs. CSNR for the deformed spiral mapping, compared to PCCOVQ optimized for an i.i.d. Laplacian source and an AWGN channel.

3.3 Achieving 4:1 Dimension Reduction by Cascading 2:1 Mappings

As the number of dimensions in the mapping increase, it becomes harder and harder to determine the optimal geometry of the mapping and optimize the associated parameters. Moreover, unless the geometry shows considerable structure or symmetry, the encoder/decoder pairs might become prohibitively complex, just like in case of high-dimensional vector quantization. Some work has been done on bandwidth compression for M:1 systems with $M \gg 2$ [Floor, 2003; Floor and Ramstad, 2006c], but still no method to determine the geometry and parameters is known to exist.

In order to circumvent those issues, one could try to reduce the complexity by decomposing the problem into smaller sub-problems just like tree-structured VQ, multi-stage VQ, shape-gain VQ etc. [Gersho and Gray, 1992]. For the bandwidth-reducing Shannon mappings, the most obvious approach is to use a tree-structure where several mappings are cascaded. First, the M source samples are combined with a given set of mappings. Then the output of these mapping are again combined with another (or possibly the same) set of mappings. This can be iterated further until there is only one sample from the output, ultimately providing a dimension reduction M:1.

Just like with tree-structured VQ, the performance is expected to be inferior to the full-search solution (if such exists). However, the reduced complexity can potentially outweigh a small performance loss.

Since the 2:1 mapping for the Gaussian source and AWGN channel is relatively close to OPTA, it seems reasonable to try to cascade two layers of 2:1 mappings, thereby achieving 4:1 compression, as was tried in [Floor, 2003]. There, the parameters of the two cascaded mappings were determined with a full search. In order to make this approach more practical, we will try to determine the parameters in a more automated fashion, using the results from Section 3.2.

In Section 3.2.1 it was mentioned that the output from the mapping is Laplacian distributed, meaning that the input to the second layer is Laplacian instead of Gaussian. This implies that the solutions from Section 3.2.2 could be used for the inner mapping. However, already suffering from the lack of rigorous optimization in the 2:1 case we cannot hope to see optimal results. At best, this is a feasibility study to see whether the results of the 2:1 case are transferable to the 4:1 case.

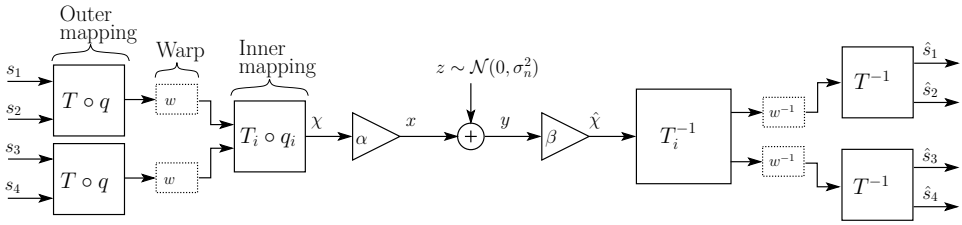

FIGURE 3.18: The 4:1 dimension reducing mapping for a Gaussian source and AWGN channel. with intermediate warping to "Gaussianize" the input to the inner mapping as was done in Section 3.2.2. Alternatively, one can omit the warping and rather change $T_i \circ q_i$ to match Laplace distribution as was done in Section 3.2.2.

3.3.1 Outer 2:1 Mapping

The input to the outer mapping is Gaussian distributed, and the regular Archimedes' spiral described in Section 3.2.1 can be employed with some modifications. Looking at Figure 3.18, we see that the noise input on the outer mapping is the total noise output from the inner mapping. According to (3.21) this was shown to be $\Delta_i^2/12$, where Δ_i denotes the spiral arm distance of the inner mapping. Using (3.19), replacing σ_n^2 with $\Delta_i^2/12$, and setting $P = 1$ we find the spiral arm distance of the outer mapping to be

$$\Delta_o = 2\pi\sigma_s \sqrt[4]{\frac{6 \cdot 0.16^2 \Delta_i^2/12}{1}} = 2\pi\sigma_s \sqrt[4]{\frac{0.16^2 \Delta_i^2}{2}}. \tag{3.34}$$

Similar to (3.21), the noise per source sample on the output of the outer mapping will be $\Delta_o^2/12$ which agrees with simulations.

3.3.2 Inner 2:1 Mapping

From Section 3.2.1, we know that the output of the regular Archimedes' spiral with the curve length approximation is Laplacian distributed. This means that if we use the approach from Section 3.2.1 in the outer mapping, the input to the inner mapping will be Laplacian. Thus, some modifications might be needed for the inner mapping. Either the input distribution can be warped into something more Gaussian by applying some non-linear function, or the mapping can be changed to better fit the Laplace distribution. We now explore these two approaches to see whether one holds an advantage over the other, as was the case for the 2:1 mapping in Section 3.2.2.

Deforming the spiral mapping

Instead of warping the input to the inner mapping, it is possible to change the inner mapping into something more suitable for the Laplace distribution. This was proposed in [Floor, 2003] and the curve which was used was the same as in (3.24). Unfortunately, a method to determine the optimal parameters was not given in the thesis. Rather, the parameters k and m were determined though trial-and-error, Δ_o and Δ_i were set to one, and the optimal channel noise power was then determined though simulation. However, since we in Section 3.2.2 found that there is a fixed relationship between Δ_i and σ_n^2, we can fit a polynomial onto the curve $\Delta_i(\sigma_n^2)$ under an mse criterion. Then, simply evaluate the polynomial at any CSNR (in dB) to determine the correct Δ_i. The fourth-order polynomial we used has the coefficients

$$\begin{aligned} p = (&6.6564 \cdot 10^{-7}, -6.8211 \cdot 10^{-5}, \\ &2.6931 \cdot 10^{-3}, -4.6654 \cdot 10^{-2}, 3.0003 \cdot 10^{-1})^t, \end{aligned} \tag{3.35}$$

where t denotes transposition, and we find the parameter of the inner spiral using the polynomial

$$\Delta_i = p(\gamma_{dB}) \cdot \sigma_n^2. \tag{3.36}$$

Warping the input distribution to fit the Gaussian spiral

Since the mapping parameter T in the outer mapping in Figure 3.18 to a great extent determines the resulting input distribution of the inner mapping, we can try to change T in such a way that the output becomes more Gaussian. This is equivalent to applying a warping operation between the outer and inner mappings, forcing the Laplace distribution into something more Gaussian. This was shown in Section 3.2.2, and we use the same warping function given in (3.33). The parameter is determined using (3.19), but as opposed to the 2:1 case, the resulting noise from the inner mapping is divided over four channel samples, yielding a distortion per source sample equal to $\Delta_i^2/24$.

3.3.3 Comparing the warping approach to the deformed inner mapping

Neither of the two approaches to used to deal with the Laplacian distributed intermediate signal in the 4:1 mapping (Section 3.3.2), are rigorously opti-

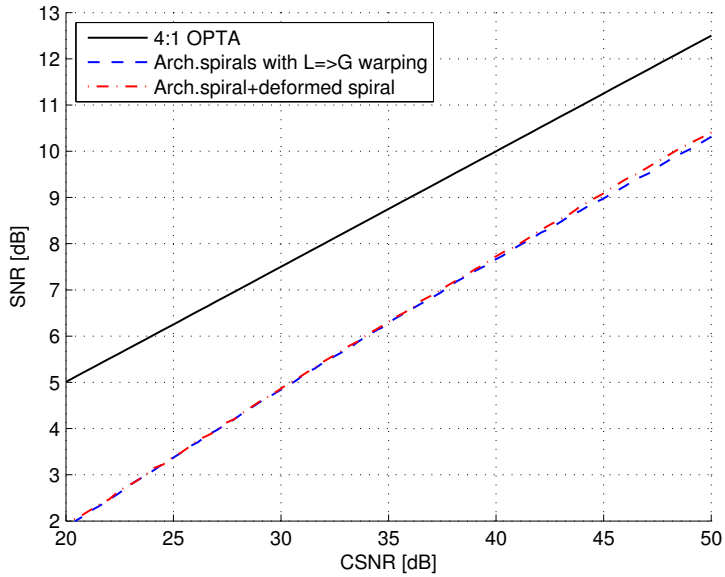

Figure 3.19: SNR vs. CSNR of a 4:1 mapping consisting of a cascade of two 2:1 mappings for a Gaussian source and an AWGN channel, where the two approaches described in Section 3.3.2 are compared.

mized. Still, it is interesting to compare their performance in order to have an indication of whether the more difficult optimization and increased encoder complexity of the deformed mapping is worth the effort. For the 2:1 Laplacian case in Section 3.2.2 there was clearly a benefit using the deformed mapping, despite the fact that its parameters were determined through an iterative search procedure not covering all parameter combinations (thus a global optimum is not guaranteed). For the 4:1 case, however, the channel noise, which is amplified in the warping process, is distributed over four source samples instead of two. This means that the benefit of the deformed mapping is less clear. Figure 3.19 shows a comparison of the warping approach and the deforming approach, and we see that they perform relatively close except at high CSNR. Compared to the 2:1 Laplacian case in Section 3.2.2, the difference is now significantly less.

Figure 3.20 shows that the robustness we saw in the 2:1 case for Gaussian sources is still intact. The reduced slope of the OPTA curve for the 4:1 leads to a more gracefully degrading performance, but also a less gracefully improving performance, when comparing to the 2:1 case. To illustrate the difficulties related to the increased dimensionality, we compare the performance of the cascaded-mapping approach to both the PCCOVQ and systems

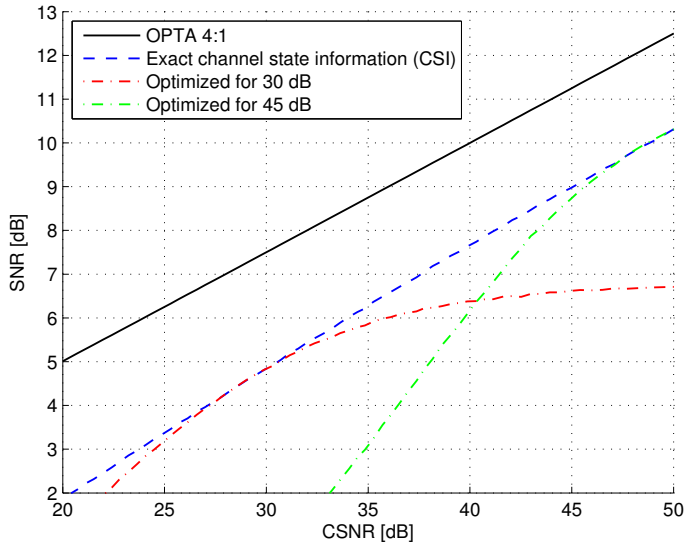

Figure 3.20: SNR vs. CSNR for a 4:1 mapping by cascading two 2:1 mappings and intermediate warping of Laplace⇒Gaussian distribution to fit the inner spiral. The dashed-dotted curves show that robustness is maintained.

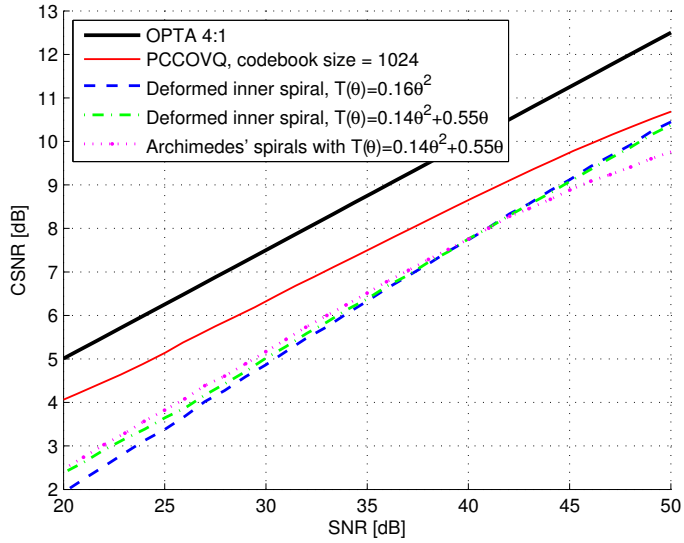

Figure 3.21: The 4:1 Shannon mapping consisting of two cascaded 2:1 mappings compared to the PCCOVQ. The PCCOVQ clearly outperforms the Shannon mappings. The lack of optimization of the deformed spiral can be seen at lower CSNR values, where even a system using only Archimedes' spirals with no warping outperforms the deformation approach.

using a different T-operator[4]. Figure 3.21 shows that the PCCOVQ clearly outperforms the proposed methods in this section by a large margin. By changing to a different T-operator, which was found to be better for the 2:1 Gaussian case in [Floor, 2003], performance can be improved for lower CSNR. In that case, however, the optimization is no longer valid as the distribution after the mapping process changes depending on the CSNR. Further improvements are expected if the systems are re-optimized with the new T-operator given as $T(\theta) = 0.14\theta^2 + 0.55\theta$ [Floor, 2003]. Even a system using only regular Archimedes' spirals and the polynomial T-operator provides better performance below 40 dB CSNR, so there is clearly room for improvements. However, compared to the PCCOVQ, the proposed method shows a 1-1.5 dB loss in performance. Although not shown in the plots here, the direct 4:1 bandwidth-reducing mapping presented in [Floor and Ramstad, 2006c] is 1.4-2 dB in SNR away from OPTA, hence outperforming the cascaded mapping (at lower CSNR). As indicated in Figure 3.21, more careful choice of T-operator is expected to improve the cascaded mapping even further, making it competitive with a real 4:1 bandwidth reducing mapping.

[4]This 2^{nd} degree polynomial curve fit on the spiral arm length (as opposed to the quadratic term used earlier)

Chapter 4

Quantization of the Shannon-Kotel'nikov Mappings

"When solving problems, dig at the roots instead of just hacking at the leaves."

- Anthony J. D'Angelo, The College Blue Book

4.1 Introduction

The S-K mappings presented in Chapter 3 show good potential, exhibiting both high spectral efficiency and robustness against channel variations. This makes them suitable for wireless communication over time-varying channels, or channels where the channel state is not exactly known at the transmitter. In the cases where the receiver is simply decoding the received signal, without the need for further transmission on digital networks or storage channels, the continuous-amplitude nature of the S-K mappings pose no problem. However, there are scenarios which require an intermediate digital representation; for example, heterogeneous networks which contain a mix of wired and wireless links of possibly different communication technologies. An example is cellular mobile communication systems which have wireless links between the mobile units and the base stations, whereas digital transport networks connect the different base stations and the rest of the telephony system. These transport networks are fully digital systems where the S-K mappings are unsuitable. It should be mentioned that today's mobile communication systems are fully digital as well, thus introducing S-K mappings

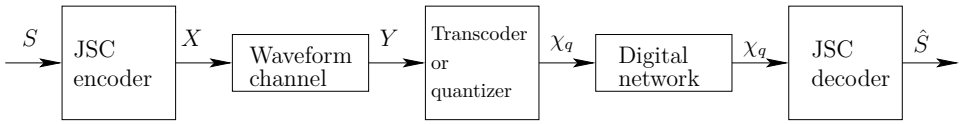

Figure 4.1: The conceptual communication chain. The wireless channel accepts continuous-amplitude channel symbols from the JSC encoder, but the digital nature of the succeeding network requires a transcoding or digitization of the channel symbols Y prior to further transmission.

into existing systems is not trivial. Another example is storage channels like hard drives and CD-ROMs, which only store binary numbers. In order to use S-K mappings in this context, we need to digitize, or transcode, the mappings to enable a digital representation.

In this chapter, we will thus explore the possibility of using S-K mappings in heterogeneous communication systems where intermediate bit-representations are necessary. We want solutions which show as little performance loss as possible, while keeping the complexity low. The need for joint optimization of the mapping and the transcoding will also be investigated. Obviously, having as little coupling as possible between the different parts in the communication chain is desirable since it provides increased flexibility with respect to later changes of system components. This means that a change in one part of the system does not call for a complete re-optimization of the entire communication chain, and new inventions can easily be integrated into existing system designs with little effort. Whenever there is a deliberately introduced coupling between different parts of a communication system, hopefully to improve system performance compared to the separate layers of the OSI model [Wikipedia, 2007a], the result is a cross-layer design (CLD) [Kawadia and Kumar, 2005; Srivastava and Motani, 2005]. The S-K mappings is an example of a CLD between the application layer and the physical layer. If we have to include the digitization of the S-K mappings in the optimization process, it becomes more and more difficult to obtain optimal solutions.

Using some of the proposed schemes in Chapter 3, we demonstrate the possibility of performing simple transcoding at the interface between the wireless and wired systems. We show that transcoding can be done separately with little loss if the quantizer rate is close to the channel capacity (of the wireless channel), whereas joint optimization of mapping and transcoding is needed if the quantizer rate is lower than the channel capacity.

4.2 Heterogeneous Communication Systems and the Need for Digital Representations

The word *heterogeneous* is of Greek origin and is a compound of *heter*, meaning different, other, another, unlike, and *geno* meaning race, kind; line of descent. The word heterogeneous would in our context be used with the meaning *different kind*. Thus, heterogeneous communication systems, or a heterogeneous network, is a communication system composed of different kinds of non-similar communication links between the sender and the receiver. An example is a person with a mobile phone calling a person with a standard fixed-line phone. The speech signal would then travel over a heterogeneous network consisting of a wireless link (mobile to base station), a digital transport network (base station to the fixed-line central) and finally a circuit-switched wired network (central to fixed-line phone). Along the way, the signal is represented in different ways; the mobile phone uses a low-rate linear prediction-based speech codec like EFR [Jarvinen et al., 1997] with channel codes and interleaving suited for the wireless channel, the transport network is usually a packet-based IP network just carrying the speech data in any form, whereas the circuit-switched connection can be for instance ISDN using A-law companded PCM [Jayant and Noll, 1984] with a 4 binary, 3 ternary line code (4B3T) [Barry et al., 2004].

The S-K mappings from Section 3 would most likely find themselves as a replacement for quantizers and channel coding on the *wireless link* in the example above. It is reasonable to assume that for wireless channels, the use of continuous-amplitude channel symbols is not a problem, since we are in principle free to determine which modulation and coding to use. However, the situation is different when we want to communicate over digital transport networks. These rely on standardized protocols adhering to the Open Systems Interconnection (OSI) model with isolated layers, implying that all data will be treated equally regardless of the origins. Hence, the same representation is required for all data. Since services like file transfer and e-mail are digital and requires error-free transmission, digital representations of analog sources would be necessary. In other words, in a heterogeneous communication systems consisting of both wireless links and transport networks, the continuous-amplitude S-K mappings need to be digitized or transcoded into a representation suitable for the digital transport network.

The conceptual communication chain to be examined in this chapter is shown in Figure 4.1, where χ_q is a digital representation of the continuous-amplitude channel symbol which can be sent over the digital network (as-

sumed transparent). At the receiver, the digitized output of the S-K mapping is decoded.

4.2.1 Alternatives for Digitizing the Mappings

There are two alternatives for creating a digital representation of a continuous-amplitude S-K mapping: Either we can decode the mappings at the intermediate wireless receiver and re-encode with a standard digital source coder suitable for the source signal, or we can transcode the mapping directly into a suitable digital representation and decode the mapping at the ultimate destination. Since the transcoding approach potentially provides lower complexity and delay, we primarily want to develop methods for efficiently transcoding the mappings. To measure the efficiency of the transcoding, we compare its performance both to an ECVQ applied to the received and decoded Y in Figure 4.1, and to a fully digital system using an ECVQ and adaptive, coded modulation (ACM).

Decode and Quantize

The most apparent way to obtain a digital representation is to first decode the S-K mapping and subsequently apply either a scalar or a vector quantizer to obtain a digital representation. When using vector quantizers with variable cell sizes, it is necessary to design the quantizer codebooks by using a training data set. The resulting codebooks would have to be stored at the decoder. Apart from the increased delay and complexity caused by the decode and re-encode operation, the necessity for storing the codebooks might be prohibitive if a large number of different rates are required.

Here, we employ a 2-D ECVQ [Chou et al., 1989] to quantize the decoded symbol. To design the codebooks of the ECVQ, we use a training set of decoded source samples from the S-K mapping. The reason for using the ECVQ is that it enables designing the codebooks with arbitrary rates, making the comparison to the transcoding approach easier. Although restricting the dimensionality of the ECVQ to two dimensions, something which can only come as close as 1.36 dB away from the R-D bound [Lookabaugh and Gray, 1989], increasing dimensionality further would be unfair to the transcoding using a scalar quantizer (which equals a 2-D VQ in the compressed state). Of course, the transcoder could also be designed using higher

dimensional vector quantizers, thereby increasing its performance. However, we want to keep the complexity low and tractable.

Transcode

The word *transcode* is used with several different meanings in the literature. Sometimes it is used to describe the process of going from one compressed format to another with intermediate decoding to raw data representation [Wikipedia, 2007b]. That is what we called decode-and-quantize in the previous section. In this dissertation, transcoding is used when we go directly from one representation to another, without any intermediate decoding to native uncompressed format (i.e. conversion is performed in the compressed domain). An example of this would be to transcode an MPEG video directly to a lower resolution without decoding into native pixel representation.

Transcoding the S-K mappings to a digital representation would simply be to take the received channel symbol, digitize it using a suitable quantizer, entropy code if necessary, then forward the digitized mapping to the receiver. At the receiver, "inverse" quantization would be done and the mapping decoded as usual. This reduces complexity compared to decode-and-quantize since it avoids inverse-mapping at intermediate nodes. Furthermore, since at least the bandwidth-reducing mappings are already "compressed" in the sense that M source symbols are represented by 1 (or N) channel symbols, simpler quantization schemes are needed to achieve the target SNR after digitization.

In the following section we will explore the simple option of transcoding by applying a uniform scalar quantizer directly on the received 1-D channel symbols from the 2:1 S-K mapping for a Gaussian source and AWGN channel. The result is compared to the decode-and-quantize approach using a 2-D ECVQ applied to the decoded signal.

4.3 Quantizing the 2:1 Archimedes' Spiral

As was mentioned in the previous section, using a scalar quantizer on the 1-D channel symbols, the transcoding is equivalent to a 2-D VQ used in the source space (Figure 4.2).

Figure 4.3 shows the mapping corresponding to the unquantized mapping in Figure 3.4. The channel space which lies along the spiral arms is quantized

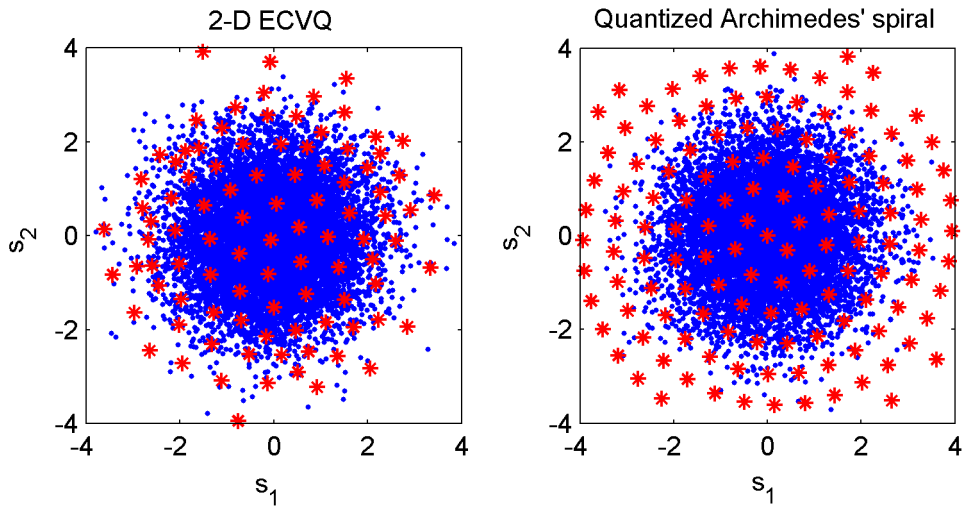

Figure 4.2: Comparison of a 2-D ECVQ and the quantized Archimedes' spiral. The blue dots represent the source distribution and the red stars represents the reconstruction points. The entropy of both system is 5.3 bits, but the quantized spiral has the advantage of an easily extensible "codebook" to cover outliers.

with an SQ. At the receiver, the inverse operation of the mapping produces a 2-D VQ, where the representation values are restricted to the subspace spanned by the approximation operation $q()$ (i.e., the spiral arms). Compared to the unquantized system in Section 3.2.1, the system now has two parameters; the spiral arm distance Δ and the quantizer step δ_Q. Assuming that both the source and noise distributions are bounded, the quantization indices are countable and can be assigned to codewords of finite length. Then any redundancy due to non-uniform probability of the indices could be removed with entropy coding.

One important question is whether or not the mapping and transcoding need to be jointly optimized, or if it is possible to use the results from Section 3.2 for the mapping operation, and then optimize the quantizer used as a transcoder separately? Moreover, is there a difference between performing the transcoding at the receiver side or at the transmitter side? The obvious benefit of a transmitter-side transcoding would be that the transmitted channel symbols on the wireless channel will be discrete multi-level symbols (as opposed to the continuous-amplitude representation in Chapter 3). Although it is out of the scope of this dissertation, it is worth mentioning that the multi-level symbols would result in simplified symbol timing recovery due to the (possible) existence of open eye curves. To do

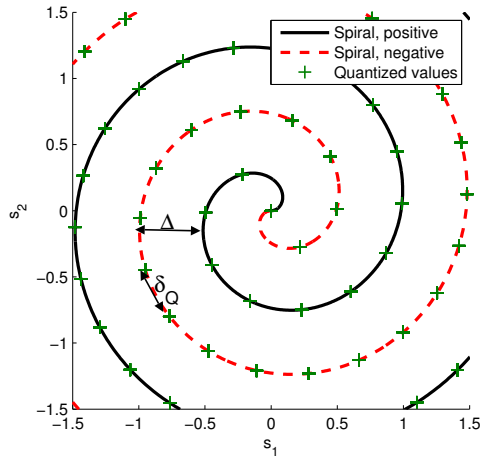

Figure 4.3: Quantized S-K mapping. The plane constitutes the source space and the spiral constitutes the channel space. The transcoding operation performs quantization directly on the received channel symbols, effectively providing a finite, countable set of representation levels along the spiral arms.

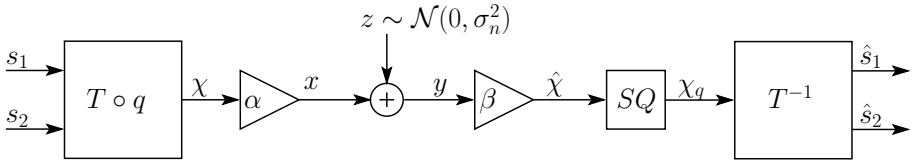

Figure 4.4: Block diagram of receiver-side transcoding.

timing recovery for the continuous-amplitude signals, some sort of pilot-based timing recovery approached must be employed [Yang et al., 2000].

4.3.1 Quantization after reception

Let us now assume that we want to transmit a Gaussian source over an AWGN channel, where the bandwidth of the channel is half of the source as in Section 3.2.1. When performing quantization at the receiver side, we are free to either separately optimize the mapping and then quantize, or jointly optimize the mapping and the quantization given the transmit power and quantizer rate constraints. In both cases the distortion terms from Section 3.2.1 remain as they are, but we get an added distortion term for the quantization noise.

The benefits of quantizing at the receiver side, is that the receiver has access to the unquantized signal. This provides the best possible quality for immediate decoding, and transcoding can be done afterwards in case of storage or further transmission. The quality of the transcoded signal can be decided at the time of transcoding. Since both storage channels and transport networks generally have much higher capacity than wireless channels, spending more bits on the transcoding part to ensure maximum robustness on the wireless link could be beneficial.

Separately Optimized Mapping and Quantization

First we optimize the S-K mapping for the wireless channel, regardless of the bit rate constraint for the subsequent transcoding. The 2:1 S-K mapping is thus optimized for maximum unquantized performance as in Section 3.2.1, then transcoded at the receiver. Since the channel symbols x and y (Figure 4.4) are one-dimensional, we can use a scalar quantizer as the transcoder, apply entropy coding, and transmit the digitized signal χ_q over the network. At the receiver side, the inverse-mapping T^{-1} is applied to recover $\hat{s}_1$ and $\hat{s}_2$. The distortion from the S-K mapping will be the sum of the approximation error and channel noise, responsible for $\Delta^2/24$, each according to (3.20). If we use the high-rate assumption for the quantizer, we can approximate the quantization error as

$$D_Q = \frac{1}{2} \cdot \frac{\delta_Q^2}{12}, \tag{4.1}$$

where δ is the quantizer step (measured along the spiral arm) and the factor half is included since the error will on average be distributed equally over two source samples. For this approximation to hold, we must assume high CSNR so that the spiral is sufficiently dense, and that the rate is high so that δ is comparable to Δ. This ensures that the line segment between two quantizer levels are approximately straight, thus producing a quantization error variance close to (4.1).

Since there is no point in operating with a high rate when the distortion is dominated by the approximation and channel noise, we want to keep the rate proportional to the channel capacity. We do this by forcing the distortion due to quantization to be independent of the CSNR. This means that the performance curve of the quantized system should be parallel to the unquantized system when we plot SNR as a function of CSNR, and the quantizer will reduce its rate as the channel gets worse. To achieve this we

set

$$\frac{D_s}{D_s + D_Q} = \omega, \tag{4.2}$$

where D_s is the distortion for the unquantized system, D_Q is the quantization error, and ω is a constant. From (3.21) we have

$$D_s = \frac{\Delta_{opt}^2}{12} = \pi^2 \sigma_s^2 \sqrt{\frac{2 \cdot a^2}{3\gamma}}, \tag{4.3}$$

where $a = 0.16$ is the constant which makes (3.9) an approximation of the spiral arm length. Rearranging (4.2) and inserting (4.1) and (4.3), we obtain

$$\frac{\delta^2}{24} = \frac{1-\omega}{\omega} \cdot \pi^2 \sigma_s^2 \sqrt{\frac{2 \cdot a^2}{3 \cdot \gamma}}. \tag{4.4}$$

The quantizer step is thus given as

$$\delta = \sqrt{\frac{2(1-\omega)}{\omega}} \cdot 2\pi\sigma_x \sqrt[4]{\frac{6 \cdot a^2}{\gamma}} = \sqrt{\frac{2(1-\omega)}{\omega}} \cdot \Delta_{opt} = \Omega \Delta_{opt}, \tag{4.5}$$

where we recognize the the Δ_{opt} from (3.19). Hence, the quantization step is proportional to the spiral arm distance, and as the CSNR decreases, the Δ_{opt} increases, and thus δ also increases. Now we need to find the Ω in (4.5) in order to determine the resulting rate. Since we know that the channel symbols χ_q are Laplacian distributed (Appendix A), with the variance given in (3.16), we can use [Jayant and Noll, 1984, eq. 4.108]

$$H_Q(\chi_q) = h(\hat{\chi}) - \log_2(\delta), \tag{4.6}$$

to determine the quantization step. The differential entropy should be calculated over the pdf resulting from the sum of the Laplacian channel symbols and the Gaussian noise (convolution of the pdf's), i.e. $f_{\hat{\chi}}(\hat{\chi})$. Assuming we have high CSNR, we can replace $\hat{\chi}$ with χ in the differential entropy term of (4.6), since the sum of a Laplacian and a Gaussian where $\sigma_L^2 \gg \sigma_G^2$ is approximately Laplacian with variance equal to σ_L^2 [1]. Solving for δ we obtain

$$\delta = 2^{0.5 \log_2\left(2e^2\sigma_\chi^2\right) - H_Q(\chi_q)}, \tag{4.7}$$

[1] This assumption is obviously not accurate for low CSNR, but as we use a Wiener filter at the receiver in the simulations, the σ_χ^2 and $\sigma_{\hat{\chi}}^2$ are close, and thus (4.6) produces the correct rate.

where we set the quantizer rate $H_Q(\chi_q) = C - R_{offset}$, and R_{offset} is a rate "offset" in bits which determines the quantizer rate given the the channel capacity C for an AWGN channel:

$$C = \frac{1}{2}\log_2(1+\gamma), \tag{4.8}$$

where γ denotes the CSNR. Inserting (3.16), (3.19) and (4.8) into (4.7), we obtain

$$\begin{aligned}
\delta &= 2^{0.5\log_2\left(2e^2 2(2\eta\frac{\pi^2}{\Delta_{opt}^2}\sigma_s^2)^2\right)} 2^{-1/2\log_2(1+\gamma)} 2^{R_{offset}} \\
&= \frac{\sqrt{2e^2 a\pi^2\sigma_s^2\sqrt{\gamma/6}}\cdot 2^{R_{offset}}}{\sqrt{1+\gamma}} \\
&\overset{a)}{\approx} \frac{2^{R_{offset}} e}{\sqrt[4]{144}} \cdot \underbrace{2\pi\sigma_x \sqrt[4]{\frac{6\cdot a^2}{\gamma}}}_{\Delta_{opt}} \approx 0.7847\cdot 2^{R_{offset}}\Delta_{opt},
\end{aligned} \tag{4.9}$$

where we in a) have used the approximation $\frac{\gamma}{(1+\gamma)^2} \approx \frac{1}{\gamma}$, valid for $1 \ll \gamma$. This is done to be able to identify Δ_{opt} for the unquantized case (3.19).

Having determined Ω in (4.5), using (4.9) enables us to easily set the quantizer step to obtain a rate of $H_Q = C - R_{offset}$ bits while having a constant loss independent of the CSNR. The theoretical total distortion for this approach is

$$D_{tot} = \frac{\Delta_{opt}^2}{12} + \frac{\delta^2}{24}. \tag{4.10}$$

Looking at Figure 4.5, we see that the transcoder is around 1.75 dB away from the unquantized system, and performing on par with the 2-D ECVQ which has higher complexity. However, as the rate is reduced below the channel capacity, the transcoder loses significantly to the ECVQ. In this case, optimizing the mapping and the transcoding jointly should improve the transcoding performance at the expense of reduced unquantized performance.

Jointly Optimized Mapping and Quantization

The results in Figure 4.5 show that if we require a bit rate which is significantly lower than the channel capacity, the SNR of the quantized spiral drops rapidly. The reason for this is the resulting mismatch between Δ and

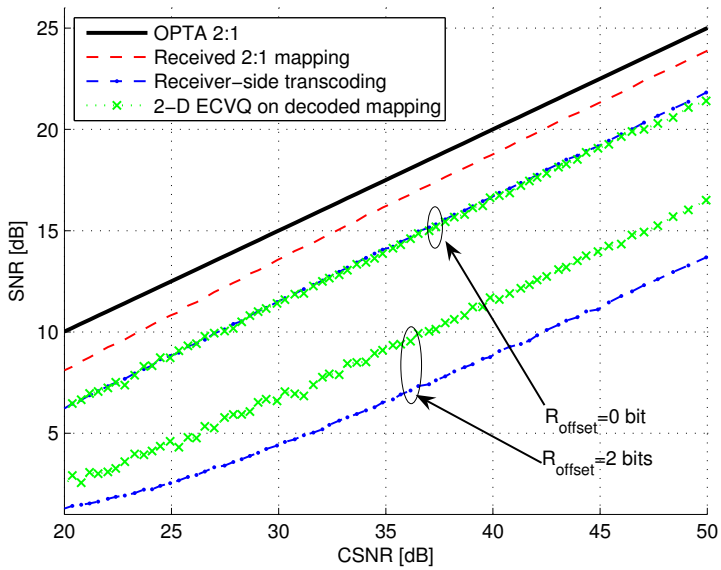

Figure 4.5: SNR vs. CSNR for the 2:1 Archimedes' spiral quantized with a uniform SQ. Gaussian source, AWGN channel. No joint optimization of mapping and transcoding. The quantizer rate is $H(\chi_q) = C - R_{offset}$. The decode-and-quantize approach clearly outperforms the transcoding for rates lower than the channel capacity.

δ. As the rate is reduced, leading to $\delta \gg \Delta$, the quantization levels in Figure 4.3 are spread out in a suboptimal manner, calling for a joint optimization of the two parameters. This co-optimization means that we will trade off some performance in the unquantized system for better quantized performance.

First we look at the case where we quantize after reception. We need to determine the optimal parameters Δ and δ (Figure 4.3), given a power constraint P on the channel and a rate constraint H_Q on the quantizer. Similar to the previous section, the channel symbols x and y (Figure 4.4) are one-dimensional. Hence, we can use a scalar quantizer as the transcoder, apply entropy coding, and transmit the digitized signal χ_q over the network. At the receiver side, the inverse-mapping T^{-1} is applied to produce the estimates $\hat{s}_1$ and $\hat{s}_2$.

Assuming that we operate in the high CSNR region and have high rate on the quantizer, the spiral will be dense and the error terms from the approximation onto the spiral and the quantization of the spiral are thus more or less orthogonal. Since the approximation onto the spiral can be

seen as a scalar quantizer in the radial direction (Figure 4.3), we use the common high-rate approximation of the scalar quantization error variance ($\Delta^2/12$) for the mapping approximation. Furthermore the high-rate uniform quantizer produces quantization noise which is uncorrelated with the input signal, so we use the common $\delta^2/12$ approximation here too. The distortion from the channel noise is simply this noise scaled with the constant β at the receiver. We end up with the following expression for the total distortion:

$$D_{tot}^{post} = D_a + D_Q + D_c = \frac{1}{2}\left(\frac{\Delta^2}{12} + \frac{\delta^2}{12} + \beta\sigma_n^2\right), \tag{4.11}$$

where the three terms represent respectively the distortion from approximation, quantization, and channel noise. We divide by two to get the per-component distortion. We set $\beta = 1/\alpha = \sqrt{\sigma_\chi^2/P}$ in the calculations for simplicity[2].

The quantizer rate is given as

$$H_Q \overset{a)}{=} h(\chi_q) - \log_2\delta = \frac{1}{2}\log_2(2e^2\sigma_\chi^2) - \log_2\delta = \log_2\left(\frac{4ae\pi^2\sigma_s^2}{\Delta\delta}\right), \tag{4.12}$$

where a) comes from [Jayant and Noll, 1984, eq. 4.108] and $h(\hat{\chi})$ is the differential entropy for a Laplacian source (assuming high CSNR so that $\hat{\chi}$ is still Laplacian), and σ_χ^2 is given by (3.16). As in Section 4.3.1 we set the quantizer rate equal to $H_Q(\chi_q) = C - R_{offset}$. The channel capacity is given as $C = 1/2\log_2(1+\gamma)$ and R_{offset} is a "rate offset" in bits. We solve (4.12) for δ and insert along with (3.16) into (4.11) to obtain

$$D_{tot}^{post} = \frac{\Delta^2}{24} + \frac{(2ea\pi^2\sigma_s^2 2^{R_{offset}-C})^2}{3\Delta^2} + \frac{(2a\pi^2\sigma_s^2)^2}{\Delta^2\gamma}, \tag{4.13}$$

where we have defined $\gamma = P/\sigma_n^2$ as the CSNR. We minimize (4.13) with respect to Δ to find the optimal spiral arm distance:

$$\Delta_{opt,joint} = 2\pi\sigma_s\sqrt[4]{\frac{(ae2^{R_{offset}})^2}{1+\gamma} + \frac{6a^2}{\gamma}}. \tag{4.14}$$

To find the quantizer step, we subsequently use (4.12) while setting $H_Q(\chi_q) = C - R_{offset} = 0.5\log_2(1+\gamma) - R_{offset}$, and solve for δ:

$$\delta_{opt,joint} = \frac{1}{\Delta_{opt,joint}} 4\pi^2\sigma_s^2\sqrt{\frac{(ae2^{R_{offset}})^2}{1+\gamma}}. \tag{4.15}$$

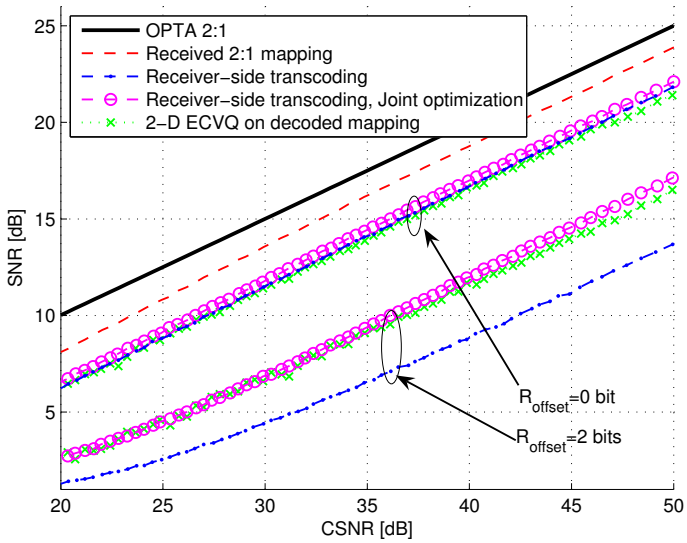

Figure 4.6: Comparison of separately and jointly optimized receiver-side transcoding of the 2:1 S-K mapping for a Gaussian source and an AWGN channel. Jointly optimized mapping and transcoding outperforms both the separately optimized transcoding and the decode-and-quantize approach.

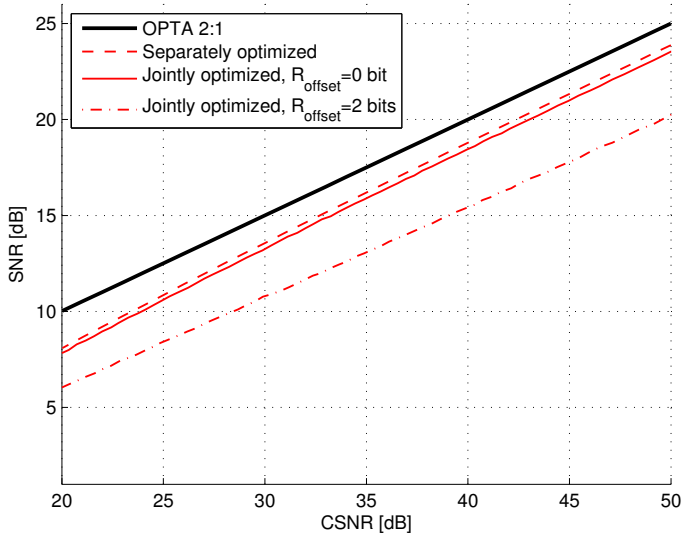

Figure 4.7: Comparison of the unquantized performance (decoded $\hat{\chi}$ in Figure 4.4) of a separately and jointly optimized mapping and transcoding. The joint optimization sacrifices the unquantized performance for increased transcoding performance as R_{offset} increases (i.e. the quantizer rate decreases).

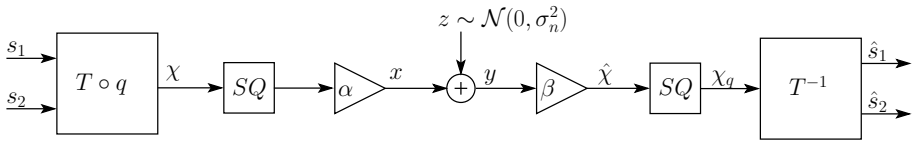

Figure 4.8: Block diagram for transmitter-side transcoding.

In Figure 4.6, we see that the joint optimization has benefits for the transcoded part. For a rate equal to the channel capacity, the joint optimization is only 1.4 dB (in SNR) away from the unquantized system from Section 3.2.1, and dropping 2.5 dB per bit removed from the quantizer. In comparison, the separately optimized transcoding is 1.75 dB away, and dropping faster as the quantizer rate is reduced. On the other hand, the unquantized performance (i.e. the decoded $\hat{\chi}$ in Figure 4.4) is reduced when jointly optimizing the mapping and transcoding. This is illustrated in Figure 4.7, where a 3.3 dB drop in SNR is seen for $R_{offset} = 2$ bits.

4.3.2 Quantization prior to transmission

Instead of quantizing at the receiver side, it is also possible to quantize the channel symbols prior to transmission. This effectively creates multi-level channel symbols which could have certain benefits over continuous-amplitude signals when given a quantizer rate for the transcoding. The detector (quantizer) at the receiver can potentially reject some of the channel noise. For lower quantizer rates, a Wiener filter should be added at the receiver to suppress some quantization noise [Øien and Ramstad, 2001; Kim and Ramstad, 2002].

Jointly Optimized Mapping and Quantization

For the transmitter-side transcoding, the quantizer rate has to be known to the transmitter. Hence, only jointly optimized mapping and quantization makes sense unless joint optimization becomes prohibitively complex. Quantizing the channel symbols and transmitting them with no error protection might seem strange, but since they are transmitted using direct PAM there

[2]The simplified receiver is acceptable for high CSNR. For low CSNR values, an MMSE receiver of the form $\beta = \sqrt{\sigma_\chi^2 P}/(P + \sigma_n^2)$ should be used.

is no bit representation with bits of different significance. This approach is robust in the sense that small-valued channel noise will only produce low distortion levels, i.e. transition to neighboring quantization intervals. Here, only the tails of the Gaussian noise distributions will give high distortion contributions, provided the noise standard deviation is comparable to the quantization interval. In comparison, with bit representations even small channel noise values can flip the most significant bit causing large jumps in the reconstructed source symbols.

Figure 4.4 shows the system we now use, where a quantizer is introduced right after the mapping operation. At the receiver, there is a similar quantizer which acts as the detector. We try to determine an expression for the total distortion, in order to optimize the system parameters. Both the approximation and quantization noise will be as in Section 4.3.1, but the channel noise will have a slightly different effect due to the discrete multi-level representation. Instead of approximating the channel noise as the scaled channel noise variance in (3.14), we use

$$D_c = \frac{1}{2}\mathsf{E}\left[\|x - \chi_q\|^2\right] = \frac{1}{2}\sum_{j=1}^{L}\sum_{i=1}^{L}\|c_i - c_j\|^2 p(j|i)\Pr[i], \tag{4.16}$$

which is the squared distortion caused by transition to neighboring levels, multiplied with the probability of a transition $p(j|i)$, multiplied by the probability $\Pr[i]$ for being in a specific interval, summed over all L intervals and all transitions. Having Gaussian noise and high CSNR, we assume that only transitions to neighboring intervals will occur, i.e. $j = \pm i + 1$. Simulations show that for parameter values close to the optimal Δ and δ, the probability of multiple transitions due to channel noise is small. However, including the transitions to all quantization levels is also possible if so desired. As the channel symbols are discrete values, we can use the common transition probability [Barry et al., 2004], which is basically the area under the tail of the noise pdf:

$$p(j|i) = 2Q\left(\frac{\frac{d_{min}}{2}}{\sigma_n}\right) = 2Q\left(\frac{\sqrt{\frac{P}{\sigma_\chi^2}}\frac{\delta}{2}}{\sigma_n}\right) = 2Q\left(\sqrt{\frac{P}{\sigma_n^2}}\frac{\delta}{2\sigma_\chi}\right), \tag{4.17}$$

where d_{min} is minimum distance of the channel symbols, δ is the quantizer step and Q is the complementary distribution function for a Gaussian standard random variable. Even though the spiral is curved and thus the true

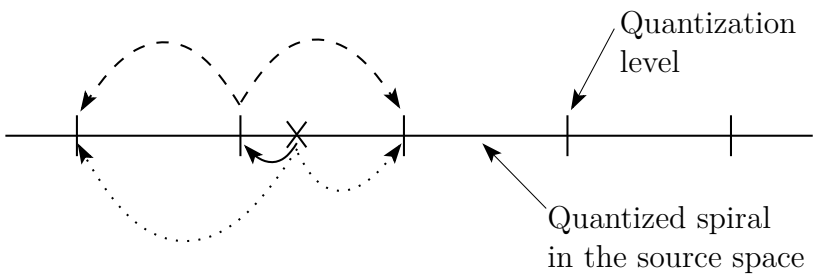

Figure 4.9: An illustration of the distortion terms from quantization and incorrect decoding. Quantization brings the source point (×) to the closest quantization level (shown by solid arrow). Channel noise can force a transition to either one of the neighboring quantization levels (shown by dashed arrows). The resulting distortion (shown by dotted arrows) depends of the direction of the transition.

distortion in the source space is the chord between two quantization levels (Figure 4.3), we approximate the distortion using the squared quantization step:

$$\|c_i - c_j\|^2 \approx \delta^2. \tag{4.18}$$

This is valid when assuming transitions to only neighboring intervals[3] and having a dense spiral (high CSNR), effectively making the line between each quantizer level approximately a straight line. Since the quantization noise should be subtracted rather than added for the cases where quantization and transitions take the signal point in opposite directions (Figure 4.9), we need to introduce a correction term to account for this. This is done by subtracting $\delta^2/12$ for half the transitions in (4.17), assuming a symmetric channel noise distribution. Inserting (4.17) and (4.18) along with the correction term into (4.16), we obtain

$$\begin{aligned} D_c &= \frac{1}{2}\sum_{i=1}^{L}\left(\delta^2 - \frac{\delta^2}{24}\right) 2Q\left(\sqrt{\frac{P}{\sigma_n^2}}\frac{\delta}{2\sigma_\chi}\right)\Pr[i] \\ &= \frac{23}{24}\delta^2 Q\left(\sqrt{\gamma}\frac{\delta}{2\sigma_\chi}\right). \end{aligned} \tag{4.19}$$

Assuming the same approximation distortion as in (3.15) and the quantization noise variance as in (4.1), and inserting (3.16) into (4.19) we obtain

$$D_{tot}^{pre} = \frac{\Delta^2}{24} + \frac{\delta^2}{24} + \frac{23}{24}\delta^2 Q\left(\sqrt{\gamma}\frac{\Delta\delta}{4a\sqrt{2}\pi^2\sigma_s^2}\right). \tag{4.20}$$

[3]This is a common assumption when approximating the BER in digital systems [Proakis, 2001].

This should be minimized with respect to both Δ and δ, subject to the rate constraint

$$H(\chi_q) = C - R_{offset} \overset{a)}{=} h(\chi) - \log_2 \delta$$
$$= 0.5 \log_2(2e^2\sigma_\chi^2) - \log_2 \delta = \log_2 \left(\frac{4ae\pi^2\sigma_s^2}{\Delta\delta} \right), \quad (4.21)$$

where a) comes from [Jayant and Noll, 1984, eq.4.108] and $h(\chi)$ is the differential entropy for a Laplacian source (the channel symbols from the spiral is Laplacian, see Appendix A). Solving this problem analytically is hard, if not impossible, because of the Q-function. Instead, this is solved numerically using a constrained non-linear optimization method (sequential quadratic programming). The result can be seen in Figure 4.10. The first observation we make is in the upper left hand plot, where we see that the optimized Δ_{opt}^{pre} is proportional to (3.19), with the proportionality factor depending on the bit rate $H(\chi_q)$. The proportionality factor can be seen in the upper right plot, and this is independent of the CSNR. In the two lowermost plots we see that the spiral arm distance Δ_{opt}^{pre} and quantization step δ_{opt}^{pre} are equal for rates below the channel capacity, hence the approximation and quantization distortion are equal. As the rate goes above the channel capacity ($R_{offset} < 0$), the Δ_{opt}^{pre} is increased and δ decreased. The model in (4.20) is not valid for rates above the channel capacity, however, and should include transitions to all levels. In that case, increasing the rate would mean that the system would tend toward the unquantized model. For rates below C, we can simply use the expression for Δ_{opt} in (3.19) together with the upper right plot in Figure 4.10 to determine Δ_{opt}^{pre}.

Looking at Figure 4.11 we see that the models in (4.10) and (4.20) agree quite well with the simulations for the high CSNR region, whereas for the receiver-side quantization there is up to a 0.45 dB discrepancy for lower CSNR. This is similar to what is seen in the unquantized system in Figure 3.5 where the model under-estimates the distortion.

The performance of the transmitter-side transcoding is shown in Figure 4.12. Two different quantizer rates are used; the channel capacity (of the wireless channel), and two bits below the channel capacity. We see that for quantizer rates equal to the channel capacity, the gains over the receiver-side transcoding in Section 4.3.1 is vanishing. Moreover, access to an unquantized version of the received channel symbol is also lost. However, as the quantizer rate decreases, the quantizer step increases. Then the transmitter-side transcoding is able to suppress more of the channel noise, and thereby outperforms the receiver-side approach.

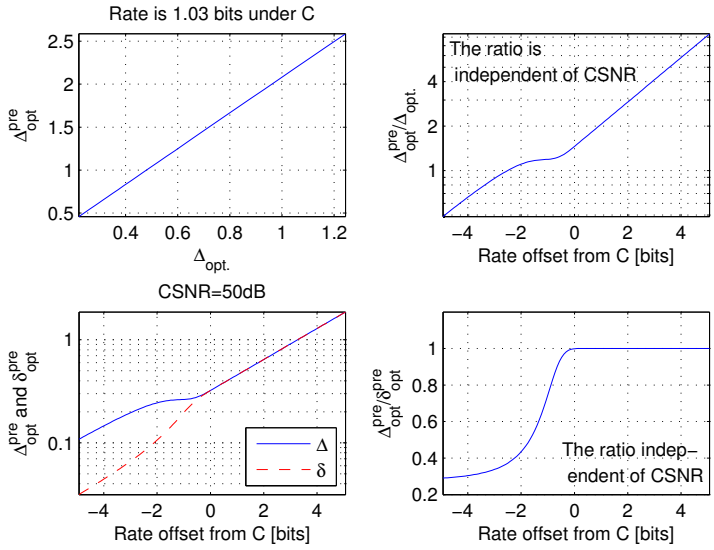

FIGURE 4.10: Jointly optimized Δ_{opt}^{pre} and δ_{opt}^{pre}. Upper left: The jointly optimized Δ_{opt}^{pre} as a function of (3.19). Upper right: Ratio of the jointly optimized Δ_{opt}^{pre} and (3.19) as a function of the rate R_{offset} (this ratio is independent of the CSNR). Lower left and right: Relation between Δ_{opt}^{pre} and δ_{opt}^{pre} for different rates R_{offset} (again independent of the CSNR).

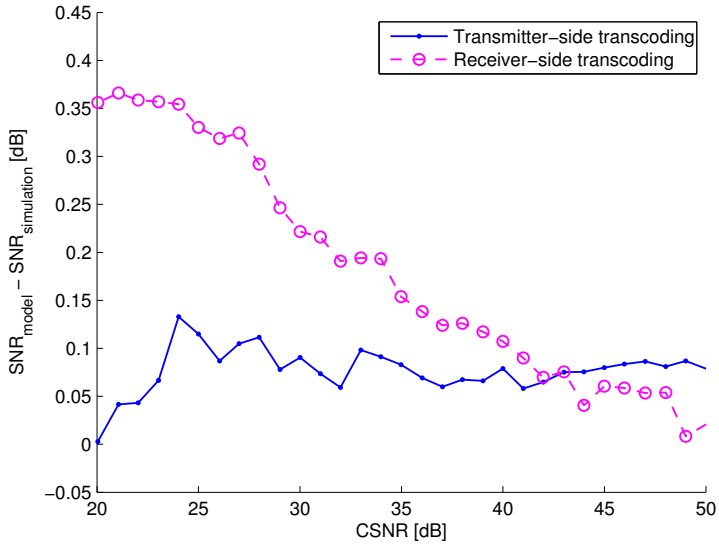

FIGURE 4.11: Comparison of simulation and distortion model for the jointly optimized transcoders operating at a rate equal to channel capacity.

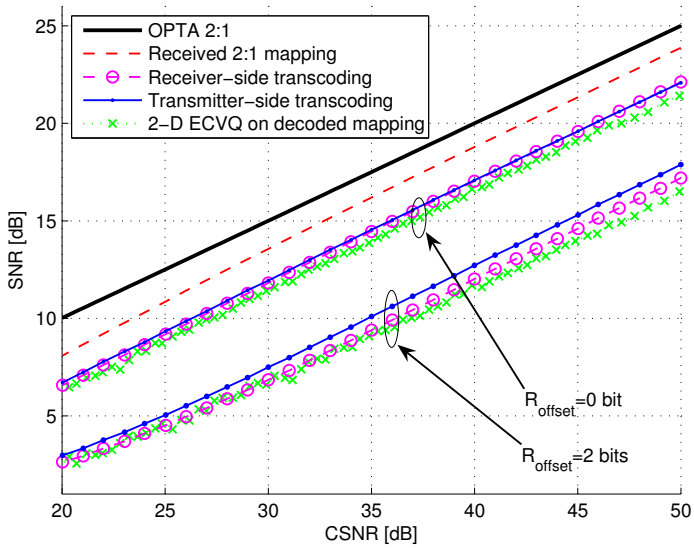

Figure 4.12: Gaussian source, AWGN channel. Both receiver-side and transmitter-side quantization is jointly optimized with the mapping operation.

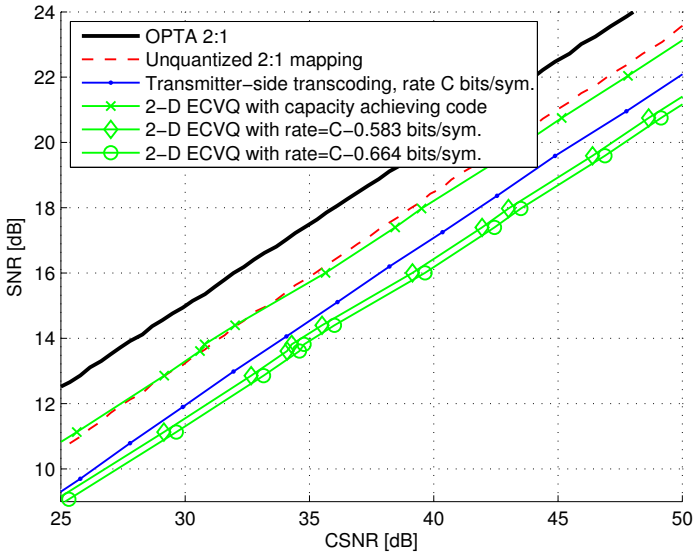

Figure 4.13: Comparison of the transmitter-side transcoding with a 2-D ECVQ with three different codes for an AWGN channel: a capacity achieving code, an LDPC code which is 3.5 dB from the Shannon bound at a target BER of 10^{-5}, and an ACM system designed for a Rayleigh-fading channel which is 4 dB away from the Shannon bound at a target BER of 10^{-3}.

In Figure 4.13, we compare the results from the transmitter-side transcoding approach to a 2-D ECVQ operating at different rates. First, the green line with x-markers show the performance for a capacity achieving code. Second, the green line with the diamond marker shows the performance of an LDPC-based system designed for AWGN channels [Eleftheriou and Olcer, 2002]. For a target BER of 10^{-5}, the distance to the Shannon bound is only 3.5 dB. This translates into a capacity loss of 0.58 bits/symbol. Finally, a system designed for slow Rayleigh-fading channels using LDPC codes [Myhre et al., 2002] are about 4 dB away from the Shannon bound for a target BER of 10^{-3}. This translates to a capacity loss of 0.664 bits/symbol. We see that the proposed system outperforms both real-world examples, whereas the unquantized system beats the capacity-achieving code at high CSNR. Instead of using the ECVQ, employing a better source coder like the entropy-constrained trellis-coded quantization [Fischer and Wang, 1992] would lift the curves another 0.7 dB provided that such a high rate could be produced. This would mean that the proposed system would now be performing on par with the system in [Eleftheriou and Olcer, 2002], but still outperform the system in [Myhre et al., 2002]. Compared to the complexity of the reference systems, the performance of the relatively simple proposed transcoder approach is quite remarkable.

4.4 Shannon Mappings in Multi-hop Scenarios

One of the current trends in the wireless communication research is the increasing interest in multi-hop networks with mesh topologies. This decentralized structure, where each node acts as both as a sender/receiver and as a relay for other nodes in the system, is applicable in many different scenarios; sensor networks [Tubaishat and Madria, 2003; Chong and Kumar, 2003], 4^{th} generation mobile systems and broadband access networks [Ghosh et al., 2005], and deep-space communication.

We define multi-hop networks to encompass all wireless communication systems where there are one or more intermediate nodes between the sender and receiver. Since we only want to discuss the applicability of the S-K mappings in a multi-hop scenario, we make several simplifications which enable a quick evaluation of the possibilities for multi-hop communication. Hopefully, the simplified model is still able to represent a realistic scenario. In essence, we disregard interference, outages and routing problems, and assume a route is established from the sender to the receiver. Furthermore, we only look at

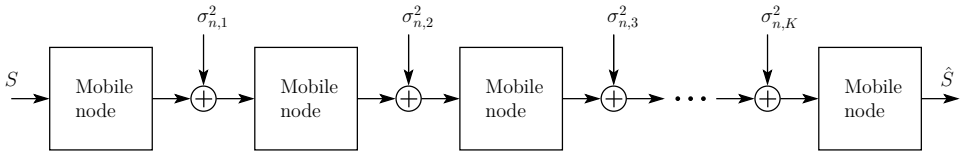

Figure 4.14: The simple serial multi-hop channel model with K hops.

a simple chain of nodes which are connected to their immediate neighbors only (Figure 4.14). Hence, no multi-hop diversity is exploited [Boyer et al., 2004].

It is worth noting that a real multi-hop network would most likely have a mesh structure, thus enabling us to exploit path diversity through for instance multiple description (MD) coding [Goyal, 2001]. In that case, the scalar quantizers in the transcoders could be replaced by MD scalar quantizers to provide robustness against lost transmissions. However, since the point here is to evaluate the possibilities of using the S-K mappings in a multi-hop scenario, we assume the structure in Figure 4.14, where each hop is an AWGN channel, and use the results for the 2:1 bandwidth reduction of a Gaussian source from Section 3.2.1 and 4.3.

In digital communications, there are two main strategies for multi-hop or relay networks. The simplest approach is to amplify the received signal, and forward it to the next relay. This provides low delay since there is no processing at intermediate nodes, but channel noise is accumulated for each link. The second approach is to decode the received signal, re-encode for the next channel and forward to the next node. This increases the delay and complexity due to the processing at each node, but channel noise is not propagated if decoding is error free at each node.

4.4.1 Amplify-and-forward

If we want to use a continuous-amplitude S-K mapping for communicating over the multi-hop network, the only thing we can do at each node is to amplify the signal and forward to the next node. Hence, channel noise would be accumulated for each hop, degrading the performance as the number of hops increases. This fact also suggest that the mapping should be optimized for the total CSNR of all the hops, as opposed to coding for the worst link. In [Boyer et al., 2004] it was shown that a serial network, the total CSNR was calculated as the resulting resistance of a parallel network of resistors,

i.e. $\gamma = \sum_{i=1}^{K} \left(\gamma_i^{-1}\right)^{-1}$. Whether it is realistic to have the knowledge of all the CSNR values is another question. However, given that the mapping shows reasonable amount of robustness, one could for instance code for the expected value of the CSNR. With the noise aggregation in mind, the performance of this scheme is assumed to be poor for anything but a few hops.

4.4.2 Decode-and-forward

For bandwidth-expanding systems the decode-and-forward strategy could be utilized with benefit if some of the channels are multi-level, as for the HSQLC mentioned in Section 2.4.2. Performing a full decoding and re-encoding for the next hop would not be beneficial for bandwidth-reducing mappings, since approximation noise would be introduced at every step. Instead we can use the transcoding results from Section 4.3.2 and optimize the quantizer step to minimize the end-to-end distortion. Then a multi-level channel symbol is transmitted, and the same quantizer is applied at each node. If we know the CSNR for each hop, we can optimize the quantizer step for the worst link to suppress the small noise while minimizing the effect of incorrectly decoded symbols. Since the decode step here only consist of a quantizer, the complexity increase over the amplify-and-forward scheme is minimal. Strictly speaking, the technique we use here does not decode the mapping, but rather transcode (quantize) the channel symbols at each node using the same quantizer. In that sense it could be called quantize-and-forward, but that term is used in [Khojastepour et al., 2004] to describe a compress-and-forward scheme, so we will refer to it as decode-and-quantize here.

4.4.3 The 2:1 Mapping in an K-hop Scenario

To assess the potential usability of the S-K mappings in an K-hop scenario, we construct a simple scenario where all the hops have the same CSNR. Then we compare the amplify-and-forward with the decode-and-forward approach. Furthermore, we compare the resulting performance with the single-hop solution to see how much the number of hops degrades the performance. Since we already have an optimized system for the 2:1 S-K mapping for a Gaussian source and an AWGN channel, we use that system even though a bandwidth expanding system would be more realistic in a multi-hop scenario.

For the amplify-and-forward approach, we use (3.19) to find the spiral arm distance Δ, where σ_n^2 is the variance of the total accumulated channel noise for all hops.

For the system using transmitter-side transcoding, we could either determine the optimal quantizer step from the hop with the lowest CSNR using the results in Section 4.3.2, or we can try to derive a new expression for the distortion given all the channels:

$$D_{MH} = \frac{\Delta^2}{24} + \frac{\delta^2}{24} + \sum_{k=1}^{K} \sum_{i=1}^{L} \sum_{j=1}^{L} d(i,j) Q\left(\frac{|i-j| d_{min}}{2\sigma_{n,k}}\right) \Pr[i], \qquad (4.22)$$

where N is the number of jumps, K is the number of hops, L is the number of quantizer levels, $d(i,j)$ is the distortion metric for receiving j when i was sent, and $d_{min} = \sqrt{P/\sigma_\chi^2}\delta$ is the minimum distance between the PAM levels. The distortion from approximation and quantization is similar to (4.20). The distortion due to channel noise should ideally be modified to include transitions to all quantizer levels. This, however, complicates matters as the distortion is no longer a straight line between neighboring quantizer levels, but rather the cord between two quantizer levels (Figure 4.3). Instead of including all the quantizer levels, we rely on the observation from Section 4.3.2 that where there were few transitions longer than to the neighbor intervals. Although this is no longer true for an increasing number of hops with a quantizer rate equal to the channel capacity, reducing the quantizer rate can make it a reasonable approximation still. This is by no means claimed to be optimal, but serves as a first step toward establishing whether a multi-hop solution for the S-K mappings is feasible.

Along with the simplifications mentioned at start of Section 4.4, we assume equal σ_n^2 on all channels and a fixed transmit power P at each node. This should be a worst-case scenario[4], since as we optimize for the worst link, any links with better CSNR would not result in increased distortion. The simple transcoding based on a scalar quantizer applied to the 1-D channel symbol is expected to be applicable to other M:1 dimension-reducing mappings as well.

[4]Worst-case scenario in the case of known CSI at the transmitter. Of course, for incorrect CSI, the result can be much worse.

Simulation

Using the results from Section 4.3.2, and assuming a quantizer rate equal to the channel capacity (of one hop), we see in Figure 4.15 that the transmitter-side transcoding is able to suppress channel noise effectively, thus enabling multihop communication. The performance is the same whether we have one or ten hops, and the assumption of transitions only to neighbor symbols is valid as long as the rate is below the channel capacity. The amplify-and-forward approach is seen to deteriorate as the number of hops increases. The difference between the decode-and-forward and the amplify-and-forward schemes is illustrated in Figure 4.16. We see that unquantized transmission is only beneficial for point-to-point (single link) communication. As soon as there are relays, decode-and-forward shows better performance.

This result shows that, contrary to immediate intuition, the S-K mappings can potentially be employed in multihop scenarios, provided that we abandon the continuous-amplitude constraint and rather use multi-level channel symbols. In a more elaborate mesh network, path diversity should be possible to implement using multiple description quantizers.

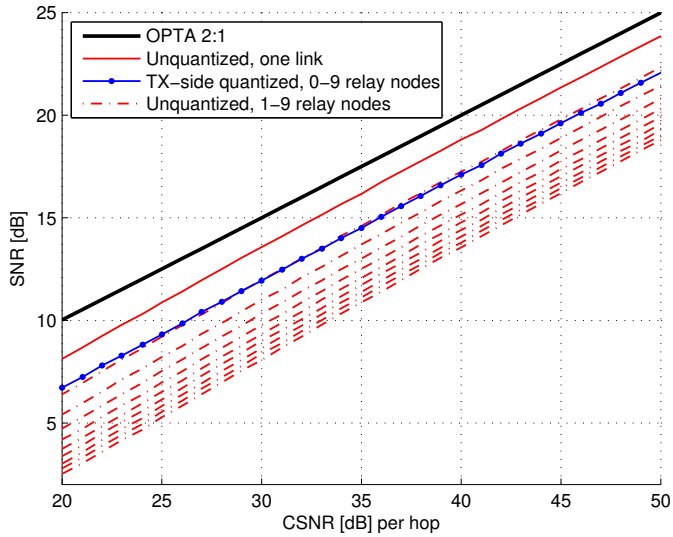

Figure 4.15: SNR vs. per hop CSNR for a multihop scenario, Gaussian source and AWGN channels. The unquantized mapping uses the results from Section 3.2.1 where the Δ is optimized for the total CSNR ($P/[K \cdot \sigma_n^2]$). The quantized mapping uses the results from Section 4.3.2 where Δ and δ are optimized with respect to one link, and the quantizer rate is constrained to the per-hop channel capacity.

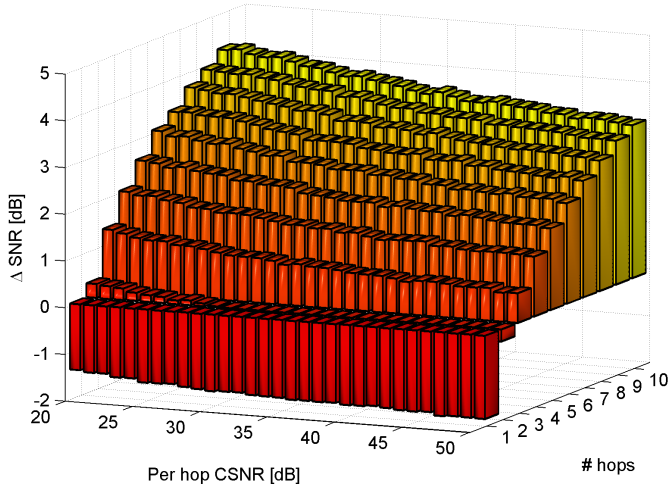

Figure 4.16: An alternative representation of Figure 4.15. Illustrates the difference in SNR between the decode-and-forward and amplify-and-forward schemes. The former (i.e. transmitter-side transcoding) has an increasing benefits as the number of hops increases.

Chapter 5

Conclusions

In this dissertation, we have investigated a lesser explored area of lossy joint source-channel coding suitable for waveform channels; that of direct source-channel mappings. The basic idea is to transmit a source over a channel by projecting a point in the source space directly onto the channel space, using a suitable map or function. We have termed this concept *Shannon-Kotel'nikov mappings* to honor their originators [Kotel'nikov, 1959; Shannon, 1949]. Both the source and channel spaces are assumed to be time-discrete (i.e. sampled) and amplitude-continuous (i.e. not quantized), and the bandwidths may be different. This implies that we can achieve compression when the source space (dimension M) is larger than the channel space (dimension N), and error-control (a form of error-protection) when the channel bandwidth is larger than the source bandwidth. When designed properly, S-K mappings provide high spectral efficiency, robustness against varying channel conditions, and low delay. High spectral efficiency is important in wireless communication since the available bandwidth is scarce. Robustness is also important in wireless systems, as the channel conditions are usually time varying, and obtaining good predictions of the channel state is hard. Thus, robustness means that we would have a system which does not break down even if the actual channel condition is different from what was assumed by the transmitter. Low delay is important in real-time communication systems where there is a strict requirement on the end-to-end delay in the communication chain.

In Chapter 2, causes of sub-optimal performance in source-channel coding systems were discussed. Although the chapter was focused on direct source-channel mappings, the results are applicable to traditional bit-based source-

channel coding systems as well. The loss factors which were identified were

1. Mismatched channel symbol distribution
2. Information rate lower than the operational channel capacity
3. Correlated channel representations
4. Mismatched source model distribution
5. Source coder imperfections
6. Sub-optimal receiver structures
7. Incorrectly decoded channel symbols (threshold effect)

Obviously, both bandwidth reducing and bandwidth expansion systems systems can suffer from sub-optimal receivers (6.), and improving the receiver is usually a matter of complexity (which might, however, become prohibitively high). For bandwidth expanding systems, trying to increase the information rate (2.) results in an increasing probability of incorrectly decoded channel symbols (7.), i.e. the same threshold effect which quickly degrades the performance of traditional channel codes. Bandwidth reducing systems, on the other hand, can be designed with zero probability of the threshold effect, and thus the information rate can increased towards (or even above) the channel capacity. As for the other loss factors, that is 1., 3., 4. and 5., their impact on the system's performance will depend on bandwidth relation M:N. For $N > 1$, it is important to minimize the channel correlation to maximize the channel utilization, so is having correct channel symbol marginals. For $M > 1$, on the other hand, reducing the source coder imperfections (5.) and having the right source model (4.) is important in order to improve the performance.

Chapter 3 introduced the concept of S-K mappings, and presented some specific examples of bandwidth reducing mappings; 2:1 for Gaussian and Laplacian sources, and 4:1 mapping for Gaussian sources. The 2:1 mappings were shown to be competitive with a power-constrained channel-optimized vector quantizer, with the benefit of simple encoding/decoding and no need for training. The 4:1 mapping is made up of cascade of two 2:1 mappings. This greatly simplifies the optimization compared to a full 4:1 mapping, but the performance is 1 dB worse than the PCCOVQ, indicating that the geometry is suboptimal.

Chapter 4 looked at the issues regarding adapting the continuous-amplitude S-K mappings to heterogeneous networks which include pure digital links. This chapter shows that a slight modification of the continuous-amplitude mappings enables transport of the S-K mappings over digital transport networks, and use in multihop scenarios. The 2:1 mapping for Gaussian sources is used as an example, and it is shown that a simple transcoding approach works well to digitize the mapping. Joint optimization of mapping and transcoding is necessary when the rate of the transcoded mapping is lower than the channel capacity of the wireless link. However, it makes more sense to lower the transmit power and quantize at a rate equal to the channel capacity, as opposed to using more transmit power and quantizing at rate lower than the channel capacity. Instead of reducing the rate to two bits below the channel capacity, one can lower the CSNR by 8.5 dB and quantize with a rate equal to the channel capacity. Then, one can optimize the mapping and transcoding separately with very little loss, providing a simpler system design.

When attempting to do multihop communication, the situation is different. The continuous-amplitude mappings will accumulate channel noise from each hop and thus the performance will degrade as the number of hops increases. To avoid this, one can transcode (quantize) before transmission and send discrete multi-level symbols instead. When the parameters are optimized for the channel conditions, most transitions happen to immediately neighboring levels. This results in negligible distortion, even for as many as ten hops.

5.1 Contributions of This Thesis

- It has been proved that the capacity loss due to mismatched channel symbol distribution for the AWGN channel with an average power constraint is equal to the relative entropy of the actual and the optimal Gaussian distribution.

- It has been proved that the rate increase due to non-Gaussian quantization noise under an squared-error distortion measure is equal to the relative entropy of the actual and the optimal Gaussian distribution.

- Other loss factors in source-channel coding systems has been pointed out.

- The sub-optimality of the HSQLC bandwidth expanding mapping has been explained using the identified loss factors.

- The optimization process of a 2:1 bandwidth reducing mapping has been shown in detail.

- A warping procedure has been proposed to adapt sources to mappings originally designed for other distributions, bypassing the problem of determining the geometry of the mappings for a given source distribution. This was shown to give negligible loss for a Laplacian source with a mapping designed for a Gaussian source.

- A 4:1 mapping consisting of a cascade of two 2:1 mappings, with an intermediate warping, has been proposed. This was shown to perform on par with a cascade of two 2:1 mapping, where the inner mapping was designed for the Laplacian input signal. The proposed system is easier to optimize and has a simpler encoder due to the more regular geometry of the mappings.

- A simple transcoding scheme for M:1 mappings has been proposed, enabling transport of the S-K mappings over heterogeneous networks. This transcoding approach was shown to be competitive with far more complex digital systems for high CSNR.

- The proposed transcoding scheme has also been demonstrated to lend itself to multihop communication, as the multi-level channel symbols are able to reject most of the channel noise. Furthermore, due to the inherent robustness of the S-K mappings, the decoding does not break down in case of erroneously detected symbols.

- Closed-loop control over wireless could benefit from the low-delay nature of the Shannon-Kotel'nikov mappings . The possibility to use the mappings in conjunction with robust control techniques would perhaps be one of the most interesting uses of the S-K mappings presented in this dissertation.

5.2 Future Work

Future research within the fields covered by this dissertation should include:

- Verification of findings in Chapter 2 on other joint source-channel coding systems, and research on how to utilize the (currently to a large degree non-constructive) knowledge of the losses to improve on current systems.
- The degree of dependence between the different loss factors should be investigated.
- The topic of inter-channel correlation for direct source-channel mapping systems needs more research in order to be able to quantify the losses, especially for low CSNR where this effect is more pronounced. Capacity reduction due to antenna correlation in MIMO systems might hold some answers.
- A method for determining the geometry of the mappings, given the source-channel-cost tuple, is needed. As for now, all we can do to determine the geometry is educated guesswork, or look at the codebooks of channel-optimized vector quantizers.
- Path diversity in more realistic multihop communication models, like mesh networks, could be exploited through the use of multiple-description quantizers in place of the scalar quantizers now used in transcoding.

Appendix A

Calculation of the Channel Symbol Distribution

The optimization of the 2:1 mapping for the Gaussian source and channel in Chapter 3 requires knowledge of the variance of the channel symbols resulting from the mapping process. To determine the variance, we first have to calculate the resulting pdf of the channel symbols. However, to calculate the pdf exactly is difficult due to the approximation step which shifts probability mass from the plane to the subspace spanned by the spiral arms. Instead of calculating the pdf along the spiral arms, we calculate the pdf along circles around the origin. This is a good approximation when the CSNR is high, since then the spiral arms are densely packed. Hence, the approximation operation can be disregarded and one rotation around the spiral is close to a circle. Obviously, this approximation does not hold for lower CSNR values as the spiral becomes looser, leading to over-estimation of the channel symbol variance. The following calculation was done in [Floor, 2003].

A.1 2:1 Channel Symbol Distribution

We assume here that the spiral is so dense that the approximation operation can be disregarded, and show that the channel signal distribution is Laplacian when using the curve length approximation $\chi = T(\theta) = \eta\theta^2$ as a mapping function, where θ is a function of s_1 and s_2. The domain of consideration will be a disc in $\mathbb{R}^2$. The channel signal χ is given as the following

function of s_1 and s_2:

$$\chi = g(s_1, s_2) = \pm\eta\frac{\pi^2}{\Delta^2}(s_1^2 + s_2^2). \tag{A.1}$$

The distribution of χ will then be given by [Papoulis and Pillai, 2002]

$$\begin{aligned} F_X(\chi) = \Pr\left[X \leq \chi\right] &= \Pr\left[(s_1, s_2) \in D_X^+ \cup D_X^-\right] \\ &= \iint_{D_X^+ \cup D_X^-} f_{S_1,S_2}(s_1, s_2) ds_1 ds_2, \end{aligned} \tag{A.2}$$

where $f_{S_1S_2}$ is the joint Gaussian distribution and

$$\begin{aligned} D_X^+ &= \left\{(s_1, s_2) \middle| s_1^2 + s_2^2 \leq \frac{\Delta^2\chi}{\eta\pi^2}, \chi \geq 0\right\}, \\ D_X^- &= \left\{(s_1, s_2) \middle| s_1^2 + s_2^2 \geq -\frac{\Delta^2\chi}{\eta\pi^2}, \chi < 0\right\}. \end{aligned} \tag{A.3}$$

Solving (A.2) over the domain in (A.3) gives the cdf

$$F_X(\chi) = \frac{1}{2}\begin{cases} 2 - e^{-\frac{\chi}{2\eta\frac{\pi^2}{\Delta^2\sigma_s^2}}}, & \chi \geq 0 \\ e^{\frac{\chi}{2\eta\frac{\pi^2}{\Delta^2\sigma_s^2}}}, & \chi < 0, \end{cases} \tag{A.4}$$

differentiating (A.4) with respect to χ, and using absolute value, gives

$$f_\chi(\chi) = \frac{1}{2\left(2\eta\frac{\pi^2}{\Delta^2}\sigma_s^2\right)} e^{-\frac{|\chi|}{2\eta\frac{\pi^2}{\Delta^2}\sigma_s^2}}, \tag{A.5}$$

which is a Laplacian pdf with variance

$$\sigma_\chi^2 = 2\left(2\eta\frac{\pi^2}{\Delta^2}\sigma_s^2\right)^2. \tag{A.6}$$

Bibliography

S. M. Alamouti.
A simple transmit diversity technique for wireless communications.
IEEE J. Sel. Areas Commun., 16(8):1451–1458, Oct. 1998.
ISSN 0733-8716.
doi: 10.1109/49.730453.

S. Arimoto.
An algorithm for computing the capacity of arbitrary discrete memoryless channels.
IEEE Trans. Inf. Theory, 18(1):14–20, Jan. 1972.
ISSN 0018-9448.

J. R. Barry, E. A. Lee, and M. D. G.
Digital Communication.
Kluwer Academic Publishers, third edition, 2004.
ISBN 0-7923-7548.

T. Berger.
Rate Distortion Theory.
Information and System Sciences. Prentice-Hall, Englewood Cliffs, New Jersy, U.S.A., 1^{st} edition, 1971.

T. Berger and J. D. Gibson.
Lossy source coding.
IEEE Trans. Inf. Theory, 44(6):2693–2723, Oct. 1998.

T. Berger and D. W. Tufts.
Optimum pulse amplitude modulation part I: Transmitter-receiver design and bounds from information theory.
IEEE Trans. Inf. Theory, IT-13(2):196–208, Apr. 1967.

C. Berrou, A. Glavieux, and P. Thitimajshima.

Near Shannon limit error-correcting coding and decoding:turbo-codes.
In *Proc. Int. Conf. on Communications (ICC)*, volume 2, pages 1064–1070, Geneva, Switzerland, May 1993.
doi: 10.1109/ICC.1993.397441.

R. Blahut.
Computation of channel capacity and rate-distortion functions.
IEEE Trans. Inf. Theory, 18(4):460–473, July 1972.
ISSN 0018-9448.

F. Bøhagen, P. Orten, and G. E. Øien.
Construction and capacity analysis of high-rank line-of-sight MIMO channels.
In *2005 IEEE Wireless Communications and Networking Conference*, volume 1, pages 432–437, Mar. 2005.
doi: 10.1109/WCNC.2005.1424539.

J. Boyer, D. D. Falconer, and H. Yanikomeroglu.
Multihop diversity in wireless relaying channels.
IEEE Trans. Commun., 52(10):1820–1830, Oct. 2004.
ISSN 0090-6778.
doi: 10.1109/TCOMM.2004.836447.

J. W. Byers, M. Luby, M. Mitzenmacher, and A. Rege.
A digital fountain approach to reliable distribution of bulk data.
In *Proceedings of the ACM SIGCOMM '98*, volume 2, pages 56–67, Vancouver, Canada, Sept. 1998. ACM.

M. Bystrom and J. Modestino.
Recent advances in joint source-channel coding of video.
In *Proc. 1998 URSI Int. Symp. on Signals, Systems and Electronics*, pages 332 – 337, Pisa, Italy, Sept. 1998.
URL `http://citeseer.nj.nec.com/bystrom98recent.html`.

X. Cai and J. W. Modestino.
Bandwidth expansion Shannon mapping for analog error-control coding,.
In *40th Annual Conference on Information Sciences and Systems (CISS)*, Mar. 2006.

G. Casella and R. L. Berger.
Statistical Inference.
Advanced Series. Duxbury, 2nd edition, 2002.

S. Catreux, P. F. Driessen, and L. J. Greenstein.
Attainable throughput of an interference-limited multiple-input multiple-output (MIMO) cellular system.
IEEE Trans. Commun., 49(8):1307–1311, Aug. 2001.
ISSN 0090-6778.
doi: 10.1109/26.939839.

B. Chen and G. W. Wornell.
Analog error-correcting codes based on chaotic dynamical systems.
IEEE Trans. Commun., 46(7):881–890, July 1998.

C.-Y. Chong and S. Kumar.
Sensor networks: evolution, opportunities, and challenges.
Proc. IEEE, 91(8):1247–1256, Aug. 2003.
ISSN 0018-9219.
doi: 10.1109/JPROC.2003.814918.

P. A. Chou, T. Lookabaugh, and R. M. Gray.
Entropy-constrained vector quantization.
IEEE Trans. Acoust., Speech, Signal Processing, 37(1):31–42, Jan. 1989.

S.-Y. Chung.
On the Construction of Some Capacity-Approaching Coding Schemes.
PhD thesis, Massachusetts Institute of Technology, Sept. 2000.
URL `http://wicl.kaist.ac.kr/pdf/sychung\%20phd\%20thesis.pdf`.
Last accessed 23.12.06.

S.-Y. Chung, J. Forney, G.D., T. Richardson, and R. Urbanke.
On the design of low-density parity-check codes within 0.0045 db of the Shannon limit.
IEEE Commun. Lett., 5(2):58–60, Feb. 2001.
ISSN 1089-7798.
doi: 10.1109/4234.905935.

T. Cover.
Broadcast channels.
IEEE Trans. Inf. Theory, 18(1):2–14, Jan. 1972.
ISSN 0018-9448.

T. M. Cover and J. A. Thomas.
Elements of Information Theory.
Wiley, New York, 1991.

H. Coward.
Joint Source-Channel Coding: Development of Methods and Utilization in Image Communications.
PhD thesis, NTNU, Trondheim, 2001.

H. Coward and T. A. Ramstad.
Quantizer optimization in hybrid digital-analog transmission of analog source signals.
In *Proc. IEEE Int. Conf. on Acoustics, Speech, and Signal Proc. (ICASSP)*, volume 5, pages 2637–2640, Istanbul, Turkey, June 2000. IEEE.

C. Edwards and D. E. Penney.
Differential Equations and Boundary Value Problems.
Prentice Hall International Editions, 1^{st} edition, 1996.

E. Eleftheriou and S. Olcer.
Low-density parity-check codes for digital subscriber lines.
In *Proc. Int. Conf. on Communications (ICC)*, volume 3, pages 1752–1757, 2002.
doi: 10.1109/ICC.2002.997149.

N. Farvardin.
A study of vector quantization for noisy channels.
IEEE Trans. Inf. Theory, 36(4):799–809, July 1990.
ISSN 0018-9448.
doi: 10.1109/18.53739.

N. Farvardin and V. Vaishampayan.
On the performance and complexity of channel-optimized vector quantizers.
IEEE Trans. Inf. Theory, 37(1):155–160, Jan. 1991.
ISSN 0018-9448.
doi: 10.1109/18.61130.

N. Farvardin and V. Vaishampayan.
Optimal quantizer design for noisy channels: An approach to combined source-channel coding.
IEEE Trans. Inf. Theory, 33(6):827–838, Nov. 1987.

T. R. Fischer and M. Wang.
Entropy-constrained trellis-coded quantization.
IEEE Trans. Inf. Theory, 38:415–426, Mar. 1992.

ISSN 0018-9448.
doi: 10.1109/18.119697.

P. A. Floor.
Ulineære avbildninger i kombinert kilde-kanalkoding.
Master's thesis, Norwegian University of Science and Technology (NTNU), O.S. Bragstads pl. 2B, 7491 Trondheim, Norway, June 2003.

P. A. Floor and T. A. Ramstad.
Noise immunity for 1:N and M:1 nonlinear mappings for source-channel coding.
In *Data Compression Conference, 2006. DCC 2006. Proceedings*, Mar. 2006a.
doi: 10.1109/DCC.2006.53.

P. A. Floor and T. A. Ramstad.
Noise analysis for dimension expanding mappings in source-channel coding.
In 7^{th} *Workshop on Signal Processing Advances in Wireless Communications*, Cannes, France, July 2006b. IEEE.

P. A. Floor and T. A. Ramstad.
Dimension reducing mappings in joint source-channel coding.
In *Proc. Norwegian Signal Processing Symposium and Workshop (NORSIG/IEEE)*, Reykjavik, Iceland, June 2006c. IEEE.

G. J. Forney and G. Ungerboeck.
Modulation and coding for linear Gaussian channels.
IEEE Trans. Inf. Theory, 44(6):2384–2415, Oct. 1998.

A. Fuldseth.
Robust subband video compression for noisy channels with multilevel signaling.
PhD thesis, Norwegian University of Science and Engineering (NTNU), 1997.

A. Fuldseth and T. A. Ramstad.
Bandwidth compression for continuous amplitude channels based on vector approximation to a continuous subset of the source signal space.
In *Proc. IEEE Int. Conf. on Acoustics, Speech, and Signal Proc. (ICASSP)*, 1997.

A. Gabay, P. Duhamel, and O. Rioul.
Real BCH codes as joint source channel codes for satellite images coding.

In *Proc. IEEE GLOBECOM*, volume 2, pages 820–824, San Francisco, CA, Nov./Dec. 2000.
doi: 10.1109/GLOCOM.2000.891253.

M. Gastpar, B. Rimoldi, and M. Vetterli.
To code, or not to code: Lossy source-channel communication revisited.
IEEE Trans. Inf. Theory, 49(5):1147–1158, May 2003.

A. Gersho and R. M. Gray.
Vector Quantization and Signal Compression.
Kluwer Academic Press, 1992.

S. Ghosh, K. Basu, and S. Das.
An architecture for next-generation radio access networks.
IEEE Network, 19(5):35–42, Sept. 2005.
ISSN 0890-8044.
doi: 10.1109/MNET.2005.1509950.

B. Girod, A. M. Aaron, S. Rane, and D. Rebollo-Monedero.
Distributed video coding.
Proc. IEEE, 93(1):71–83, Jan. 2005.
ISSN 0018-9219.
doi: 10.1109/JPROC.2004.839619.

A. Gjendemsjø, D. Gesbert, G. E. Øien, and S. G. Kiani.
Optimal power allocation and scheduling for two-cell capacity maximization.
In *Modeling and Optimization in Mobile, Ad Hoc and Wireless Networks, 2006 4th International Symposium on*, pages 1–6, Apr. 2006a.

A. Gjendemsjø, G. E. Øien, and P. Orten.
Optimal discrete-level power control for adaptive coded modulation schemes with capacity-approaching component codes.
In *Proc. Int. Conf. on Communications (ICC)*. IEEE, June 2006b.

J. Goblick, T.
Theoretical limitations on the transmission of data from analog sources.
IEEE Trans. Inf. Theory, 11(4):558–567, 1965.
ISSN 0018-9448.

A. Goldsmith, S. Jafar, N. Jindal, and S. Vishwanath.
Capacity limits of MIMO channels.
IEEE J. Sel. Areas Commun., 21(5):684–702, 2003.
ISSN 0733-8716.

doi: 10.1109/JSAC.2003.810294.

A. J. Goldsmith and S. G. Chua.
Adaptive coded modulation for fading channels.
IEEE Trans. Commun., 46(5):595–602, May 1998.
ISSN 0090-6778.
doi: 10.1109/26.668727.

A. J. Goldsmith and P. P. Varaiya.
Capacity of fading channels with channel side information.
IEEE Trans. Inf. Theory, 43(6):1986–1992, Nov. 1997.

V. K. Goyal.
Multiple description coding: compression meets the network.
IEEE Signal Processing Mag., 18(5):74–93, Sept. 2001.
ISSN 1053-5888.
doi: 10.1109/79.952806.

R. M. Gray and T. Linder.
Mismatch in high-rate entropy-constrained vector quantization.
IEEE Trans. Inf. Theory, 49(5):1204–1217, May 2003.

J. Hagenauer.
Rate-compatible punctured convolutional codes (RCPC codes) and their applications.
IEEE Trans. Commun., 36(4):389–400, Apr. 1988.
ISSN 0090-6778.
doi: 10.1109/26.2763.

J. Hagenauer.
Source-controlled channel decoding.
IEEE Trans. Commun., 43(9):2449–2457, Sept. 1995.
ISSN 0090-6778.
doi: 10.1109/26.412719.

J. Hagenauer and T. Stockhammer.
Channel coding and transmission aspects for wireless multimedia.
Proc. IEEE, 87(10):1764–1777, Oct. 1999.
ISSN 0018-9219.
doi: 10.1109/5.790636.

S. Heinen and P. Vary.
Source-optimized channel coding for digital transmission channels.
IEEE Trans. Commun., 53(4):592–600, Apr. 2005.

ISSN 0090-6778.
doi: 10.1109/TCOMM.2005.844936.

F. Hekland and T. Ramstad.
Digitising the 2:1 Shannon mappings for transport over heterogeneous networks.
In *Data Compression Conference, 2006. DCC 2006. Proceedings*, pages 455–455, Mar. 2006a.
doi: 10.1109/DCC.2006.23.

F. Hekland and T. A. Ramstad.
Digitising Shannon mappings for heterogeneous networks and storage.
In *Proc. Norwegian Signal Processing Symposium and Workshop (NORSIG/IEEE)*, pages 93–97, Stavanger, Norway, Sept. 2005. Norsig.
ISBN ISBN 82-993158-7-5.

F. Hekland and T. A. Ramstad.
Optimal rate-constrained transcoding for a 2:1 bandwidth reducing Shannon mapping.
In *Signal Processing Advances for Wireless Communications, Proceedings of.* IEEE, July 2006b.

F. Hekland, G. Øien, and T. Ramstad.
Using 2:1 Shannon mapping for joint source-channel coding.
In *Data Compression Conference, 2005. Proceedings. DCC 2005*, pages 223–232, Mar. 2005.
doi: 10.1109/DCC.2005.92.

F. Hekland, G. E. Øien, and T. A. Ramstad.
Quantifying performance losses in source-channel coding.
In *Proc. European Wireless (EW)*, Paris, France, Apr. 2007.

F. Hekland, P. A. Floor, and T. A. Ramstad.
Shannon-Kotel'nikov mappings in joint source-channel coding.
IEEE Trans. Commun., Submitted.

M. J. Hossain, P. K. Vitthaladevuni, M. S. Alouini, V. K. Bhargava, and A. J. Goldsmith.
Adaptive hierarchical modulation for simultaneous voice and multiclass data transmission over fading channels.
IEEE Trans. Veh. Technol., 55(4):1181–1194, July 2006.
ISSN 0018-9545.
doi: 10.1109/TVT.2005.863345.

K. Jarvinen, J. Vainio, P. Kapanen, T. Honkanen, P. Haavisto, R. Salami, C. Laflamme, and J.-P. Adoul.
GSM enhanced full rate speech codec.
In *Acoustics, Speech, and Signal Processing, 1997. ICASSP-97., 1997 IEEE International Conference on*, volume 2, pages 771–774, Munich, Apr. 1997.
doi: 10.1109/ICASSP.1997.596038.

N. S. Jayant and P. Noll.
Digital Coding of Waveforms, Principles and Applications to Speech and Video.
Prentice-Hall, Inc., Englewood Cliffs, New Jersey, 1984.

V. Kawadia and P. R. Kumar.
A cautionary perspective on cross-layer design.
IEEE Wireless Commun., 12(1):3–11, Feb. 2005.
ISSN 1536-1284.
doi: 10.1109/MWC.2005.1404568.

M. Khojastepour, A. Sabharwal, and B. Aazhang.
Lower bounds on the capacity of gaussian relay channel.
In *38th Annual Conference on Information Sciences and Systems*, Princeton, New Jersey, Mar. 2004.

S. G. Kiani, D. Gesbert, J. E. Kirkebø, A. Gjendemsjø, and G. E. Øien.
A simple greedy scheme for multi-cell capacity maximization.
In *In Proc. International Telecommunications Symposium (ITS-2006)*, Fortaleza, Brazil, Sept. 2006.

A. N. Kim and T. A. Ramstad.
Comparing performance of entropy constrained scalar quantizer and other scalar quantizers.
In *International Conference on Digital Signal Processing*, volume 2, pages 1341–1344, July 2002.
doi: 10.1109/ICDSP.2002.1028342.

V. A. Kotel'nikov.
The Theory of Optimum Noise Immunity.
New York: McGraw-Hill Book Company, Inc, 1959.

I. Kozintsev and K. Ramchandran.
Robust image transmission over energy-constrained time-varying channels using multiresolution joint source-channel coding.
IEEE Trans. Signal Process., 46(4):1012 – 1026, Apr. 1998.

A. Kurtenbach and P. Wintz.
Quantizing for noisy channels.
Communications, IEEE Transactions on [legacy, pre - 1988], 17(2):291–302, Apr. 1969.
ISSN 0096-2244.

F. Labeau, J.-C. Chiang, M. Kieffer, P. Duhamel, L. Vandendorpe, and B. Macq.
Oversampled filter banks as error correcting codes: theory and impulse noise correction.
IEEE Trans. Signal Process., 53(12):4619–4630, Dec. 2005.
ISSN 1053-587X.
doi: 10.1109/TSP.2005.859314.

E. Lam and J. Goodman.
A mathematical analysis of the DCT coefficient distributions for images.
IEEE Trans. Image Process., 9(10):1661–1666, Oct. 2000.
ISSN 1057-7149.
doi: 10.1109/83.869177.

J. N. Laneman, E. Martinian, G. W. Wornell, and J. G. Apostolopoulos.
Source-channel diversity for parallel channels.
IEEE Trans. Inf. Theory, 51(10):3518–3539, Oct. 2005.
ISSN 0018-9448.
doi: 10.1109/TIT.2005.855578.

K.-H. Lee and D. P. Petersen.
Optimal linear coding for vector channels.
IEEE Trans. Commun., COM-24(12):1283–1290, Dec. 1976.

T. Lookabaugh and R. Gray.
High-resolution quantization theory and the vector quantizer advantage.
IEEE Trans. Inf. Theory, 35(5):1020–1033, Sept. 1989.

J. Max.
Quantizing for minimum distortion.
IEEE Trans. Inf. Theory, 6(1):7–12, Mar. 1960.
ISSN 0018-9448.

D. McRae.
Performance evaluation of a new modulation technique.
IEEE Trans. Inf. Theory, 19(4):431–445, Aug. 1971.
ISSN 0096-2244.

U. Mittal and N. Phamdo.
Hybrid digital-analog (HDA) joint source-channel codes for broadcasting and robust communications.
IEEE Trans. Inf. Theory, 48(5):1082 – 1102, May 2002.

R. Motwani and C. Guillemot.
Tree-structured oversampled filterbanks as joint source-channel codes: application to image transmission over erasure channels.
IEEE Trans. Signal Process., 52(9):2584–2599, Sept. 2004.
ISSN 1053-587X.
doi: 10.1109/TSP.2004.832027.

B. Myhre, V. Markhus, and G. E. Øien.
LDPC-coded adaptive modulation on slowly varying Nakagami-fading channels.
In *Proc. European Wireless 2002*, volume 1, Florence, Italy, Feb. 2002.

A. Nosratinia, J. Lu, and B. Aazhang.
Source-channel rate allocation for progressive transmission of images.
IEEE Trans. Commun., 51(2):186–196, Feb. 2003.
ISSN 0090-6778.
doi: 10.1109/TCOMM.2003.809256.

G. Øien and T. Ramstad.
On the role of wiener filtering in quantization and dpcm.
In *Proc. Norwegian Signal Processing Symposium and Workshop (NORSIG/IEEE)*, 2001.

A. Papoulis and S. U. Pillai.
Probability, Random Variables and Stochastic Processes.
New York: McGraw-Hill higher education, Inc, 4^{th} edition, 2002.

N. Paul, J. Brouet, C. Thirouard, J. Antoine, A. Wautier, and L. Husson.
Efficient evaluation of voice quality in GERAN (GSM EDGE radio access network).
In *Vehicular Technology Conference, 2001. VTC 2001 Fall. IEEE VTS 54^{th}*, volume 3, pages 1402–1406, Atlantic City, NJ, Oct. 2001.
doi: 10.1109/VTC.2001.956427.

A. J. Paulraj, D. A. Gore, R. U. Nabar, and H. Bölcskei.
An overview of MIMO communications - a key to gigabit wireless.
Proc. IEEE, 92(2):198–218, Feb. 2004.
ISSN 0018-9219.
doi: 10.1109/JPROC.2003.821915.

C. Poulliat, D. Declercq, C. Lamy-Bergot, and I. Fijalkow.
Analysis and optimization of irregular LDPC codes for joint source-channel decoding.
IEEE Commun. Lett., 9(12):1064–1066, Dec. 2005.
ISSN 1089-7798.
doi: 10.1109/LCOMM.2005.1576589.

J. G. Proakis.
Digital Communications.
Electrical Engineering Series. McGraw-Hill, 4^{th} edition, 2001.
ISBN: 0-07-232111-3.

K. Ramchandran, A. Ortega, K. M. Uz, and M. Vetterli.
Multiresolution broadcast for digital HDTV using joint source/channel coding.
IEEE J. Sel. Areas Commun., 11(1):6–23, Jan. 1993.
ISSN 0733-8716.
doi: 10.1109/49.210540.

T. A. Ramstad.
Shannon mappings for robust communication.
Telektronikk, 98(1):114–128, 2002.
URL `http://www.telenor.com/telektronikk/volumes/pdf/1.2002/Page_114-128.pdf`.

P. Robertson and T. Wörz.
Bandwidth-efficient turbo trellis-coded modulation using punctured component codes.
IEEE J. Sel. Areas Commun., 16(2):206–218, Feb. 1998.
ISSN 0733-8716.
doi: 10.1109/49.661109.

T. Robinson.
Shorten: Simple lossless and near-lossless waveform compression.
Technical report, Cambridge University Engineering Department, Trumpington Street, Cambridge, CB2 1PZ, UK, 1994.

M. J. Ruf and J. W. Modestino.
Operational rate-distortion performance for joint source and channel coding of images.
IEEE Trans. Image Process., 8(3):305–320, Mar. 1999.
ISSN 1057-7149.
doi: 10.1109/83.748887.

A. Ruscitto and E. M. Biglieri.
Joint source and channel coding using turbo codes over rings.
IEEE Trans. Commun., 46(8):981–984, Aug. 1998.
ISSN 0090-6778.
doi: 10.1109/26.705390.

A. Said and W. A. Pearlman.
A new, fast, and efficient image codec based on set partitioning in hierarchical trees.
IEEE Trans. Circuits, Syst. for Video Technol., 6(3):243–250, June 1996.
ISSN 1051-8215.
doi: 10.1109/76.499834.

K. Sayood and J. C. Borkenhagen.
Use of residual redundancy in the design of joint source/channel coders.
IEEE Trans. Commun., 39(6):838–846, June 1991.
ISSN 0090-6778.
doi: 10.1109/26.87173.

C. E. Shannon.
A mathematical theory of communication.
The Bell System technical journal, 27:379–423, 1948.

C. E. Shannon.
Coding theorems for a discrete source with a fidelity criterion.
IRE Nat. Conv. Rec., 7:142–163, 1959.

C. E. Shannon.
Communication in the presence of noise.
Proc. IRE, 37:10–21, Jan. 1949.

H. Skinnemoen.
Combined source-channel coding with modulation organized vector quantization (MOR-VQ).
In *Proc. IEEE GLOBECOM*, volume 2, pages 853–857. IEEE, Nov. 1994.

M. Skoglund, N. Phamdo, and F. Alajaji.
Design and performance of VQ-based hybrid digital-analog joint source-channel codes.
IEEE Trans. Inf. Theory, 48(3):708 – 720, Mar. 2002.

M. Skoglund, N. Phamdo, and F. Alajaji.
Hybrid digital–analog source–channel coding for bandwidth compression/expansion.

IEEE Trans. Inf. Theory, 52(8):3757–3763, Aug. 2006.
ISSN 0018-9448.
doi: 10.1109/TIT.2006.878212.

J. Song and K. J. R. Liu.
Robust progressive image transmission over OFDM systems using space-time block code.
IEEE Trans. Multimedia, 4(3):394–406, Sept. 2002.
ISSN 1520-9210.
doi: 10.1109/TMM.2002.802845.

V. Srivastava and M. Motani.
Cross-layer design: a survey and the road ahead.
IEEE Communications Mag., 43(12):112–119, Dec. 2005.
ISSN 0163-6804.
doi: 10.1109/MCOM.2005.1561928.

Y. Sun and Z. Xiong.
Progressive image transmission over space-time coded OFDM-based MIMO systems with adaptive modulation.
IEEE Trans. Mobile Comput., 5(8):1016–1028, Aug. 2006.
ISSN 1536-1233.
doi: 10.1109/TMC.2006.120.

D. S. Taubman and M. W. Marcellin.
JPEG2000 Image Compression Fundamentals, Standards and Practice.
Engineering and Computer Science. Kluwer Academic Publishers, 1st edition, 2002.

C. Thomas, C. May, and G. Welti.
Hybrid amplitude-and-phase modulation for analog data transmission.
IEEE Trans. Commun., 23(6):634–645, June 1975.
ISSN 0096-2244.

U. Timor.
Design of signals for analog communication.
IEEE Trans. Inf. Theory, 16(5):581–587, Sept. 1970.
ISSN 0018-9448.

M. Tubaishat and S. Madria.
Sensor networks: an overview.
IEEE Potentials, 22(2):20–23, apr/may 2003.
ISSN 0278-6648.
doi: 10.1109/MP.2003.1197877.

G. Ungerboeck.
Channel coding with multilevel/phase signals.
IEEE Trans. Inf. Theory, 28(1):55–67, Jan. 1982.
ISSN 0018-9448.

V. A. Vaishampayan.
Combined Source-Channel Coding for Bandlimited Waveform Channels.
PhD thesis, University of Maryland, 1989.

V. A. Vaishampayan and S. I. R. Costa.
Curves on a sphere, shift-map dynamics, and error control for continuous alphabet sources.
IEEE Trans. Inf. Theory, 49(7):1658–1672, July 2003.

R. E. van Dyck and D. J. Miller.
Transport of wireless video using separate, concatenated, and joint source-channel coding.
Proc. IEEE, 87(10):1734–1750, Oct. 1999.
ISSN 0018-9219.
doi: 10.1109/5.790634.

S. Vishwanath and A. Goldsmith.
Adaptive turbo-coded modulation for flat-fading channels.
IEEE Trans. Commun., 51(6):964–972, June 2003.

Q. Wang, S. Kulkarni, and S. Verdu.
Divergence estimation of continuous distributions based on data-dependent partitions.
IEEE Trans. Inf. Theory, 51(9):3064–3074, Sept. 2005.
ISSN 0018-9448.
doi: 10.1109/TIT.2005.853314.

E. W. Weisstein.
Laplace distribution.
From MathWorld–A Wolfram Web Resource.
URL `http://mathworld.wolfram.com/LaplaceDistribution.html`.
Accessed 01. Feb. 2007.

K. Wieland.
DigiWorld 2006: FTTH costs coming down.
Webpage, Nov. 2006.
URL `http://www.telecommagazine.com/newsglobe/article.asp?HH_ID=AR_2572`.
Accessed 28. Nov. 2006.

Wikipedia.
OSI model — wikipedia, the free encyclopedia, 2007a.
URL http://en.wikipedia.org/w/index.php?title=OSI_model&oldid=108297747.
[Online; accessed 15-February-2007].

Wikipedia.
Transcode — wikipedia, the free encyclopedia, 2007b.
URL http://en.wikipedia.org/w/index.php?title=Transcode&oldid=105421812.
[Online; accessed 16-February-2007].

J. M. Wozencraft and I. M. Jacobs.
Principles of Communication Engineering.
New York: John Wiley & Sons, Inc, 1965.

Q. Xu, V. Stankovic, A. Liveris, and Z. Xiong.
Distributed joint source-channel coding of video.
In *Proc. IEEE Int. Conf. on Image Processing (ICIP)*, volume 2, pages 674–677, Sept. 2005.
doi: 10.1109/ICIP.2005.1530145.

Y. Yamada, S.-I. Nakagawa, Y. Kurosawa, T. Kawazawa, H. Taga, and K. Goto.
2 Tbit/s (200*10 Gbit/s) over 9240 km transmission experiment with 0.15 nm channel spacing using VSB format.
IEE Electronics Letters, 38(7):328–330, Mar. 2002.
ISSN 0013-5194.
doi: 10.1049/el:20020231.

B. Yang, K. B. Letaief, R. S. Cheng, and Z. Cao.
Timing recovery for OFDM transmission.
IEEE J. Sel. Areas Commun., 18(11):2278–2291, Nov. 2000.
ISSN 0733-8716.
doi: 10.1109/49.895033.

S. Zahir Azami, P. Duhamel, and O. Rioul.
Joint source-channel coding: Panorama of methods.
CNES Workshop on Data Compression, Toulouse, France, Nov. 1996.

A. I. Zayed.
Advances in Shannon's Sampling Theory.
CRC Press, 1993.
ISBN: 0-8493-4293-7.

H. Zheng and K. J. R. Liu.
The subband modulation: A joint power and rate allocation framework for subband image and video transmission.
IEEE Trans. Circuits, Syst. for Video Technol., 9(5):823 – 838, Aug. 1999.

W. Y. Zou and Y. Wu.
COFDM: an overview.
IEEE Trans. Broadcast., 41(1):1–8, Mar. 1995.
ISSN 0018-9316.
doi: 10.1109/11.372015.

D. Zwillinger.
CRC Standard Mathematical Tables and Formulae.
CRC Press, Boca Raton, Fla., 31^{st} edition, 2003.
ISBN 1-58488-291-3.

"Your time is limited, so don't waste it living someone else's life. Don't be trapped by dogma - which is living with the results of other people's thinking. Don't let the noise of other's opinions drown out your own inner voice. And most important, have the courage to follow your heart and intuition. They somehow already know what you truly want to become. Everything else is secondary."

- Steve Jobs (1955 -)